FLUID FLOW IN OSCILLATING CAVITIES

By

Srivathsan Ragunathan

RECOMMENDED: Debendra K Das

Advisory Committee Chair

Chair, Department of Mechanical Engineering

APPROVED:

Dean, College of Science, Engineering and Mathematics

Dean of the Graduate School

December 16, 2003

Date

FLUID FLOW IN OSCILLATING CAVITIES

A
THESIS

Presented to the Faculty
of the University of Alaska Fairbanks
in Partial Fulfillment of the Requirements
for the Degree of

MASTER OF SCIENCE

By

Srivathsan Ragunathan, B.E.

Fairbanks, Alaska

December 2003

Abstract

Oscillatory flows have gained considerable research attention in the recent decades following an interest in transport enhancement in micro-electronic devices. Heat transfer enhancement due to flow modulation has an inherent advantage over conventional mechanical heat transfer components in terms of reduction in weight and space. The present work is aimed at studying fluid flow in oscillating square cavities as a first step towards heat transfer enhancement. A commercial CFD code, Fluent, was used to model a test case consisting of Stokes' second problem, with a source code written in the C programming language. The simulated results were in good agreement with the analytical results found in the literature. Since the description of an oscillatory boundary condition in complex geometries would prove to be a difficult exercise because of the presence of spanwise walls, Newton's second law of motion for accelerating reference frames was used. This method proved to be an effective one computationally and the results agreed well with the analytical results. The cavity problem was analyzed using Fluent with the Non-Newtonian formulation described above. Fluid dynamic characteristics were studied with respect to dimensionless parameters and they exhibited an explicit dependence on these parameters.

Table of Contents

List of Figures

List of Tables

Nomenclature

δ	Stokes layer thickness
ρ	Density of the fluid
ω	Angular velocity
ν	Kinematic viscosity of the fluid
V_a	Wall velocity amplitude
d	Cavity size
V_w	Wall velocity
η	Similarity variable
Re_d	Cavity-size-based Reynolds number
Re_a	Amplitude-based Reynolds number
St	Strouhal number

List of Appendices

Acknowedgements

My most sincere thanks go to my advisor, Dr. Douglas J Goering, who was instrumental in making me work on this project. I will always be grateful to his patience when I failed to produce results; kind comforting words that goaded me to work beyond my limited potential. Dr. Debendra K Das's graduate class on Fluid Mechanics will forever be etched in my memory and so will be his kind approach. Dr. Ronald Johnson has been a father figure for me; he has been a great inspiration.

I would like to thank the Center for Nanosensor Technology (CNT), UAF, for the funding they provided for this project. I would also like to thank the Arctic Region Supercomputing Center (ARSC) for the technical support they provided during this project.

My father does not know a lot of Engineering, but is very proud when I use technical words in front of him. I will always remember with grateful tears, the sacrifices he has made for me. I would also like to acknowledge my mother's support in all my activities.
I am the only child in my family; Ipshita Majhi has been a great sister. I have shared my deepest concerns with her and she has helped me overcome all my emotional hiccups with her soothing presence.

The friends' list is huge and I would like to acknowledge all of them. My roommates deserve a special mention. Arun, Baala and Vijay have listened to my specious arguments and only smiled wisely. Dev Kulkarni has made me laugh; P.K has laughed during difficult times. Ashish, Ragu, Aditi, Manasi, Rae, all of us have had a lot of fun together. Saritha Munnangi has been a great friend too; I have learnt a lot from her composure. Finally, I would like to thank the omnipresent Providence, the great Lord Srinivasa without whom I would not have learnt to walk down the road of life.

Chapter: 1

Introduction and Literature Review:

(1.1) Introduction:

The subject of fluid mechanics continues to offer new challenges to scientists and engineers alike; many new independent research frontiers have gelled over centuries and many peaks conquered. Fluid mechanics can be assumed to be omnipresent; the atmosphere that surrounds us is a huge mass of fluid. The latest in the line of challenges offered is the area of microfluidics, where, the equations governing continuum fluid flow are sometimes challenged. Fluid-structure interaction is another area where additional governing equations (that of the stresses induced in the solid structure) are required to be solved along with the equations for fluid flow (continuity and momentum equations) (see [1] for example).

Oscillations about a mean point are inherent in every aspect of life (even life trends are not devoid of such oscillations; highs and lows about a normal point are a part of life!). In science and mathematics, oscillations have always imparted gross unsteadiness; they exploit the non-linearity in the governing equations and complicate the underlying physics. Steadiness in physical phenomena that are controlled by oscillations often appears after the passage of time in the form of periodicity; obviously things are still changing but these changes occur in a well-defined periodic manner (I can't help thinking of the analogy life offers; it takes time for highs and lows in life to sink in infuse equanimity in a person!)

Stokes was one of the first persons to study the effect of oscillations on fluid flow. In his 1845 paper (see [1]), he studied the effect of an infinitely long oscillating planar wall above an expanse of fluid. He derived analytical solutions for this problem (called Stokes' second problem) through the similarity variable technique. Oscillatory flows have gained considerable attention in the recent decades following an interest in fluid transport enhancement.

Steady subsonic flow in cavities was found to give rise to self-sustained flow oscillations as was first shown by N.K.Ghaddar et al in 1985 at MIT. Oscillating the incoming flow in resonance with these self-sustained oscillations was found to enhance heat transfer rates. At the outset it should be pointed out that this phenomenon has a great potential for cooling in the micro-electronics industry, since mechanical heat transfer devices like fins add weight to the device, so that the word "micro" would be a misnomer. Micro electronic chips these days have very high power densities; natural convection cooling often does not suffice.

How does a fluid respond to a grooved wall oscillating below it? A part of the answer lies in Stokes' second problem. In his paper, Stokes proved that the momentum of the oscillating wall diffused up to a thickness that was dependent on the angular velocity of the oscillation and the kinematic viscosity of the fluid. This was called the *Stokes Layer Thickness.* (See [1] for example).

The oscillation of a grooved wall with a stationary fluid is a different problem (and has been less explored) because of the presence of spanwise walls oscillating in a direction perpendicular to the fluid boundary. Fig. 1.1 illustrates this geometry. The problem becomes complicated if the spanwise wall starts moving in the streamwise direction.(X is the streamwise direction here).

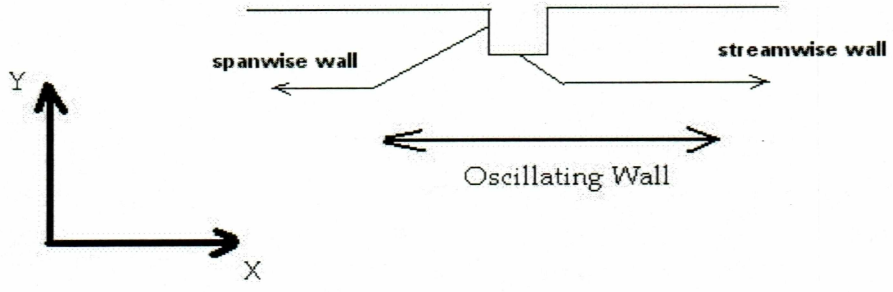

Figure 1.1: The cavity problem

The problem shown in Fig. 1.1 is the subject of the present study. On account of strong non-linearities associated with this problem, computational methods were employed. The original problem actually required moving grids attached to the grooved wall that would

have complicated the problem further. Newton's second law of motion for accelerating reference frames was used to make the problem setup simpler. A reference frame was attached to the wall and fluid motion was viewed from this frame (the wall seems to be at rest and the fluid appears to be oscillating). This is explained in detail in Chapter3.

Fluent, a CFD software package, was employed to solve this problem. The problem setup employed the use of the non-Newtonian reference frame and a momentum source term. This method was found to give accurate solutions to Stokes' second problem which was used as a bench mark case for all experimentations on grids, computational parameters *et cetera.* Much more information on this is given in Chapter 3 of this work.

The oscillating cavity problem showed a lot of interesting results that might have a significant impact on transport rates. Vortex shedding, their growth, fluid sloshing and separation were found to differ drastically depending on the dimensionless parameters described in chapter 4. These results are described in Chapter 5 and some ideas for future developments are given in Chapter 6.

(1.2) Literature Review:

A lot of work has been completed on general oscillatory flows. A survey of literature on oscillating walls and fluid flow was carried out. A brief summary of the literature consulted is given here. Papers are arranged in a chronological order (except one). The first two papers describe general oscillatory problems and their stability. The paper on turbulent flows can also be included in this list but its focus was on transition in such oscillatory flows. The fourth paper (composed of two parts) is the first we have on specific geometries and oscillatory flows in them. Separation is an important phenomenon in oscillatory flows and is indicative of the movement of vortices. The seventh paper (composed of two parts) treats channel flows and analyses enhancement of transport through resonance. Other papers consulted were for general reference in the context of vibrating walls and their effects.

Unsteady Cavity flows : Oscillatory Flat box flows: V.O'Brien , 1975

This paper was supposedly the first attempt at extending previously studied closed rectangular cavity flows to oscillatory cavity flows. Three numerical parameters were

said to govern flow, namely, peak Reynolds number, reduced frequency (or Stokes number) and the height-to-length ratio of the cavity. The flow fields were obtained by finite difference solutions and analytic solutions of the Navier-Stokes equations.

(In our cavity problem three length scales that could possibly affect the flows were identified and these were (1) the Stokes Layer thickness, (2) the displacement amplitude of the vibrating wall and (3) the cavity dimensions (only a square cavity was considered). The Stokes layer thickness and the displacement amplitude were dependent on each other; only two different Reynolds number formulations were possible. These considerations are explained in chapter 4.)

This paper also discussed the dependence of flow on the shape of the box and the Reynolds number.

An analytical approach was given for flat box flows, wherein, a box with dimensions H and L (height of the box and length respectively) was considered. The unsteady vorticity equations were considered with one wall oscillating back and forth with a normalized driving velocity of $\cos(\acute{\omega}t)$ where $\acute{\omega}$ is the driving frequency of the wall. An analytical solution to this equation with viscous no-slip conditions at the walls and zero net flux over the section as boundary conditions was given. The solution obtained was different than the oscillatory Stokes flow problem given that this particular solution considered an induced pressure gradient in contrast to the latter that considered a zero pressure gradient. Parallel Flow was predicted for $H/L < 1$ in the central part of the box.

Experiments were in good agreement with the predicted analytical results; photographing of a dyeline during the cycle was done. The details of the experiment itself were described in a different paper (see additional references [1]). Experiments showed that the results agreed more with the "composite theory" (having both the induced pressure gradient as well as tangential shear) than the original Stokes' oscillatory flow.

A finite difference model to solve this problem was also explained in this paper. An important observation made was that the accuracy of the numerical solution depended on

the mesh size. The mesh size, in fact, was governed by the oscillatory Stokes' layer thickness, a fact that was well observed in our test run for Stokes' problem.

The results of this work can be summarized as follows:

(1) At higher oscillating frequencies of the wall, this paper claimed, all the interesting viscous effects were confined to the boundary layers of the walls, a fact that was clearly observed with Fluent solutions for Stokes' second problem in our test runs. The amplitude profiles flattened out in the central portion of the box for higher driving frequencies.

(2) Experimental setups were modified to vary frequency, fluid viscosity and box height H and thus N and Reynolds number were varied. The Reynolds number went from 1 to 10000, but flow in the central part remained essentially parallel and independent of Re for *small* H/L ratios.

Linear Stability theory of Oscillatory Stokes layers: Kerczek *et al* 1974:

This paper, published prior to the previous one, dealt with stability theories of oscillatory stokes layers under different conditions. Two quasi static linear theories and integration of full time-dependent linear disturbance equations were discussed in detail. The conditions for stability in each of these theories were discussed.

This paper provided a basis for the non-dimensional groups we used in the fluid dynamics part of our work. One is the Reynolds number based on the Stokes length (this paper uses a different expression for Stokes' length $(2\nu/\omega)^{1/2}$, we have used White's[1] expression for Stokes length as explained in Chapter 3.

The most interesting portion of the whole paper lies in its discussion of dynamic stabilization and destabilization due to superposed modulation. Donnelly (1964), through experiments in a concentric cylinder found that modulation at small amplitudes caused stability in flow because the critical Taylor number for instability was increased. Grosch and Salwen (1968) found stability at small modulation amplitudes in plane Poiseuille flow and destabilization at higher amplitudes.

Earlier attempts at establishing energy stability theory on one example of a finite stokes layer were summarized briefly and the results given. One theory (linear-theory stability analysis by Collins (1963)) assumed a quasi-static state and an instantaneous "frozen" profile were used. Limitations on this theory were also briefly discussed. Such stability theories and modulation provided much insight into the Heat Transfer aspects of the cavity problem. It was envisioned that oscillations of a wall with cavities may have tremendous potential for heat transfer enhancement.

Another very important discussion in this work bearing relevance to our problem is that of the critical Reynolds number for transition to turbulence in oscillatory flows. An experimental work done during the mid-60s suggested that the critical Reynolds number for transition to turbulence was 566. Although this could not be directly related to our work, it proved useful in establishing the range of Reynolds numbers for laminar flow solutions to work with.

The limitations of various theories were summarized in the concluding part of this paper.

This paper had results for a general time-dependent stability problem, so it helped generate stable results for the range of Reynolds numbers considered. Transition to turbulence is a very interesting digression that is not a part of this work. This is mentioned in Chapter 6.

A new approach to oscillatory rough turbulent boundary layers: Jonsson, 1980

This is a purely experimental work with velocity measurements in an oscillatory turbulent layer over a rough wall using a large water tunnel.

The measurements on the oscillatory boundary layer were done previously by oscillating the wall and this paper approached the problem by oscillating the fluid. Much theoretical work was discussed in this paper which established the existence of certain velocity and phase relations in oscillatory rough turbulent boundary layers. The paper formulated expressions for friction factor, shear stress and dissipation factor. Reynolds numbers based on different length scales were discussed here which had significant relevance to

Reynolds number formulations for the cavity problem. The expression for shear stress provided an insight into the fluid dynamics aspects of our cavity problem.

On Flow through furrowed channels: Parts 1 and 2 Ian Sobey, 1980

This work studied flow thorough a furrowed channel, steady and unsteady. Part 1 dealt with the prediction of the flow structure with numerical solutions of unsteady Navier – Stokes equations. This work was motivated by the development of a highly efficient membrane oxygenator which achieved very high mass flow rates with furrowed channels. (The present work on cavity flows might fortuitously also lead to such life-saving applications even though it is currently being studied to achieve high transport rates especially in small devices).

Dimensionless parameters that govern the steady flow were described in one section and they are: (1) the dimensionless frequency (similar to the expression described later in this chapter), (2) the Strouhal number and (3) The peak Reynolds number (based on mean flow). The structure of the channel itself was odd; it had periodically arranged furrows and all these furrows were shaped in the form of a sine wave.

A numerical code based on the finite difference version of the Navier Stokes equations was written and two cases were analyzed. Second order upwind differencing was used for the non-linear terms in the governing equations, and a two time-level Dufort-Frankel substitution for the time-dependent terms. The cavity problem was first analyzed with a first order upwind differencing scheme and then with a second order scheme. A lot of information was given in this paper (on flow through furrowed channels) about the mesh spacing and the time step sizing. A very fine mesh near the furrow and a coarse mesh elsewhere were used.

Firstly steady flow was analyzed through this channel and these results were compared with the modern boundary layer theory of Smith. Flow separation at high Reynolds numbers was predicted. Reynolds numbers and geometric parameters of the cavity were varied and the effect of these quantities on flow was studied. Of particular interest to our work on cavity flows is the prediction of the presence of vortices and their location with respect to the furrow. The location of these vortices was studied as a function of the

dimensionless parameters mentioned above. The predicted results through numerical analyses were in excellent accord with the analytical results.

The numerical method was then applied to a case of unsteady flow, where a pulsatile flow was studied over the furrowed sections. At least five parameters were said to characterize the flow, the pulsatile Reynolds number, the Strouhal number, the hollow length, depth D and the time history of the flow. Flow patterns were predicted; the presence and location of vortices and their motion were studied as a function of the above mentioned parameters.

Part 2 of this work dealt extensively with experiments on flows through such furrowed channels. Flow patterns were observed to concur with the numerically predicted results in Part 1 of this work.

This paper was of a lot of help to us in visualizing vortices in the cavity problem. These vortices are very important given that they help enhance transport.

The occurrence of separation in oscillatory flow: Ian J. Sobey, 1983

This work is concerned with the prediction of separation in oscillatory flow in furrowed sections. Flow patterns were studied with small, medium and large Strouhal numbers. This work goes on to illustrate the limitations of the quasi-steady theory for unsteady flows. Results from the previous paper for steady and unsteady flows were used for predicting separation as a function of physical and geometric parameters.

Separation in steady flow was predicted when the Reynolds number for flow was greater than a critical Reynolds number for a fixed geometry. Any further increase in Reynolds number resulted in the separation region growing as the vortex formed inside the furrow kept expanding into the channel fluid column. A separation envelope (a plot of the separated region against the Reynolds number) was presented and this was used for characterizing separation in unsteady flows also. The quasi-steady flow assumption is also shown to be applicable in some unsteady cases. In summary, this paper provided us with a good idea of the physics involved in such oscillatory flows. In the cavity problem

also, vortices and separation regions were encountered. Chapter 5, section 5.1 is dedicated solely to physical explanation of the flow patterns that were observed.

Numerical Investigation of incompressible flow in grooved channels: Parts 1 and 2

Ghaddar, et al, 1986.

This work dealt (comprising 2 parts) with the fluid mechanics and heat transfer in periodically grooved channels. The first part of this paper deals with flows in grooved channels and their linear stability. For a range of Reynolds numbers (based on mean flow unlike our problem where there is no mean flow) less than a critical value, flow was steady comprising an outer channel flow, a shear layer at the groove lip and a weak recirculating vortex in the groove. (A lot of this information was used in our cavity problem though it was under different boundary conditions. For example, a weak vortex was found inside the cavity too at certain times; this is explained in Chapter 5). The linear stability of this flow was then analyzed and resemblance to standard channel waves was found. This work put forward a theory for frequency prediction based on the Orr-Sommerfield dispersion relation and verified it by varying the geometric parameters of the cavity. (It should be mentioned that geometric parameters variation is another interesting digression, in fact, flow patterns can also be affected by geometric parameters of the cavity; this is not a part of our work). The instabilities were found to give rise to "self-sustained oscillations" driven by an unstable groove vortex sheet. The above mentioned phenomenon could be very beneficial in transport enhancement.

The numerical method used is of little direct significance in this work but could prove to be useful if we attempt writing a computer code for the cavity problem. The meshing information in this problem though proved to be very useful since a similar cavity geometry and computational domain were used in our cavity problem.

The detection of self-sustained oscillations due to linear instability forms the next section of this work. Transition to such oscillatory flow corresponded to a regular Hopf bifurcation.

Part 2 of this work extended subcrictical results to the case of forced flow where it was proved that excitation of the flow at its natural frequency of oscillation resulted in significant transport enhancement. Heat Transfer characteristics were determined for grooved channels and compared with ungrooved channels and it was shown that there was significant enhancement in heat transfer.

The thermal boundary condition used was Neumann boundary type; uniform heat flux at the grooved bottom wall and an adiabatic top surface. The steady state heat transfer characteristics of an unmodulated groove flow were studied as a baseline case to evaluate the effects of oscillation on heat transfer. Nusselt number was defined for both of these cases and a heat transfer enhancement parameter, which was a ratio of these two Nusselt numbers, was defined.

Overall, this paper provided a lot of insight into flow patterns and magnitudes of heat transfer enhancements in oscillatory flows.

A spectral collocation method for confined unsteady flows with oscillating boundaries: D. Mateescu, et al , 1994

This work dealt with the development of a spectral collocation method for the study of fluid flow with periodically oscillating boundaries. The important fluid dynamic parameters were expanded using Chebyshev polynomials and Fourier functions. An important feature was the use of complex exponential time and frequency functions for time discretization. These were applied to classical test cases and the results were found to be in accord with the analytical results.

An introduction to spectral methods was given. A spectral collocation method is a special case of the method of weighted residuals in which the test functions are "translated Dirac Delta functions centered at the collocation points". The earlier spectral methods collocation used a combination of spectral spatial discretization and finite difference based time discretization, making the computation arduous and possible only on a supercomputer. The present method though, discretized both space and time by spectral

expansions by using complex exponential functions thereby making computation very simple and possible on any computer.

This paper was consulted only for qualitative comparison with our results. Since a custom CFD code Fluent was used for our problem, this paper was of no direct use. In future if a code is attempted to solve for fluid dynamics and heat transfer for the cavity problem, this paper could come in handy.

Vortex Structure and Fluid Mixing in Pulzatile Flow through Periodically Grooved Channels at Low Reynolds Numbers: NISHIMURA, *et al, 1997*

This work dealt with both experimental and numerical aspects of pulsatile flows in channels with rigid top walls and square and rectangular grooves located at regular intervals. This work was primarily concerned with vortex structure and fluid mixing through grooved channels as a function of Reynolds number (based on mean flow, see [10] for example) and Womersly numbers (a frequency based number). The main features of this study were the prediction of primary and secondary vortices in the groove proper and in the vicinity of the upper wall respectively. Numerical results are predicted with visualization plots with stream functions while the experimental results are visualized with streaklines.

A flow rate of the fluid comprising a steady part and an oscillatory fraction was considered and flow effects due to this were studied through periodically grooved channels. The numerical practice here was particularly interesting; the dimensionless vorticity transport equation and the stream function equation (see [10] for details) were considered and a central difference approximation method was applied to discretize the governing equations. A Thomas algorithm was used to solve the algebraic equations with the result that the use of upwinding procedures was done away with.

The next part of this paper is a technical description of the activity inside the cavity and outside it. Flow separation is observed at the rear edge of each rib at the start of the deceleration phase. This produces a clockwise rotating vortex that starts filling the groove. Growth of this vortex in the cavity is complete when flow rate is maximum.

During the deceleration phase the vortex grows and covers the rib while another counter-clockwise rotating vortex occurs near the top wall. At zero flow rate these two vortices fill up the entire domain. The vortex near the upper wall disappears immediately after this and the vortex generated inside the cavity remains there for some more time. This process is repeated for succeeding cycles.

Experiments were done to validate numerical results and they were found to concur with numerical results.

Peristaltically driven channel flows with applications to micromixing: Selverov, 2001

This work studied flows driven by transverse, small amplitude traveling sinusoidal wave along the boundary of a closed rectangular container. Results were studied more closely for high frequency waves. This work carried more significance to microfluidic devices where internal mechanical elements cannot be accommodated due to restrictions in size. One of the walls of a rectangular channel with both ends closed underwent a sinusoidal oscillation in the form of a traveling wave. The results for both Eulerian and Lagrangian approaches were compared.

An important parameter, non-dimensional frequency $\alpha = (\omega h^2/\nu)^{1/2}$ where ω is the driving frequency, h is the height of the channel and ν is the kinematic viscosity of the fluid, was discussed.

It was found that all quantities exhibited an explicit dependence on dimensionless frequency for high frequencies. A detailed description of the boundary layer structure both near the oscillating wall and the fixed wall was given. "Reflux" which is net fluid flow in a direction opposite to that of the traveling wave, was studied using the Lagrangian approach.

The resulting flow was found to have a boundary layer structure with maximum "pumping" effect near the boundary of the moving wall. The velocity field was found to be dependent on the dimensionless frequency α at different locations across the channel. Near the walls, flow was in the direction of the wave and away from the walls, motion

was in the opposite direction (because of the closed channel configuration). These effects were seen both in the Lagrangian and Eulerian descriptions of flow.

Interesting results were found for low frequencies: The net flow near the walls was in a direction opposite to that of the traveling wave while away from the walls, fluid motion was in the direction of the wave.

Stability of flow in a channel with vibrating walls: Floryan, *et al,* 2002.

This paper dealt with the effects of wall vibrations in the form of traveling waves on the stability of flow in a channel. It was found that such vibrations affected flow instability only if they consisted of modes with wavelength and frequency close to those of "neutral Tollmien-Schlichting" waves. Vibrations in resonance with these waves though initially causing instability that increased linearly with time, had the potential to significantly reduce the critical Reynolds number.

The growth of small-amplitude disturbances responsible for the transition from laminar to turbulent flow was described by a classical linear operator. The stability parameters were determined from the Eigenvalues of this operator. Even if all the Eigenvalues were stable, the disturbances might undergo an initial transient growth and this growth might "trigger a bypass transition".

Detailed mathematical equations were given and these were solved for vibrations of small amplitudes. The stability of flows with different vibration modes was studied.

This paper also served as a caution for transition to turbulence in our problem if any.

Analytical studies of flow effects due to vibrating walls: Carlsson,

Under consideration for publication in the Journal of Fluid Mechanics (submitted Dec5, 2002)

This paper presented an analytical approach to the study of flow induced by vibrating solid boundaries. Transverse motions in the form of standing waves vibrated at small amplitudes were considered. Steady streaming occurred at the second order in the

perturbation solution. Two dimensionless parameters were found to affect this steady flow, the frequency of oscillation and the channel half-width. If the channel was large enough, the flow was determined solely by the frequency of the oscillation. The resulting cell structure was of three types. If the wavelength and the channel half-width were comparable, irrespective of the frequency, full circulatory flow existed in the channel. The other two cell structures depended on the frequency of the oscillation.

The flow field generated by flexible walls vibrating transversely in the form of standing waves was studied. The flow obtained was symmetric and periodic with respect to a given wavelength of the vibrating surface and there was streaming in cellular flow patterns. Standing waves produced circular wave patterns that could be used to mix viscous liquids.

The theoretical analysis consisted of perturbation methods to investigate the steady streaming produced due to the transverse vibrations of the walls. Streaming motions were studied for different values of the dimensionless frequency and the channel half-width.

The time averaged second order velocity was determined to study streaming. This was repeated for different values of dimensionless frequency (α) and channel half-widths (H). In each case it was found that the form of the resulting cellular structure strongly depended on both these factors.

If α and H were small, the flow was dominated by viscous effects. If α was increased, inertial effects began to dominate, breaking the fluid domain into two layers, the layer near the wall governed by viscous effects and the outer inviscid region.

If H was increased, the significance of the opposite wall decreased and solution began to resemble that of a semi-infinite domain.

This paper was of no direct use either but it provided a reasonable insight into the flow patterns we were to expect in our cavity problem.

Spatio-temporal dynamics of a periodically driven cavity flow:

Vogel, *et al,* 2003

This work studied the flow in a rectangular cavity driven by the sinusoidal motion of the floor in its own plane, both experimentally and theoretically. The primary interest of this paper was in determining the stability limits of time-periodic, two dimensional base state. Three flow regimes were found in the parameter space considered: (1) a 2-D time-periodic flow (2) a time-periodic 3-D flow with a cellular structure in the span-wise direction and (3) a 3-D irregular flow in space and time. The system possessed space-time symmetry with a reflection about a vertical mid-plane together and a half-period translation in time(R-T symmetry). The numerical results computed by solving the 2D Navier Stokes equation agreed with the experimental results. Two classes of flows were investigated, one with a rigid top and another with a free surface.

The geometry considered was a rectangular cavity with stationary spanwise end walls, the floor oscillating sinusoidally and either a free surface or a rigid wall at the top. The spanwise sidewalls played a major role in determining the flow pattern. The streamwise sidewalls played a major role in setting up another oscillatory flow at the top. The streamwise sidewalls rolled up the Stokes layer near the walls like in a lid driven cavity flow but in this case the rolling was unsteady.

The Reynolds number based on the amplitude and frequency were formulated and the velocity of the floor described by these two scaled parameters. These two dimensionless parameters were varied; velocity fields and vorticity were studied for a rigid top as well as for a free surface at the top.

This study showed that flow in periodically driven oscillatory cavity could be described as 2D in some bounds. This paper also provided us some idea of the flow patterns to be expected in oscillatory problems. Vorticity proved to be a very important fluid dynamic phenomenon in the cavity problem. Its occurrence and shedding are very critical in all transport properties including heat transfer.

Chapter 2

Introduction to Fluent:

(2.1)Introduction:

Since the whole problem was run using the CFD code Fluent on ARSC computers, this chapter is devoted to a discussion of the modeling and solution process using Fluent and its associated software. Fluent comprises the 3-D solver that initializes and runs the fluid flow problem. Geometric modeling and grid generation were done using the user-friendly, GUI supported software packages Gambit and Tgrid. Through Gambit, the user can also set boundary condition types on edges, faces and volumes so that a well-defined model is input to Fluent (the actual numbers though have to be set in Fluent). Once the grid is generated, it is exported to Fluent and the model initialized and run there. This chapter briefly discusses Gambit (T Grid is not described here because Tgrid was not used in our problem). The source code for the Fluent solver is written in the C++ computer programming language. As a general word of caution, the following is only a short summary of the Fluent features used in this work, for complete information Fluent's website, www.fluent.com, can be consulted.

(2.2) General Procedure for Numerical Analyses:

Numerical analyses enjoy some advantages over conventional experimental analyses. Some of them are:

(1) Low Cost

(2) Speed.

(3) Ability to model complex flows

(4) An excellent starting point for an experimental analysis for which a definite mathematical solution is non-existent (for example, unsteady recirculating flows).

The following paragraph describes, in general, steps that are required for any numerical analyses:

(a) **Problem Definition:** This includes mathematical description of the physical phenomena to be studied, i.e., the differential equations and boundary conditions that govern the problem.

(b) **Discretization:** This includes setting up of discrete points in the region(s) of interest and calculating various dependent variables through the discretized equations. Discretized equations are generally algebraic expressions evolving from differential equations governing the physical phenomena. In commercial CFD software like Fluent, the user needs to create geometries to represent the calculation domain of interest and *mesh* it to represent discrete points where the user wants dependent variables calculated. Since boundary conditions are also included in the set of discretized equations to be solved, the user needs to input boundary conditions also. In commercial software like Fluent, there are user-friendly options that facilitate this process.

(c) **Solution:** This is a major process in the numerical procedure. For non-linear differential equations where exact solutions are very difficult to obtain (sometimes impossible), numerical methods are the only retreat. Many methods employ iterative procedures to obtain solutions for algebraic equations, but it must be mentioned that there are also direct solvers for these algebraic equations **[3].** Gauss-Siedel, Newton-Raphson, Runge-Kutta are examples of iterative procedures. These iterative procedures start with an initial guess for the values of the variables and improve these with iterations. A solution is said to be *converged* if the values obtained from two successive iterations are equal or almost equal. Since a lot of assumptions go into such solution procedures, various parameters are studied so that the user makes an "educated guess". These parameters influence the accuracy of the final solution and the computational speed. Some of these terms are described briefly later in this chapter.

(d) Post Processing: This is the final stage in a computational procedure. Commercial software codes like Fluent have user-friendly graphics options which make interpretation of results easy. Normally, commercial software codes work with dimensionless numbers that makes analyses very efficient and elegant.

(2.3) Gambit:

Gambit is a graphics platform where a physical representation of the computational domain can be realized by means of user-friendly utilities, each of which is described briefly. Gambit consists of the following components:

(2.3.1) The Graphical User Interface (GUI):

The GUI makes the job of drafting basic geometries and in general, visualization easier. The advent of the *mouse* as an input device has made this job an attractive one too. Gambit's GUI has the following components:

(a) The Graphics Window: This is the region where the model drawn by the user is displayed. This occupies a major portion of the Gambit screen and has many subcomponents. The graphics window is made up of four quadrants for viewing in different origin orientations. These quadrants can be customized and resized using preset configurations. The mouse can be used in all these applications.

(b) The Main Menu Bar: The main menu bar has "Microsoft Windows-Like" menu items that assist in the creation, editing and the general solver setup of a CFD model. The main menu has an online help menu too which is becoming a must in commercial software today.

(c) The Operation Tool Pad: The Operation Tool Pad consists of a group of command buttons that actually create and mesh the model. A figure below shows how an operation tool pad looks:

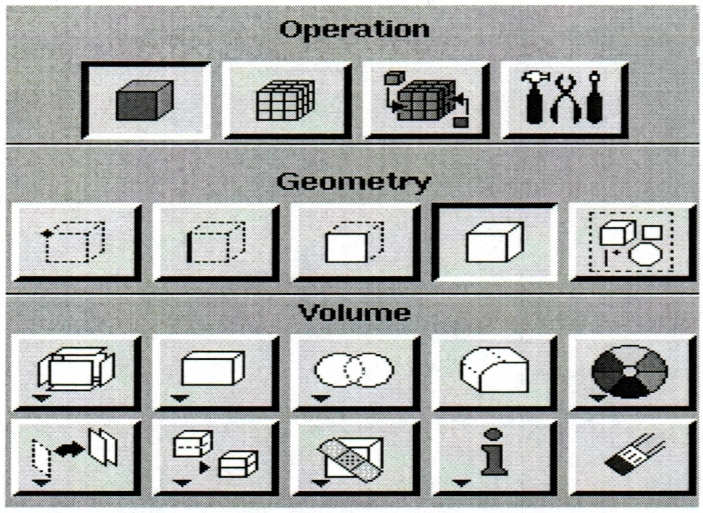

Figure 2. 1: The Operation tool pad in Gambit (Source: www.fluent.com)

The topmost on this group is the main pad has different tools that are for creation, meshing, boundary condition specification, *et cetera.* The next layer has subpads that are to be used in combination with the main pad. The selection of one main pad item leads to the opening of a particular subpad. For example, the selection of the Geometry main pad leads to the opening of subpads that create geometries like vertices, edges, faces, volumes and groups. Boolean operations between different geometric entities are allowed. For the cavity problem, adding different edges formed a group called the "lower wall". This will be explained in detail in chapter 4.

Since the meshing process has a great effect on the solution, careful reading and thought have to be applied to it. There are different meshing options available in Gambit once the basic geometry is drawn. The user can mesh edges, faces and volumes depending on the need. The following are the face meshes available in Gambit:

(1) Triangular

(2) Quadrilateral

(3) A combination of quadrilateral and triangular meshes.

(All versions of Fluent above v4 support unstructured meshes).

The above mentioned meshes can be mapped, submapped, or meshed with a combination of both as the need warrants. Gambit automatically determines the combination of the meshes and the meshing type according to the node distribution and the geometry. Gambit can be programmed to draft geometries and create meshes. The programming utility was not used in our present work.

(2.3.2) Boundary Condition and Continuum Element description in Gambit:

The user can set up the continuum and the boundary condition types in Gambit. The third button in the operation tool pad, when enabled, displays two options; one is for continuum element description and one for boundary condition description. Numerous boundary condition types are available with Gambit like wall, fan, velocity inlet, pressure inlet, to name a few. The user can have either a solid or a fluid continuum.

(2.3.3) Mesh Saving and Exporting:

Once the boundary and continuum types are set, the model can be saved. This saved model along with the grid is exported into Fluent through the **"File"** menu.

(2.4) Fluent:

Fluent is a general purpose 3-D CFD solver that is being used in all of our calculations. The following paragraphs are devoted to a brief description of the solution procedure using Fluent.

The problem domain was described in Gambit and meshing was done there. This physical domain along with the grid is imported into Fluent. This is done with the "File" menu in Fluent.

The **"File"** menu helps the user to read files, save them and export them to other platforms. There is an option under "**Save"** to save files automatically. This option was used to track velocities at frequent intervals of time for both the Stokes problem and the cavity problem.

(2.4.1) Grid:

A fairly detailed explanation is needed for grid recognition and usage in Fluent, since the grid is one of the most important elements in a CFD model.

(a) Grid terminology: This explains how Fluent reads a grid. The figure (self-explanatory) is from www.fluent.com.

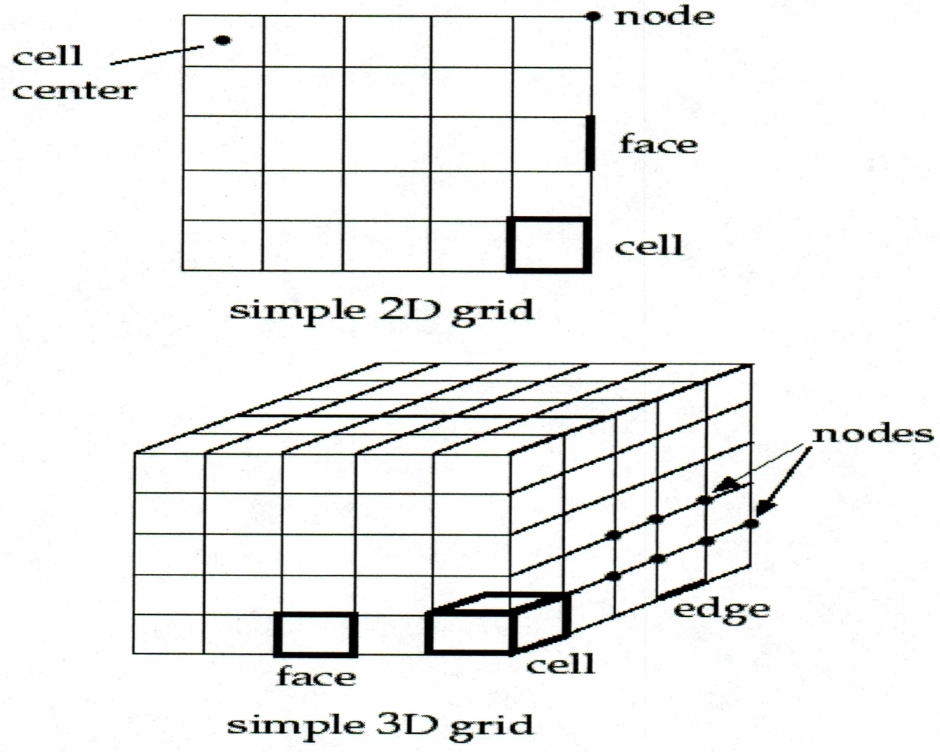

Figure 2. 2:Grid Terminology in Fluent

(b) Grid Check: This is an important step in Fluent and is recommended to be done immediately after the grid is read into Fluent. All versions of Fluent above Fluent 4 can handle unstructured meshes and this is why grid check is required in most of the cases before solving the problem. Grid check performs the following:

(1) Displays the maximum and minimum domain extents

(2) Displays the maximum and minimum *cell* volumes in m^3. If the minimum cell volume is negative, one or more cells have improper connectivity. Fluent warns the user about this.

(3) Displays the maximum and minimum face areas in m^2.

(4) Checks topological information about the grid; checks the number of faces and nodes per cell, face handedness for each zone is verified to be right-handed, checks element consistency, checks for boundaries *et cetera.*

(5) Simplex counters are verified and compared with corresponding entries in the grid header file.

(c) Acceptable grid topologies:

All versions of Fluent above version 4 have the ability to deal with unstructured meshes and odd-shaped elements. The grids acceptable to Fluent fall under two categories: 2-D cell types like triangular, quadrilateral and 3-D cell types like prism/wedge and pyramid. Examples of grids that are valid for Fluent are O-type grids, C-type grids, non-conformal grids etc.

(d) Scaling: The default units in Fluent are SI units. The user can change it to the unit system he/she wants.

Parallel: A grid can be spilt for parallel-processing to reduce computational time.

(2.4.2) Define-Menu:

This menu contains all the necessary options for specifying solver controls, material properties, operating conditions, boundary conditions, custom field functions, importing user-defined functions, *et cetera.*

(a) Model: Using this option, the type of solver, equations to be solved (options of viscous flow, inviscid flow, turbulent flow, energy, non-Newtonian flow, multi-phase flow to name a few, are available) can be selected.

(b) Solver: This allows the user to select the type of solver the user wants. A figure (from www.fluent.com) would serve the purpose of depicting these choices better. The **"Solver"** panel appears as shown below in Figure 2.3.

Mathematical details of the solver options are described well in textbooks (see for example [3]) documented well in Fluent's website. They are described in a later section (2.5) only briefly. However it must be mentioned that a lot of experimentation was done on these solver properties and significant effects were found with the use of various parameters. Some of these are results are described

in chapter 3 and chapter 4. For example, use of the first order implicit unsteady formulation resulted in asymmetry for Stokes second problem over a cycle. The use of the second order formulation, however, helped overcome this difficulty.

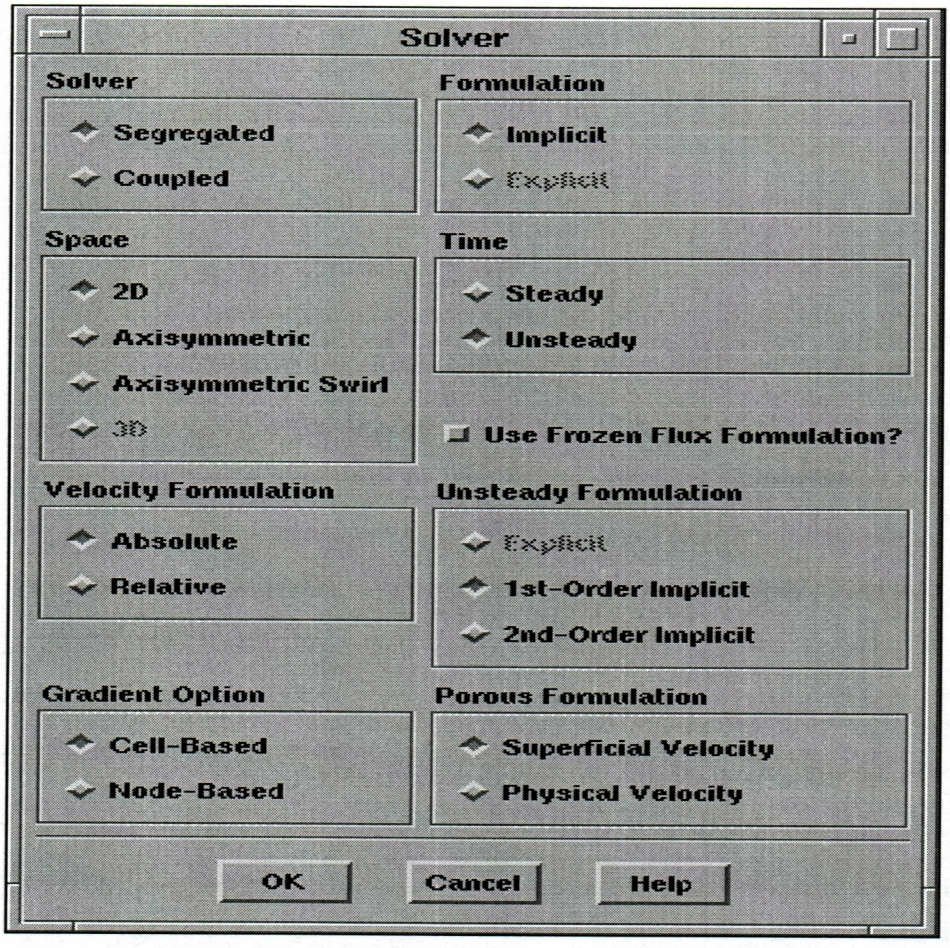

Figure 2. 3 : Solver Options in Fluent

(c) Material Properties: Fluent has a huge materials database to choose from and the user can assign physical properties to these materials.

(d) Operating conditions: Through this panel, the user can set parameters like operating pressure, gravity effects and density parameters for the model.

(e) Boundary Conditions: If the model is created in Gambit and exported into Fluent, zones and their boundary types appear in this panel. The user, however, can change these boundary conditions. The user can assign values

for these boundary types and they form the boundary conditions for the model to be solved. If a user-defined boundary condition macro is read into Fluent, this option also appears in the list of boundary conditions available. Altogether, Fluent offers a very comprehensive as well as a very flexible boundary condition panel. Use was made of the user-defined macro option in all our cases.

(f) Custom field functions: Apart from the usual variables available for graphics display, Fluent can also calculate and display user defined variables. Use was made of this also for viewing results in the Newtonian reference frame.

(g) User-Defined functions: This allows the user to make Fluent read user-written macros. UDFs are usually written in the C programming language.

(h) Solve-Menu:

The **"Solve"** menu is used for setting solution parameters, initializing a solution, iterating, *et cetera.*

(1) **Solution Controls Panel:** Through this panel, the user can make use of the options available for discretizing the convection terms in the equations selected for solving, set under-relaxation factors (for convergence. See for example [3]). In the cavity problem, initially use was made of the first order upwind scheme for the momentum equations and later the second order upwind scheme was used.

(2) The user can also set residual criteria for the solutions. Residuals in Fluent are "scaled residuals". Scaling is explained well in Fluent's website. These residuals can be plotted and printed on a Fluent graphics window as iterations proceed.

(3) **Initialize:** An iterative solver needs a starting point (normally an educated guess) and this is done through the "**Initialize"** menu.

(4) **Iterate:** This is the last step in the solution process. The solver iterates till it meets the convergence criteria set by the user.

(2.4.3) Display-Menu: This menu is used for visualization of the results obtained. Contours and vectors of variables like velocity, temperature, pressure, density, vorticity etc can be obtained through this menu. If custom field functions are defined, these can also be displayed. Fluent can also animate results so that a sequence of events is nicely visualized.

(2.4.4) Plot –Menu:

Plot menu helps in the plotting of various variables with respect to the physical dimensions of the domain. If custom field functions are defined by the user, these can also be displayed.

(2.5) Governing Equations and the solution process in Fluent:

The purpose of this section is to describe in general, the governing equations considered for the treatment of fluid flow and heat transfer problems in Fluent, the discretization process to convert a group of non-linear governing partial differential equations and associated boundary conditions into tractable algebraic equations that can be solved for dependent variables, and the linearization process to linearize the equations for solvability.

The four general steps that were described in the previous section are all applicable to the Fluent solution process also with certain modifications that are explained below.

Fluent is a finite-volume based solver; fluid properties are based on a *control volume*, i.e., conservation equations (mass, momentum and energy) are expressed for a control volume.

(2.5.1) Governing equations :

Fluent supports the following models and selects a set of governing equations based on the model the user selects. In general, Fluent considers the mass conservation equation (continuity equation) and the momentum equations (up to 3, one for each direction) as they are required for all problems involving fluid flow. In addition to these equations, the energy equation is considered for a heat transfer problem; temperatures in addition to velocities are solved for.

Apart from traditional fluid flow and heat transfer problems, Fluent is capable of solving many other problems of engineering interest, for instance, complex turbulent flows, swirling and rotating flows in turbomachinery, chemically reacting flows, multiphase flows, flows in porous media, combustion phenomena, to mention a few. All of the problems mentioned above involve additional scalar transport equations in addition to the continuity and the momentum equations. Since the work presented here requires solution of the continuity and momentum equations a brief discussion of the solution process involving the continuity and the momentum equations is presented here.

(2.5.1.1) Continuity equation (conservation of mass):

The continuity equation is a simple scalar expression involving mass conservation for a fixed volume. It can be written as:

$$\partial\rho/\partial t + \mathbf{div}\ (\rho \mathbf{v}) = S_m \qquad (2.1)$$

where ρ is the density (the first expression in the right hand side is the time rate of change of density and is zero in incompressible flows), v is the velocity vector and div is the divergence operator, S_m is the source term (may be the mass added by a dispersed secondary phase as an example).

(2.5.1.2) Momentum equation(s):

The momentum equations for fluid flow are applications of Newton's second law of motion (relating the forces on a body and the time rate of change of momentum) the difference being that they are written with respect to a Eulerian reference frame (the use of substantial derivatives in place of ordinary derivatives). Solution of the momentum equations gives the velocity field, provided, the continuity equation is satisfied.

The momentum equation(s) can be written as:

$$\rho Dv/Dt = \rho g + \nabla . \tau_{ij} - \nabla p \qquad (2.2)$$

where Dv/Dt is the substantial derivative of the velocity vector v given by

$Dv/Dt = \partial v/\partial t + (v.\ \nabla)v$

∇ is the "del" operator given by $\vartheta/\vartheta x + \vartheta/\vartheta y + \vartheta/\vartheta z$,

τ_{ij} is the stress tensor and p is the pressure.

In their full form , the momentum equations are highly non-linear because of the fact that the dependent variables (u,v and w) are expressed as a product of their own derivatives (there can be other non-linearities too, for example an oscillating boundary condition can give rise to strong non-linearities)

(2.6) Discretization and Linearization:

The highly non-linear partial differential equations (there are actually 3 momentum equations, one for each direction) are *discretized* over a control volume to produce a system of algebraic equations for the unknown variables in each computational cell. These are then linearized so that they can be solved by direct or iterative solvers. Discretization is done by integrating the governing equations about each control volume; this is called a control-volume method. A simple steady state scalar equation concerning the transport of a scalar Φ is considered here to explain the process of discretization.

$$\oint \rho \Phi \mathbf{V}.\, d\mathbf{A} = \oint \mathbf{D} \nabla \Phi.\, d\mathbf{A} + \int_V S_\Phi \, d\mathbf{V} \qquad (2.3)$$

where V and A are vectors (velocity and surface area vectors respectively), D is the diffusion co-efficient for the scalar variable Φ and S_Φ is the source term which is integrated over a volume. Values of Φ are to be calculated at the cell-centers in the finite control volume shown below.

A two-dimensional control volume is shown in figure (2.4)

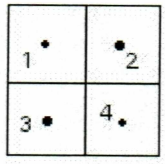

An example of a finite control volume. The dots represent cell-centers.

Figure 2. 4: An Example of a finite control volume

where 1, 2, 3 and 4 represent cell centers where finite values of the scalar Φ are to be stored. Vectors like velocity are calculated at face centers.

The equation for continuity, equation (2.1) when integrated, gives a set of algebraic equations that are to be solved for the dependent variable Φ.

$$\sum_f^N \rho_f v_f \Phi_f . A_f = \sum_f^N D (\nabla \Phi)_n . A_f + S_\Phi \qquad (2.4)$$

where N is the number of faces enclosing the cells, Φ_f is the value if Φ convected through the face f, the term $\rho_f v_f . A_f$ represents mass flux through the face f, $(\nabla \Phi)_n$ represents the magnitude of $\nabla \Phi$ normal to the face f. Equation (2.4) represents a system of algebraic equations that can be solved for the scalar variable Φ.

(2.7) Calculation of vectors and Upwind schemes:

Vectors, however, are not calculated at cell centers; rather they are calculated from values of Φ at the faces (interpolated from cell-center values of Φ). This interpolation is accomplished using a process called *upwinding*. Upwinding means that the face values of Φ are approximated from quantities in the cell upstream relative to the direction of the normal velocity.

There are different ways of interpolating (a scientific approximation process) and Fluent offers a variety of such upwinding procedures and they are:

(1) First order upwind scheme

(2) Second order upwind scheme

(3) Power-Law scheme

(4) QUICK scheme

(5) The central differencing scheme.

Only the first and the second order schemes are described here briefly; but the reader is referred to [2] or Fluent's website www.fluent.com for a more detailed explanation.

A first order scheme assumes that values at cell centers represent cell-average and hold throughout the entire cell; the face values are identical to the cell quantities. When a first order scheme is selected, the face value Φ_f is set equal to the cell center value *in the upstream cell.*

For better accuracy, a second order scheme is selected. A second order scheme interpolates cell values through a Taylor's series expansion about the cell centroid to evaluate face values of the quantities. This method takes into account the gradient of the values in the upstream cell unlike the first order upwind and is thus more accurate.

Fluent is an iterative solver; it starts with an initial guess for the dependent variables and keeps updating their values iteratively until a converged solution is obtained. The equations themselves have to be linearized in some way to render them viable for a numerical method. The process, as the name indicates, is called linearization and is a very critical step in a numerical method. Depending on the method used to linearize the system of governing equations, they are classified as implicit or explicit.

An *explicit method* is the easier of the two; the unknown variables are written in a form that involves only existing values from neighboring cells.

An *implicit method* is inherently more complex in its formulation; the unknown value of a variable is calculated using an equation that involves both known and unknown values from neighboring cells, so, such equations have to be solved simultaneously to give the values of the variables.

(2.8) Segregated and Coupled solvers:

Fluent offers two types of solvers; segregated and coupled. A segregated solver solves the continuity, x, y and z momentum and energy equations one by one whereas a coupled solver solves all of these equations simultaneously.

(2.9) Temporal (time) Discretization:

Unsteady flow problems have to be discretized in time as well as in space. This is done in Fluent in two different ways:

(1) Explicit method: This option is available only when the coupled solver is selected in Fluent. This method is based upon the evaluation of variable values at the current time level. This method, obviously is very easily formulated because of its "explicitness", and has faster convergence times, but is *only* conditionally stable (depending upon the time-step size, it cannot use large time step sizes).

(2) Implicit method: This option is available in both coupled and segregated solvers. An implicit discretization method makes use of past, current and future values of variables in time. This is a better approximation method, but yields a system of algebraic "implicit" solutions that have to be solved simultaneously to yield final values. No doubt, this method takes a longer time to converge, but is *unconditionally* stable. Fluent offers two levels of accuracy here; the first-order accurate and the second-order accurate temporal discretization methods. The first-order accurate formulation has variable values in time based upon the current time and the future time whereas the second-order accurate formulation includes all three values in time; the past time, the current time and the future time.

Chapter 3

A Bench-mark case: Stokes's second problem:

(3.1) Introduction:

To validate the use of Fluent for flow problems with wall oscillations, a benchmark case with known analytical results was tested. Stokes' second problem is essentially an unsteady, laminar fluid flow problem with oscillating boundaries. An oscillatory boundary condition on one of the walls was imposed by utilizing a user-defined macro in Fluent. The appropriate computational domain, grid resolution and time step size resolution for computational efficiency were experimented with and fixed. Plotting of fluid velocities was done and these were compared to analytical results. The results were in good agreement with the analytical results.

In order to avoid the use of moving grids and possibly a solution distortion in very complex oscillating flow problems, a much "cleaner" method was utilized. Newton's law for non-inertial frames of reference was used in calculating an oscillating source term to be added to the x-momentum equation in Fluent. A user-defined macro was used for this purpose and the problem was solved in a non-inertial reference frame with the walls remaining stationary and the fluid oscillating. This formulation took lesser number of iterations to converge as compared to the previous formulation in which the wall was oscillating. The results were viewed in the inertial reference frame and compared to the analytical case. The accuracy of these results motivated the use of this formulation for the cavity problem.

(3.2) Problem description:

An excellent treatment of Stokes' second problem and its analytical solutions is given in White [14]. Stokes's second problem is essentially a laminar flow problem above an infinitely long planar wall which is oscillating steadily (say with $\mathbf{U_0}$ **sin (ωt)**). A parallel flow assumption is made so that $u = u(y, z, t)$ and $v=w=0$. Also the no slip condition on

the wall requires $u(0,t)= U_0 \sin(\omega t)$, no initial motion of the fluid requires $u(y,0)=0$. The unsteady Navier-Stokes equations were solved with these boundary and initial conditions. The analytical solution was found to be

$$u = U_0 \exp(-\eta) \sin(\omega t-\eta) \qquad (3.1)$$

Where

$$\eta = y\,(\omega/2\nu)^{1/2} \qquad (3.2)$$

These results were plotted in a Microsoft Excel spreadsheet to be compared with Fluent results.

(3.3) Modeling the problem with Fluent:

The final model for Stokes' second problem *evolved* through a series of experiments on grids, solver options, boundary conditions, *et cetera.* Some of them were found to have a great effect on the solution obtained. These effects are described in detail in the following paragraphs. Experimentation was done on this simpler problem with known solutions to make a more complex oscillatory problem like the cavity problem easy.

(a) Model generation and grid resolution study

The above-described problem was modeled using Fluent (a CFD software which is described in detail in the previous chapter). White [14] discusses the characteristics of the Stokes layer, a fluid layer with finite thickness from the oscillating wall within which all velocity fluctuations are confined, in essence, the problem exhibits a boundary layer behavior within the Stokes layer.

The Stokes layer thickness (δ) was found to be a function of the angular velocity (ω) of the wall oscillation and the kinematic viscosity (ν) of the fluid and is expressed as:

$$\delta = 6.5*(\nu/\omega)^{1/2} \qquad (3.3)$$

Outside the Stokes layer, along the cross-streamwise direction (in this case, the y direction), velocity gradients are very negligible or zero. Also (3.1) shows that the

velocities are independent of the streamwise coordinate (in this case x), so not many grid points were needed in the streamwise direction. Approximately 10 grid points were used in the streamwise direction.

The expression for Stokes layer thickness and its physical meaning provided a basis for grid generation. Since almost all velocity fluctuations were confined within the Stokes layer, a computational domain of four Stokes layers was thought of as sufficient. Additionally, because of the above mentioned reasons, a very fine grid was needed in the vicinity of the wall (up to a cross streamwise distance equal to the Stokes layer thickness) to capture large velocity gradients, whereas a coarse grid far away from the Stokes layer would not affect the solution. An expanding grid from the lower wall was used for this purpose and approximately 40 grid points were used from y=0 to y=0.25cm, where 0.25cm signifies the Stokes layer thickness for our problem (with a kinematic viscosity of $0.0093cm^2/s$ and an angular velocity of 2π rad/s). A very fine grid approaches a continuum calculation but also increases the computation time. For computational efficiency, a trade-off was made between accuracy and computation time. The number of grid points was increased till any more additions ceased to give appreciably better accuracy.

For brevity, a rectangular computational domain (1 cm x 0.5 cm) was chosen. This domain was constructed from basic CAD elements in Gambit. Connected edges were drawn to form a rectangle and the region inside these four edges was defined as a face. A fluid continuum element was tagged to this face. To create expanding grids on the face efficiently, expanding nodes were created on these edges first (only in the y direction). A sub-mapping scheme was selected by Gambit automatically for face meshing. Since Gambit can also prescribe boundary condition types, on edges, boundary conditions that were set on the edges are shown in the next page (Figure: 3.1). The longitudinal edges were defined as walls and the other 2 edges were defined as pressure inlet and exit respectively. A fluid continuum element was defined also for the domain.

This model was exported into Fluent using the mesh export tool provided in Gambit.

A 10 x 100 grid (10 points in the x direction and 100 in the y direction), yielded an average error of 0.25 when the residuals were set to 1e-03 (this is a very high residual limit, used only for fixing the grid size). This took about 300 iterations per time step to converge. 100 points probably was the higher limit. A lower limit grid arrangement of 10x60 was then experimented with. This setup converged much faster per time step but the average error was high. Finally 10x80 grid was experimented with and gave reasonable accuracy (average error was 0.255, comparable to the higher limit grid set-up). This 10x80 grid was used in all calculations with regard to the Stokes problem.

(b) Fluent Solution process:

The model is read and standard procedures such as grid check and scaling were done. The CGS system of units (cm for distance units and cm/s for velocity units) were used for the model.

Water was chosen as the fluid with kinematic viscosity 0.0093cm^2/s and density 1000 kg/m^3. These small adjustments in the values of viscosity and density were needed to make the Stokes layer thickness 0.25 cm. Figure 3.1 shows the final grid for the Stokes problem.

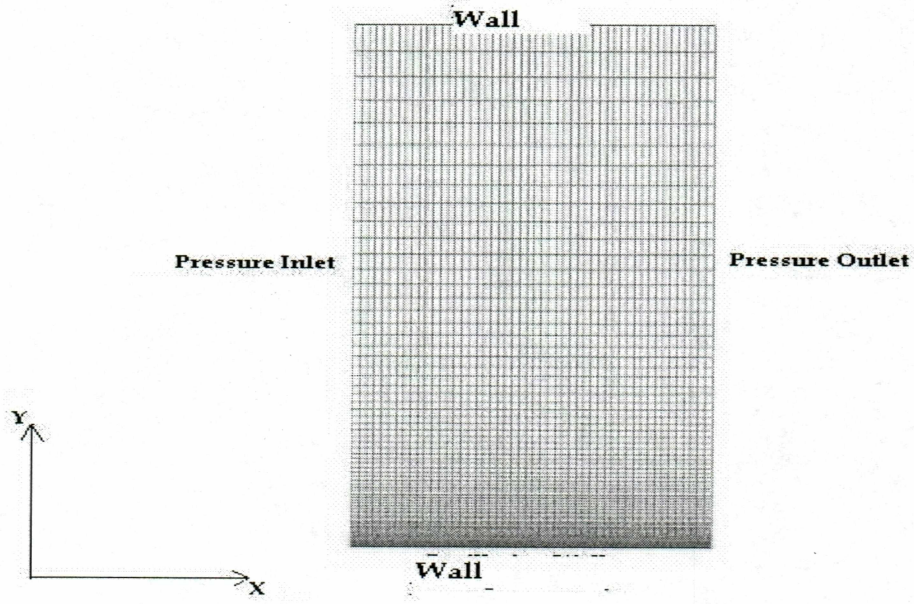

Figure 3. 1: Grid for the Stokes problem

The next step in the solution process was the assignment of values for the boundary conditions. The lower wall had to be prescribed an oscillating velocity which was not a boundary condition type in Fluent. A simple user-defined macro, written in the C programming language was used to define a sinusoidal oscillating velocity

$$\mathbf{V_w = V_a \sin(\omega t)} \qquad \mathbf{(3.4)}$$

where V_a is the velocity amplitude and t is the current flow time in seconds. The value of V_a was fixed as 1cm/s for simplicity in calculations and visualization. The program used is given in the appendix (A1). The upper wall was defined as a zero shear layer essentially resulting in a free surface at the upper end of the computational domain. The angular velocity was adjusted to be 2π rad/s so that the time period for the prescribed oscillation was 1s. However, there was a difficulty encountered when pressure inlet and pressure outlet boundary conditions were used at the left and right boundaries of the domain (see figure 3.1). The problem under consideration should display velocities exactly parallel to the wall; there should be no vertical velocities. When the above-mentioned boundary conditions were used, vertical velocities were displayed, even when there was no pressure gradient across the domain. A velocity contour plot illustrating this phenomenon is shown below. Only straight lines were expected, but the velocity contours showed elliptical lines indicative of appreciable y- velocities.

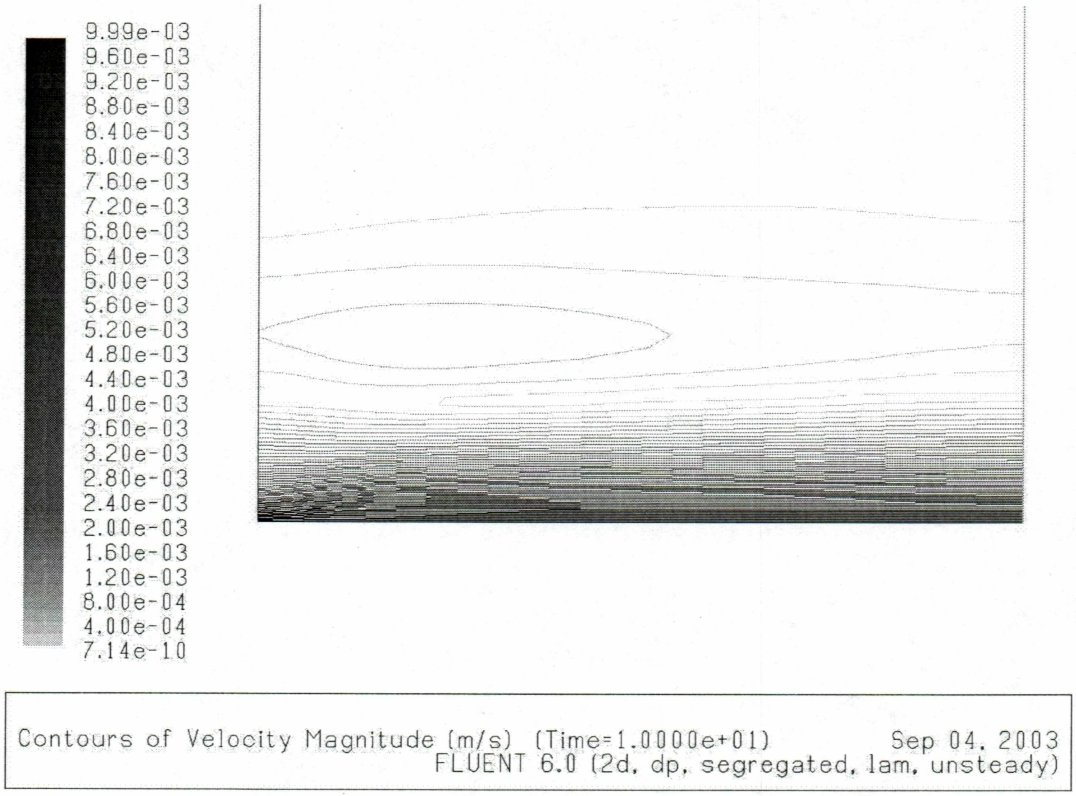

Figure 3. 2: Velocity contours with pressure inlet and outlet boundary conditions

It was inferred that pressure inlet and exit boundary conditions at the boundary nodes interfered with what was actually happening and this conflict gave rise to these erroneous vertical velocities. Since the cycle was time-periodic, it was thought that periodic boundary conditions at these boundary nodes would be a better representation of the reality. Thus, periodic boundary conditions were imposed on these edges and they gave better results. A contour plot of this is shown below:

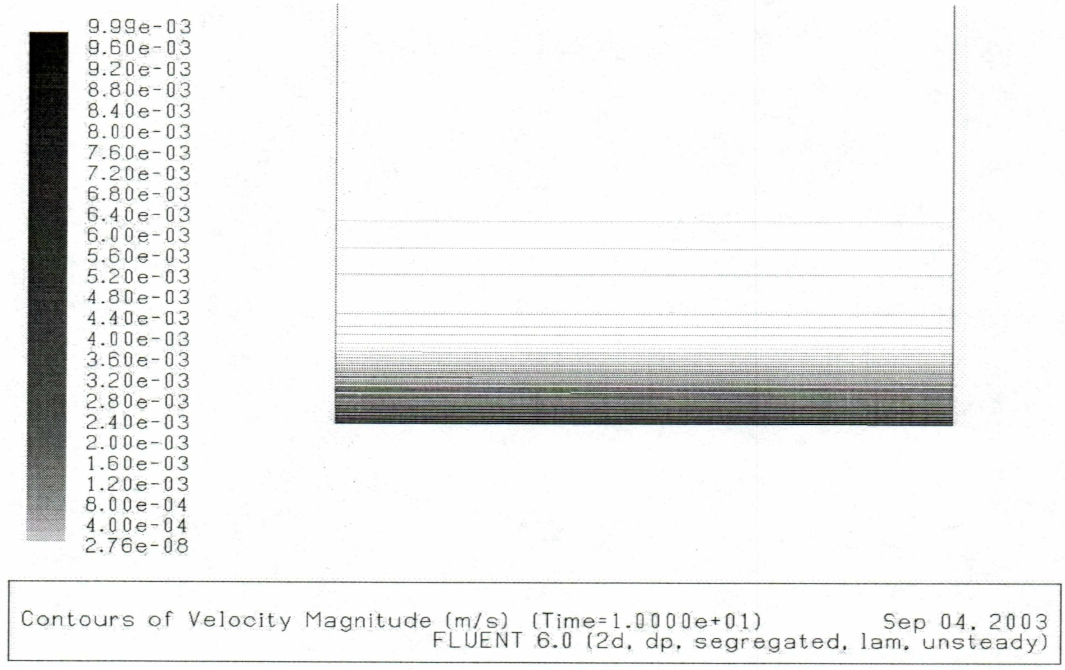

Figure 3. 3: Velocity contours with periodic boundary conditions

(c) Time step size resolution:

In a numerical method, time-step size has the same effect on the solution as grid spacing does. The final result at a particular time is achieved through a sequence of time steps, values at each time step having an influence on the next. Ideally, the time step size should be as small as possible for better accuracy, but this also increases the computation time.

To achieve a compromise between computational speed and accuracy, the time step size was experimented with. A lot of test cases were run with different time step sizes. Finally, a time-step size of 0.01s was fixed so that 100 increments completed one cycle. The problem was run through 10 cycles of oscillation to allow transients (due to the initial conditions) to die down gradually.

(d) Solver Controls:

Proper choice of solver properties may have a phenomenal influence on the solution process (accuracy, convergence etc). A segregated, unsteady solver was used for our problem. There was a problem however with the choice of the unsteady formulation to be used. There are 3 choices available to a user in Fluent for unsteady formulations: (1) the

explicit formulation (with an inherent disadvantage of a limited range of "grid Fourier numbers"), (2) the first order implicit formulation and (3) the second order implicit formulation. The first order formulation was used initially and it was found to give asymmetric results over a cycle in a symmetric problem. The second order formulation was used and this difficulty was overcome to an extent. It was inferred here that the problem lay with the discretization process in Fluent, the time values each of these formulations took into consideration. Since the user-defined macro uses the current time as one of its input, the Fluent solver has to pass the current time to macro every time, calculate the wall velocity at a particular instant and return it to the solver. It was found out that the second order implicit formulation returned a value of velocity that was very close to the correct velocity at that particular instant.

(e) Residual Criteria:

Fluent allows the user to set up accuracies based on decimal places in the residual criteria menu. Figure 3.4 is a comparison between error values obtained using different residual criteria.

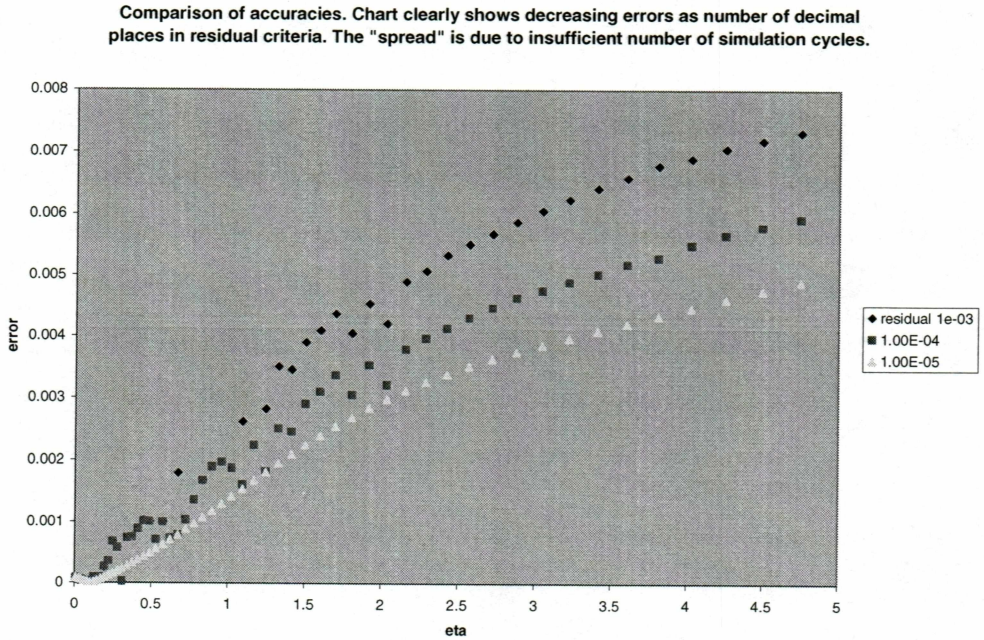

Figure 3. 4: Comparison of accuracies with different residual criteria

(f) Post Processing:

Velocities were plotted at regular intervals versus the vertical distance from the oscillating wall and these were compared to the analytical results from [1]. Only some of those plots are shown below, but accordance with analytical results was found in all of these plots. All the velocities were computed along a vertical line running through the center of the domain.

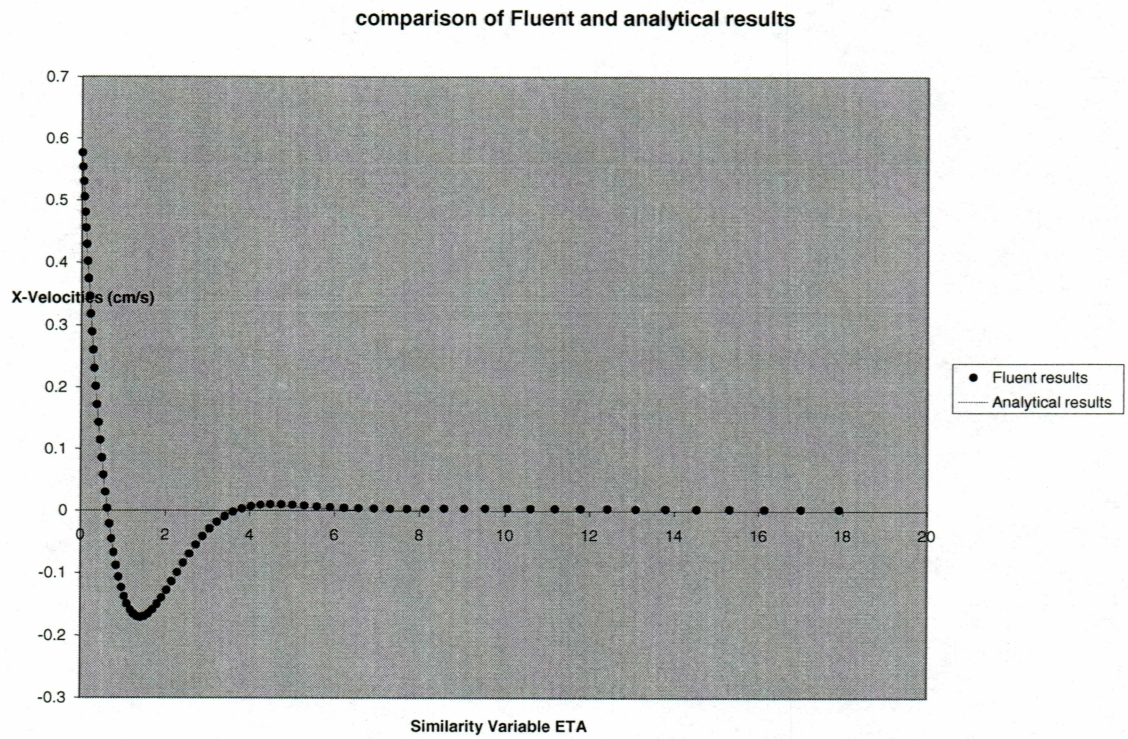

Figure 3. 5: Comparison between Fluent and analytical results for time = 10.1 s

Figure 3.5 shows a comparison of Fluent and analytical results for time equal to 10.1s. An average error of 0.001% (in terms of the wall velocity amplitude) was calculated between the values given by Fluent and the analytical results. The similarity variable eta used for this graph is just a dimensionless distance, so it can be seen that all velocity fluctuations are confined inside a distance of 0.25 cm(the value for the similarity variable being 4 for this value of y) which is the Stokes layer thickness for this problem.

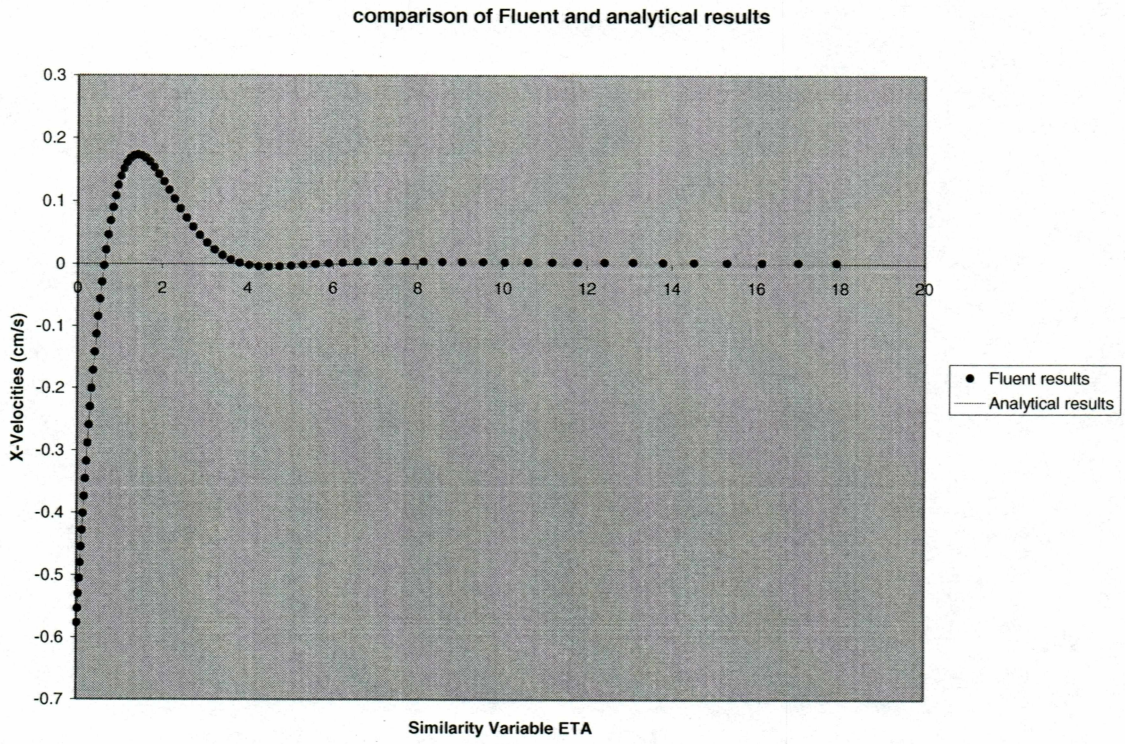

Figure 3. 6: Comparison between Fluent and analytical results for time = 10.6s

(3.4) Newton's second law of motion for non-inertial reference frames:

Reference frames that accelerate with respect to any other fixed reference frame are called non-inertial reference frames. Newton's second law of motion (in its simplest form, F=ma) must be modified for bodies when studied with respect to accelerating reference frames. The relative acceleration has to be accounted for in such cases. The following analysis is from [15].

Consider two frames of reference in which the acceleration of a particle (say A) of mass m is calculated, let one of these frames be stationary and the other reference frame accelerating. The diagram is identical to the one found in [15] except that this one is a two-dimensional simplification.

XOY denotes the fixed reference frame and xoy is the frame that is accelerating. If we observe the particle A of mass m from both of these reference frames, we can write an

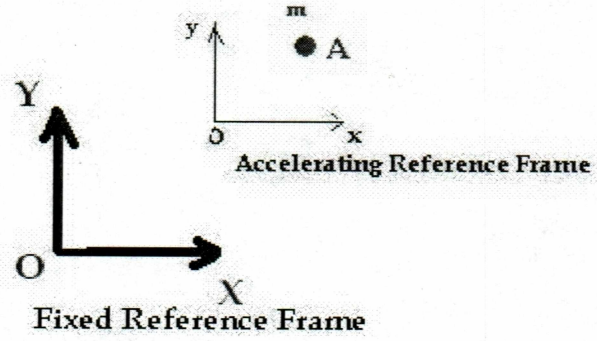

Figure 3. 7: Newton's second law for non-inertial frames of reference

expression for the absolute acceleration of the particle A (as seen from O) in terms of the relative acceleration (as seen from o).

$$\mathbf{a_A = a_{o/O} + a_{A/o}} \qquad \textbf{(3.5)}$$

where $\mathbf{a_A}$ is the absolute acceleration of the particle, $\mathbf{a_{o/O}}$ is the acceleration of the moving reference frame with respect to the fixed reference frame and $\mathbf{a_{A/o}}$ is the acceleration of the particle with respect to the moving reference frame. Thus Newton's second law of motion for this accelerating reference frame can be written as

$$\mathbf{\Sigma F = m_A a_A = m_A\,(a_{o/O} + a_{A/o})} \qquad \textbf{(3.6)}$$

Where ΣF is the total force acting on the particle. Equation (3.6) is Newton's second law of motion for accelerating reference frames (and such reference frames will be called non-inertial reference frames henceforth).

The Navier-Stokes equation describing fluid flow has a form similar to Newton's second law of motion and, fortunately, this fact can be exploited in writing equations for a non-inertial reference frame concerning fluid flow. Such a formulation was found to increase the speed of the solver, possibly because there are no moving grids involved. To explain

how Equations (3.5) and (3.6) could be applied to our problem, the following analysis is to be considered. Please refer to Figure 3.8 and let XOY be the stationary (absolute) reference frame and xoy be the accelerating reference frame as shown in the figure above. In the first formulation, fluid velocities were observed from the absolute reference frame with the wall actually oscillating. This might prove to be a difficult exercise when vertical walls like those in a square cavity, are encountered. Newton's law for non-inertial reference frames can be used to circumvent this problem.

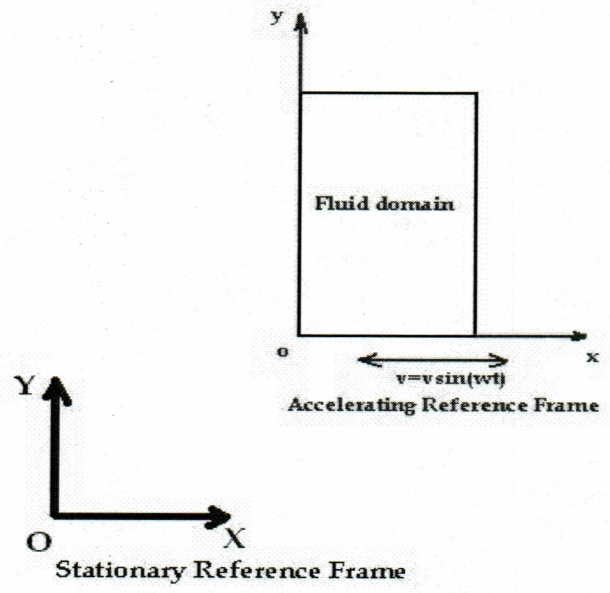

Figure 3. 8: Application of Newton's second law for non-inertial frames

Let the wall itself become the frame of reference from which the velocities and accelerations are observed (the wall velocity would become zero to the observer sitting on the wall). Let $\mathbf{a}_{f/o}$ be the acceleration of the fluid with respect to the accelerating reference frame xoy and $\mathbf{a}_{f/O}$ be the acceleration of the fluid with respect to the absolute reference frame XOY. Let $\mathbf{a}_{o/O}$ be the acceleration of the wall with respect to the absolute reference frame. Then by Equation (3.6), we get

$$\mathbf{a}_{f/O} = \mathbf{a}_{o/O} + \mathbf{a}_{f/o} \qquad (3.7)$$

The acceleration terms in Equation (3.7) are vectors and they are to be applied with a sense of direction to them.

For a person sitting on the wall, the top-most fluid layer which is actually at rest appears to have a negative acceleration (as described by equation (3.6)). The fluid layers near the wall have some motion because of the momentum transport from the moving wall. If the acceleration described by Equation(3.8) is input as a source term to the momentum equations, one only needs Equation(3.5) to calculate the velocity field in the Newtonian reference frame (absolute reference frame).

$$\mathbf{a}_{f/o} = - \mathbf{a}_{o/O} \qquad \textbf{(3.8)}$$

(3.8) allows us to calculate a "force" term.

$$\Sigma \mathbf{F} = \mathbf{m}_f \mathbf{a}_f = \mathbf{m}_f \, (\mathbf{a}_{f/o}) \qquad \textbf{(3.9)}$$

where m_f represents the mass of the fluid and a_f is the absolute acceleration of the fluid. A source term having the acceleration term equal to the wall acceleration was added to the momentum equations and the wall held fixed. A user-defined macro was written in the C language for this purpose and this was added to the x-momentum equation in Fluent. This program is listed in appendix A2.

(3.4.1) Source Term addition to Fluent solver:

Fluent allows addition of source terms to its solver, through user-defined macros written in the C programming language. Such source terms have to be balanced for units in the equations they are added to, for example if a source term is added to one of the

momentum equations, it should have a force unit per volume (i.e, mass*acceleration/volume).

In the present problem, the lower wall oscillation is driving the otherwise stationary flow, and it is imparting acceleration to the fluid layers above it. Since the wall velocity is defined, fluid acceleration with respect to the wall and the force term that produces this apparent acceleration can be calculated.

$$V_{o/O} = -V_w \sin(\omega t)$$

$$a_{o/O} = -V_w \omega \cos(\omega t)$$

$$a_{f/o} = -a_{o/O} = V_w \omega \cos(\omega t)$$

$$F = m V_w \omega \cos(\omega t)$$

$$F/v = (m/v)\, V_w \omega \cos(\omega t)$$

$$\mathbf{F^* = \rho V_w \omega \cos(\omega t)} \qquad \mathbf{(3.10)}$$

where $\mathbf{F^*}$ is the force per unit volume is the volume, V_w is the wall velocity, ω is the angular velocity of the oscillation t is the instantaneous time, and ρ is the density of the fluid. Equation (3.10) is the source term to be input into Fluent. The program is included in the appendix.

Velocity plots from Fluent utilizing the source term technique, were compared to the analytical solutions obtained from [1] and they were in good agreement with each other. Some velocity plots are shown here. The results shown here are in the absolute reference frame (using equation (3.5)).

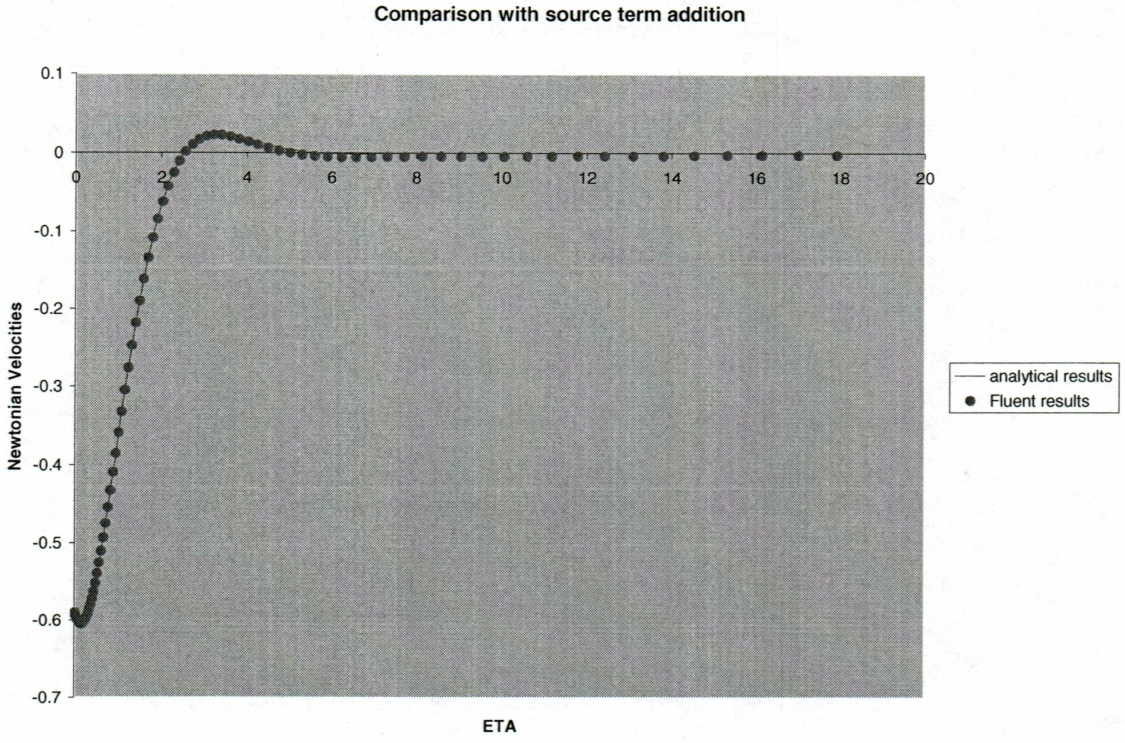

Figure 3. 9: Comparison of Fluent and Analytical results with a source term addition for time t=10.4 s,

Figures 3.8 and 3.9 are comparisons between Fluent and analytical solutions for time t = 10.4 s and t =10.9 s respectively. An average error of 0.002cm/s was observed. Considering the reduction in the number of iterations (120 as compared to 230 in the Newtonian formulation), this error was considered reasonable.

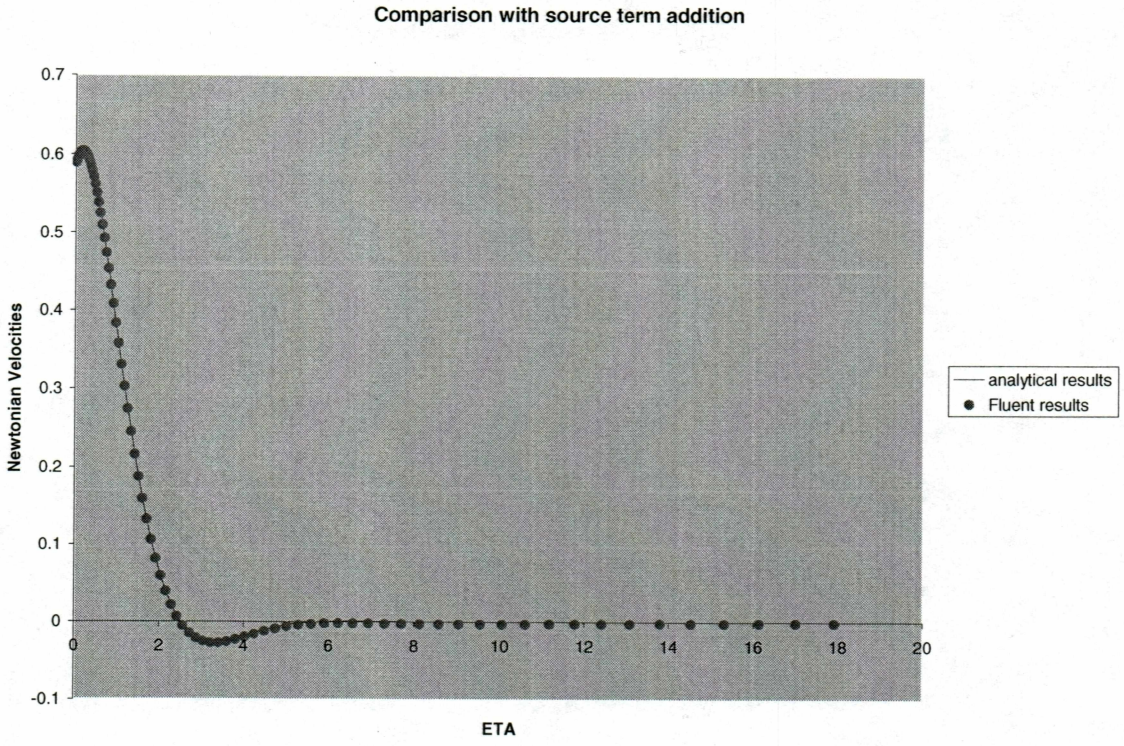

Figure 3. 10: Comparison of Fluent and Analytical results with a source term addition for time t = 10.9s

(3.5) Conclusion:

The main aim of this chapter was to use Fluent to benchmark a simple case with known analytical solutions so that it could be used for more complex problems. Fluent responded well to the challenge and this motivated us to use the same user-defined macros for the cavity problem. This problem also gave us an idea about the grid spacing that is needed or more correctly, the concentration of these grid points at the correct places, the correct time step size resolution, the number of cycles the problem needed to be run for transients to vanish, *et cetera.* The source term addition to the solver made the problem set-up simpler; the problem modeled using the non-Newtonian frame of reference required fewer iterations to converge (120 iterations per time step as compared to 230 for a

Newtonian model, for a residual size of 1e-06). It also avoided the use of moving grids and possibly solution distortion.

Chapter 4

Fluid Flow in Oscillating Cavities:

(4.1) Introduction:

Two dimensional channel flows with rectangular cavities have been a subject of several previous studies, some of which were discussed in the literature review part of this work. The most interesting work pertinent to our present problem considerations is being discussed here. Ian Sobey [4] dealt with sinusoidally furrowed channels and predicts separation at extremely high Reynolds numbers, vortex generation in pulzatile flow and transport enhancement due to the movement of these vortices. N.K.Ghaddar et al, References [7], [8] worked extensively on incompressible flow through periodically grooved channels and they describe transport enhancement due to resonance. Work on 3-D oscillatory cavity flows by M.J.Vogel *et al,* Reference[13] is yet to be published. The common feature of all work discussed so far is a "channel flow" with rigid top walls. Almost all of the work mentioned so far depended on mean flow. References [7] and [8], for example, discuss a flow rate that is oscillating sinusoidally in resonance with the frequency of the self-sustained fluid oscillations inside the cavity. In comparison, to our knowledge, little work has been done on flow effects due to oscillations of a wall with cavities. The essential difference in the flow pattern between Stokes' second problem and the cavity problem is the presence of vertical velocities (because of the presence of the cavity itself) in the form of vortices.

Flow is investigated in a two-dimensional cavity oscillating back and forth sinusoidally, with the commercial CFD software Fluent. Two dimensionless parameters affecting flow were identified and these were varied to understand their effects on the flow field. As with Stokes' second problem, the use of moving grids was done away with to make the problem set-up simpler. Newton's second law of motion for non-inertial reference frames was used and the problem was solved with respect to a non-inertial reference frame. A user-defined macro written in the C programming language was added to the X-

momentum equation for this purpose. A detailed explanation of this was given in Chapter 3.

The cavity problem may not have practical import in the near future but presents a very interesting general study. Such a study was initially directed at transport enhancement, especially heat transfer enhancement. Heat Transfer depends on the flow field; therefore the problem has to be solved for flow before any heat transfer analysis can be attempted. Work with the flow field showed a lot of interesting results which may have a great impact on heat transfer. As mentioned in Chapter1, this problem may have unforeseen applications in other fields too.

(4.2) Problem Description:

As mentioned before, the only variation in this problem is the presence of a cavity in an infinitely long plane wall. The wall is made to oscillate sinusoidally with a velocity V defined by

$$V_w = V_a \sin(\omega t) \qquad (4.1)$$

Where V_w is the velocity at any instant of time t, V_a is the velocity amplitude of the oscillation, ω is the angular velocity. The continuity equation and the x and y momentum equations are to be solved with the above mentioned boundary condition and the initial condition that the velocity is zero at time t=0. The problem can be easily understood by examining Figure 4.1.

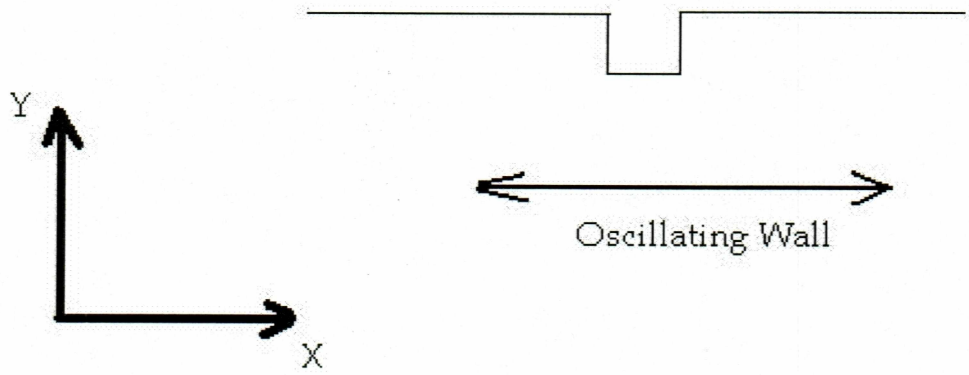

Figure 4. 1: The cavity problem

The presence of the convective acceleration terms in the momentum equations makes this problem highly non-linear and the task of attempting an analytical solution (for instance by using a similarity variable) is a very challenging one. Instead it was decided to make use of numerical methods to solve the problem. Also, only a square cavity was considered because of its simplicity. The above-mentioned problem was modeled and solved using Fluent.

Any numerical procedure starts with a good "scientific" intuition of the physical occurrences in the problem. Since it was envisioned that the presence of a cavity would influence the flow field, our interest in this problem primarily lay in the vicinity of the cavity.

(4.3) Dimensionless Parameters for Flow:

In general, fluid flow depends on many parameters like velocity, length, viscosity, *et cetera,* it is very inconvenient to examine the effect of each of these parameters individually on flow. For this reason, dimensionless numbers (all of these parameters combined in some way) are used in Fluid Mechanics to characterize fluid flow. The most prominent among these numbers is the Reynolds number, a ratio of the inertial and viscous effects in a flow field. In its simplest form, Reynolds number can be defined as:

Re = (a reference velocity) * (a reference length)/ (kinematic viscosity of the fluid)

Normally the length term would signify the size influence on the flow, for instance, in tube flows, the length term would be the diameter of the tube. The cavity problem has a free surface and there is no formal "entry" length scale like the tube flow problem. However, three different length scales were identified with the oscillating cavity and they were:

(1) The cavity dimensions (since a square cavity was considered, its length was considered)
(2) The displacement amplitude of the oscillation.
(3) The Stokes layer thickness, given by Equation (3. 3)

As mentioned in Chapter 1, all of these length scales were not independent of each other since the displacement amplitude and the Stokes length could not be independently controlled.

To resolve this problem, we resorted to the use of Buckingham's Pi theorem. This theorem was formulated to identify sets of dimensionless numbers from fundamental parameters affecting physical processes.

(4.3.1) Buckingham's Pi theorem:

Physical parameters are made up of fundamental dimensions: mass designated as M, length designated as L and time by T. Buckingham's Pi theorem states that in a physical situation controlled by 'n' physical quantities made up of 'm' basic dimensions, the quantities can be arranged to form 'n-m' independent dimensionless parameters [4].

(4.3.2) Dimensionless parameters for the cavity problem:

The physical quantities that affected the cavity problem were identified to be (1) the cavity size (say d), (2) the velocity amplitude V_a, (3) the kinematic viscosity of the fluid ν and (4) the angular velocity of oscillation ω. Following (4.3.1), n=4. The fundamental

dimensions for all these quantities are either L or T or both L and T. so m=2. The number of independent dimensionless parameters that could be formulated for this problem is n-m=4-2=2.

Based on a thorough search of literature available for oscillatory problems, two dimensionless parameters were arrived at:

(1) Reynolds number based on the cavity size and velocity amplitude.

$$\mathbf{Re_d = (V_a * d)/\nu} \qquad \mathbf{(4.2)}$$

(2) The ratio of the Stokes layer thickness and the amplitude of oscillation (incidentally, a ratio of the Reynolds numbers based on the stokes layer thickness and the displacement amplitude would yield the same result since the velocity term and the viscosity term are the same), or the Ratio of the Stokes layer thickness and the cavity size d. Only one of these terms could be the second dimensionless parameter; assigning a value to one of these numbers fixes the other one.

Armed with this knowledge of dimensionless numbers, we set out to explore the cavity problem.

Fluid flow patterns were studied by varying the Reynolds number based on the cavity size and the ratio of the Stokes layer thickness and the cavity size (automatically fixing the ratio of the Stokes layer thickness and the displacement amplitude). This process is described in detail in Section 4.5.

(4.3.2.1) A relation between cavity-size-based Re and displacement-amplitude-based Re:

White [14] and other authors cited in Chapter 1 of this work discuss a conventional dimensionless frequency (called the Strouhal number) and its importance in oscillatory flow phenomena. The present work on oscillatory flow does not discuss the effect of Strouhal number on flow separately; but it can be shown that the conventional Strouhal number is hidden in our description of the cavity-size-based Reynolds number. In fact, it

reduces to a product of the Strouhal number and the displacement amplitude-based Reynolds number. The derivation is as follows:

$$\mathbf{Re_d = V_a * d/\nu}$$

Where d is the cavity size, V_a is the velocity amplitude of oscillation and ν is the kinematic viscosity of the fluid. $V_a = (\omega * a)$ where 'ω' is the angular velocity and 'a' is the displacement amplitude of the oscillation. Also the frequency of oscillation f is $(\omega/2\pi)$.

The above expression after some modifications will look like

$$\mathbf{Re_d = (2\pi)\ (f*d/v_a)\ (v_a*a/\nu)}$$

$$\mathbf{Re_d = 2\pi*St*Re_a} \qquad \mathbf{(4.2.1)}$$

Where St is the conventional Strouhal number defined by $\mathbf{St = f*d/v_a}$

(4.4) Modeling the oscillating cavity problem with Fluent:

Gambit was used for initially drafting the computational domain. A good initial intuition was required even in the drafting stage because of the complexity of the problem. References [5], [6], [7], and [8] describe flow separation and vortex generation in flow through furrowed sections. All these papers discuss marked changes near the "lip" of the furrow which necessitates proper mesh arrangement and distribution in this zone. The other zone of importance, of course, was the cavity proper (see for example references [7] and [8]). In addition, results from the benchmark case (Stokes' second problem) helped in the general understanding of the mesh spacing and distribution near oscillating solid boundaries (A reference frame fixed to the moving wall was used; the fluid appears oscillating and the wall appears stationary).

Initially, a cavity size equal to the Stokes layer thickness (0.25 cm for a kinematic viscosity of 0.0093 cm^2/s and an angular velocity of 2π rad/s) was considered (a square cavity with dimensions 0.25 cm). Figure 4.2 shows the general arrangement of the computational domain.

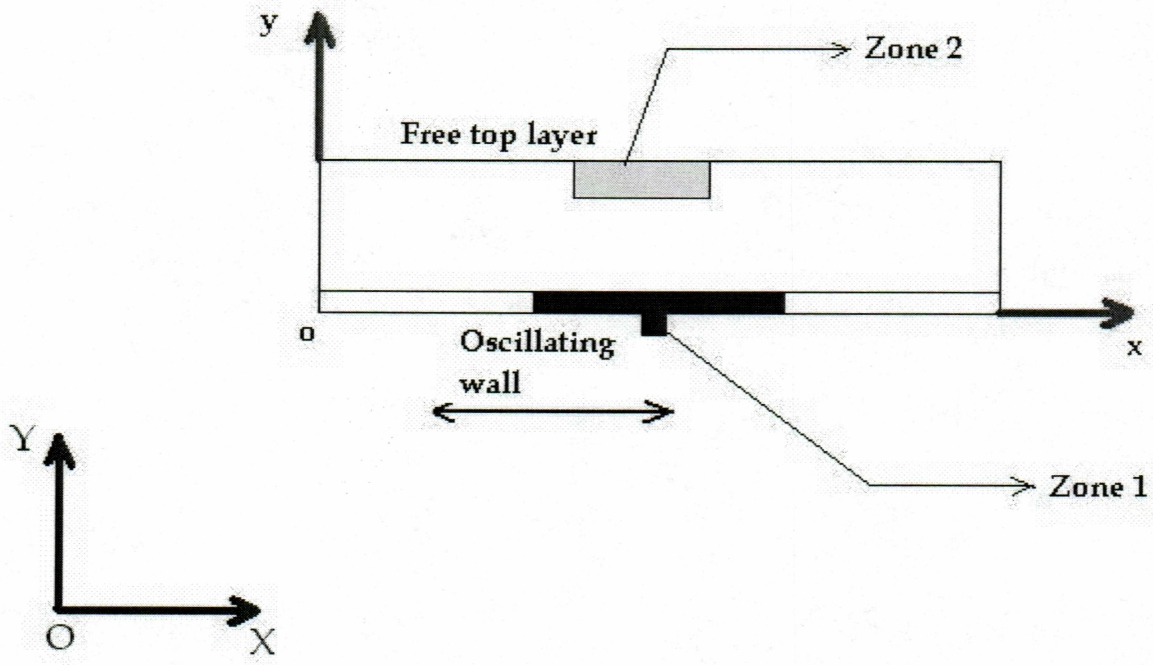

Figure 4. 2: Preliminary modeling considerations

In Figure 4.2, XOY and xoy are the fixed (non-accelerating) and accelerating reference frames, respectively. The lower wall with the cavity is oscillating sinusoidally, zone 1 is identified easily with the discussion in the previous paragraph; it represents the cavity and its immediate vicinity. Zone 2 has an interesting significance that is explained in the later part of this chapter. The top wall is a zero shear layer indicating the upper end of the computational domain. It had to be placed far away from the lower wall to have no effect on the solution. A height of 3 cm from the lower wall (about 12 times the Stokes layer thickness) was considered to be sufficient because of experimentations with the computation domain size. The Stokes layer thickness was the most critical factor in

finalizing the size. It was seen that velocity fluctuations occurred up to a distance that was only a little larger than the Stokes layer thickness.

(4.4.1) Meshing considerations:

As in the Stokes problem, meshing proved to be a very critical factor in determining the solution. Also, the final grid for the cavity problem evolved through a series of experiments for well-converged solutions. From the initial considerations explained in the previous section, the cavity was very closely meshed using Gambit. Uniformly spaced quadrilateral elements were used to mesh the cavity section and it contained 2500 node points.

Outside the cavity though, a little more consideration was needed. Only zone 1 in Figure 4.2 needed very fine meshing, a coarser mesh sufficed for places away from this zone. An expanding grid was used in Gambit for the above-mentioned purpose. The same applied for meshing along the cross-streamwise direction too, so that only zone 1 remained finely meshed. The entire domain contained roughly 26,000 grid points

(4.4.1.1) Effect of mesh density:

To test the effect of a very fine mesh on the solution a lower limit of fineness had to be reached. As mentioned before, a finer grid has a lot more grid points and tends to the continuum calculation but also increases the computation time as variables have to be determined for so many grid points. For example, the finest grid with 2500 grid points inside the cavity and roughly 62,000 grid points outside it, took 10 hours to run through a complete cycle.

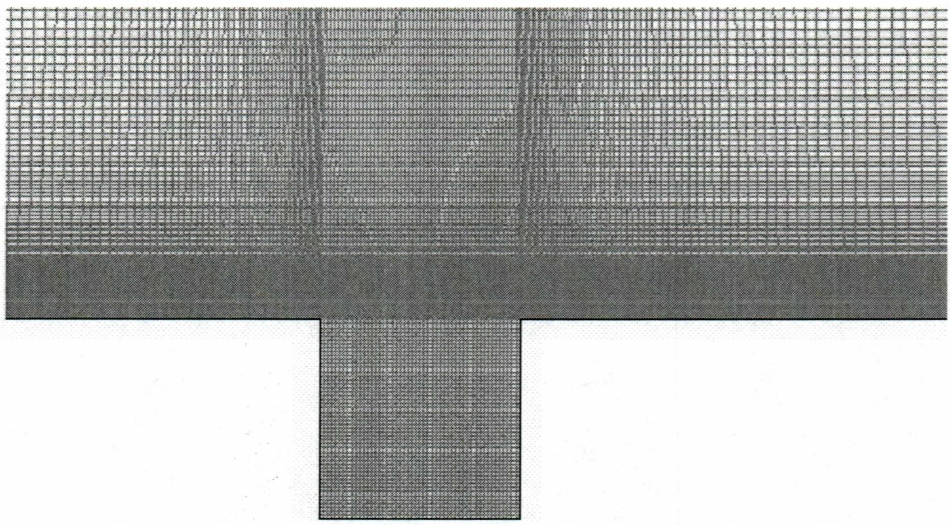

Figure 4. 3: A Very Fine Grid

Figure 4.3 depicts the finest mesh that was used. As for the Stokes problem, the problem required at least 10 complete oscillation cycles for minimization of transients and generation of stable results. The time taken for computation for this fine mesh though, was thought of as unacceptable. The necessity for computational efficiency also forced us to look for a coarser mesh that was still able to capture many of the important details without utilizing a lot of computation time.

Many such grids were treated with the basic mesh considerations (described earlier in sections 4.4 and 4.4.1) in mind. Finally, a mesh design having roughly 2500 grid points inside the cavity and 22,000 points outside it was decided as a good tradeoff between computation time and accuracy and the results with these meshes showed no major difference with respect to the finer mesh results. Figure 4.4 shows the final mesh in the vicinity of the cavity. All cases were treated with this mesh. One interesting point with regard to the meshing arrangement worth adding at this stage is the way the mesh arrangement was made just outside the cavity. The distance between the nodes just outside the cavity was adjusted to be a third of the distance between nodes inside the cavity. This arrangement was supposed to capture all the subtle occurrences (see references [5], [6], [7], [8]), if any, just outside the cavity. It was found later that this

arrangement was indeed efficient in capturing subtle effects. Figure 4.5 shows this arrangement.

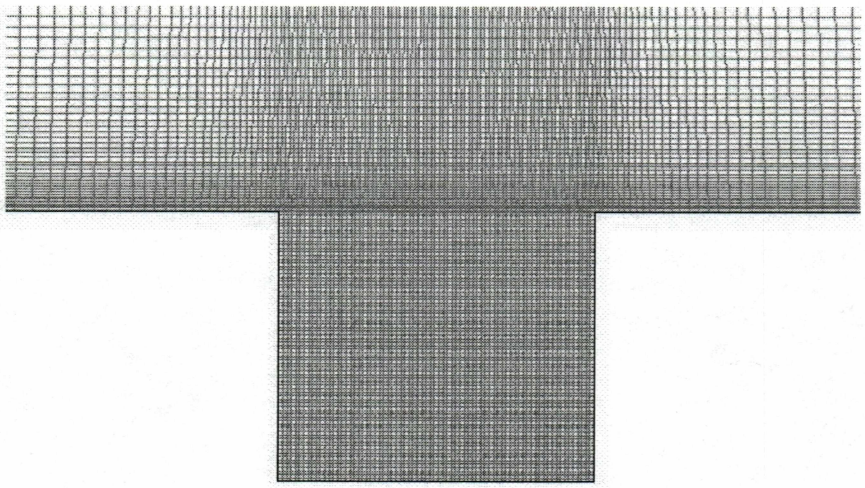

Figure 4. 4: Final Grid

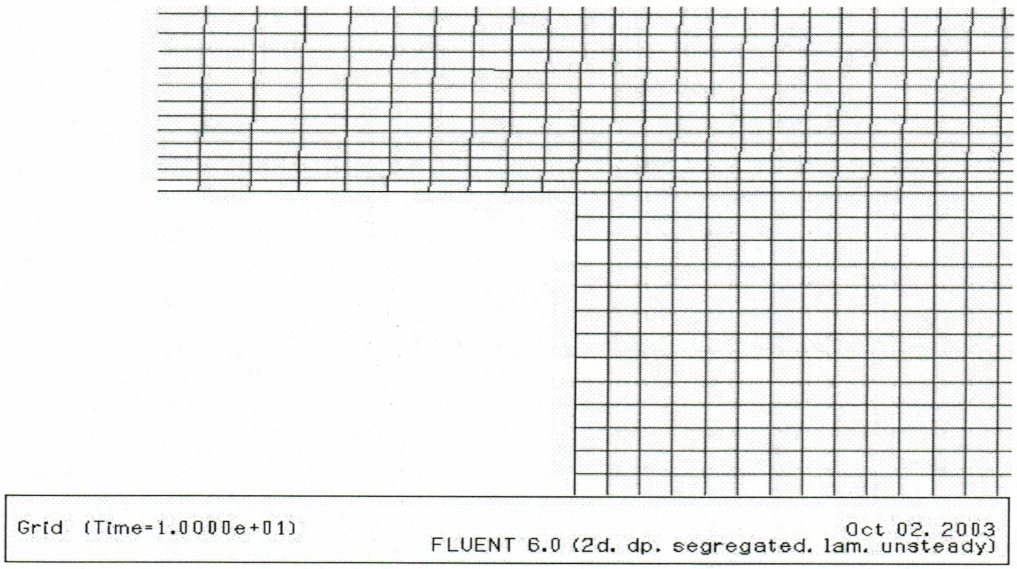

Figure 4. 5: Meshing in the vicinity of the lip of the cavity

(4.4.2) Boundary condition types:

The boundary condition types were set for different edges in Gambit. The lower wall, as mentioned before, was made by logically adding different edges, so that these edges constituted one single geometrical element as shown in Figure 4.1. Apart from this logical manipulation of the lower wall, the boundary conditions types were identical to those for the Stokes problem. Edges 3 and 4 in Figure 4.2 were assigned pressure inlet and outlet boundary condition types in Gambit. , Edges 1 and 2 were defined as solid walls and fluid continuum elements were defined for the computational domain.

(4.4.3) Fluent Solution Process:

The mesh thus defined in Gambit was imported into Fluent using the mesh import/export capability provided in Fluent. Standard procedures such as grid check and scaling were done in Fluent. Units of cm for length scales, cm/s for velocities and cm^2/s for acceleration were used.

As mentioned before, the actual numerical values for boundary conditions have to be specified in Fluent. The lower wall was defined as a "no-slip" solid surface (it must be remembered here that the problem is being solved in the accelerating reference frame which makes the lower wall stationary and it is actually oscillating in the Newtonian reference frame) and the upper wall was assigned a "zero shear" solid surface (meaning a free surface). It was decided to follow the Stokes problem for boundary condition definitions for edges 3 and 4 (spanwise edges), so periodic boundary conditions were imposed on these edges.

Water with kinematic viscosity $0.0093cm^2/s$ and density $1000\ kg/m^3$ was used as the fluid for all computational purposes. As described in the previous chapter, a momentum source term macro written in the C programming language was added to the X-momentum equation in Fluent. This program is included in the appendix. With our experience in symmetry issues, we used a second order unsteady formulation for numerical solutions.

The above-described model was initialized and run for 10 cycles of complete oscillations. Apart from the decisions on the grid, there were other parameters that needed to be

refined based on the solutions for this particular model. They are described briefly, one by one.

(4.4.3.1) Solver Controls:

As mentioned in Chapter 2, solver controls can have a very significant effect on the solutions obtained. Sobey *et al* [4] mentions the use of second order upwind differencing for accurate solutions in oscillatory flows. Use was made of both the first order and the second order formulations and it was found that second order upwind differencing captured more effects than first order upwind differencing. Thus it was decided to use second order upwind differencing in all future calculations. The above mentioned fact also helped in reducing the grid size as much better accuracy was acquired with fewer number of grid points and the overall computation time was reduced.

(4.4.3.2) Residual Criteria:

As mentioned before, an iterative process is said to have attained a *converged* solution if it meets the residual criteria set by the user. Fluent provides the user with an editable menu of residual criteria for continuity, each of the momentum equations (x, y, and z) and energy (if enabled). The residuals in Fluent are calculated based on a reference value, in other words, they are *scaled residuals.* The user has to set values for these residuals; lesser the values, more is the convergence time and vice versa. More stringent (lesser) values of these residuals were found to have a profound effect on the solutions obtained.
Zone 2 (Figure 4.2) was defined as a zero shear layer; with a residual criteria of 1e-03 for continuity, and the x and y momentum equations, appreciable (non-zero) perpendicular velocities were found in zone 2 which was out of place for the present problem considerations which should result in only horizontal velocity vectors in this zone. This contradiction is shown in figure 4.6

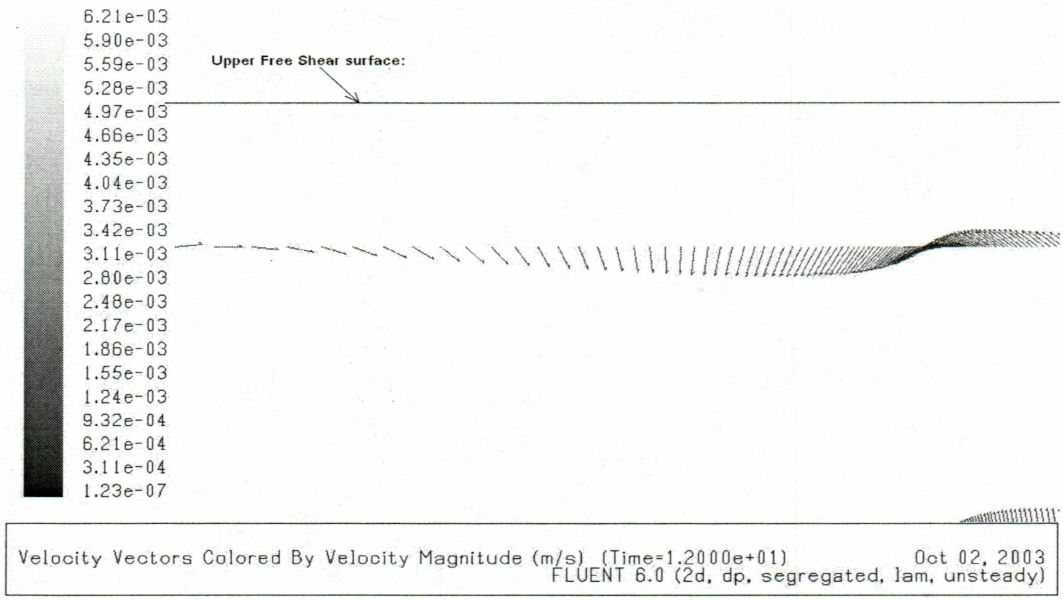

Figure 4. 6: Perpendicular velocities due to insufficient residuals.

Reducing the residual criteria though showed excellent improvement in that these perpendicular velocities gradually disappeared and became exactly parallel to the upper wall. These residual criteria were decreased until there were no appreciable perpendicular velocities near the upper wall, and in the end, were fixed at 1e-06. Thus the initial model was refined continuously by adjusting various parameters and solution controls until it yielded a stable, accurate solution. With this final refined model in hand, a parametric study was undertaken. Fluid flow patterns were studied by varying the cavity size-based Reynolds number and the length ratio of the cavity and the Stokes layer thickness. These variations are explained in Section 4.5.

(4.5) Parametric Study of Fluid Flow in an oscillating cavity:

Section 4.3 of this work described in brief, the dimensionless parameters affecting flow. An effort was made to study the effects of these parameters on flow in an oscillating cavity. Three different cases were identified and they can easily be understood from the matrix in the next page. 'a' denotes the displacement amplitude of oscillation, "cavity" denotes the size of the cavity, and 'δ' denotes the Stokes layer thickness.

Table 4.1 : Cases considered for analyses:

Parameters	Case 1	Case 2	Case 3
Re_d	42	42	42
δ/d	1	0.5	2
a/d	1	2	1

(4.6) Results and Post Processing:

Contours of stream function were plotted through a complete cycle for each of these three cases. They are shown below. Discussion of these results is done in Chapter 5 of this work.

It was decided to use an instantaneous cycle time t* that goes from 0 to 1 instead of the actual time that varied for each case.

Since the angular velocity was varied in each case, the time period values varied in each case. The following were the time period values for each case:

Case 1: T = 1s

Case 2: T = 0.25s

Case 3: T = 4s

Base Case:

This was the case used for refining the grid; setting control parameters and other computational issues. So no further explanation was required for this case, but for consistency, the following computational parameters should be borne in mind. The angular velocity of oscillation was 2π rad/s and the time period of the oscillation was 1 second. Proper choice of time step sizes was also described as an important numerical tool; since the time period was 1s, a hundredth of this value, i.e., 0.01 was thought of as an appropriate time step size. Figures 4.7 through 4.15 show velocity vector and stream function plots at different instants in time during a cycle.

Case 1:

Figures 4.7 through 4.15 show velocity vectors and stream function plots for Case1. Case1 had a Stokes layer thickness that was between those for Cases 2 and 3. It can be seen that as time progresses, fluid is being sloshed out and entrained and a vortex is being shed. This is explained in detail in Chapter 5.

Case 2 : Figures 4.16 through 4.24 show velocity vector plots and stream function plots for Case 2.It can be seen that as the Stokes layer thickness is decreased, the primary and secondary vortex are being shed at different locations. The whole process of fluid sloshing and entrainment is also changed.

Case 3 : Figures 4.25 through 4.38 show velocity vector plots and stream function plots for Case 3 when the Stokes layer thickness was increased. It can be seen here that the vortices are being shed very far away from the cavity because the viscous layers extend much more into the computational domain than the other two cases.

All three cases exhibited an explicit dependence on the Stokes layer thickness. Perturbation in the boundary layer was seen in all the three cases. These are summed up in Chapter 5 of this work.

It should be mentioned here that a couple of test cases were run by varying the cavity-size-based Reynolds number but since no dramatic changes in the results were seen, these are discussed here in detail.

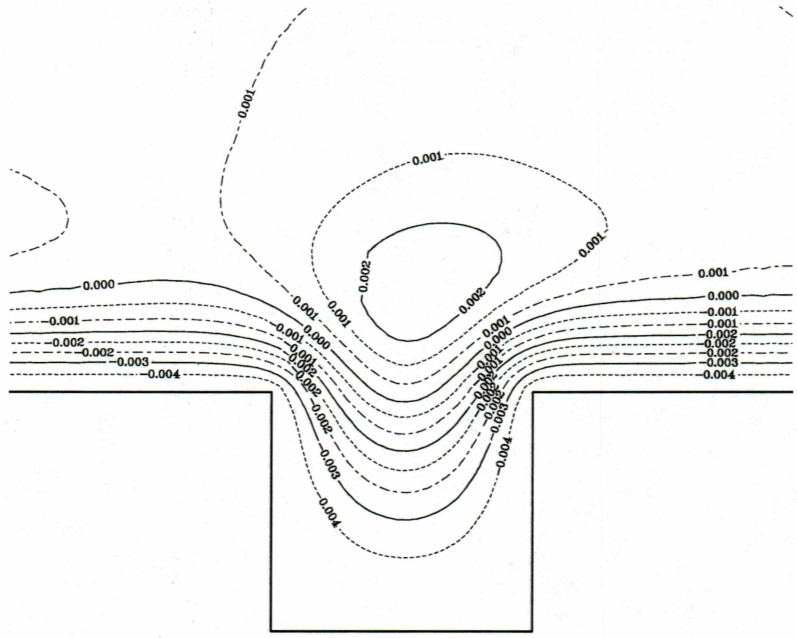

(a)

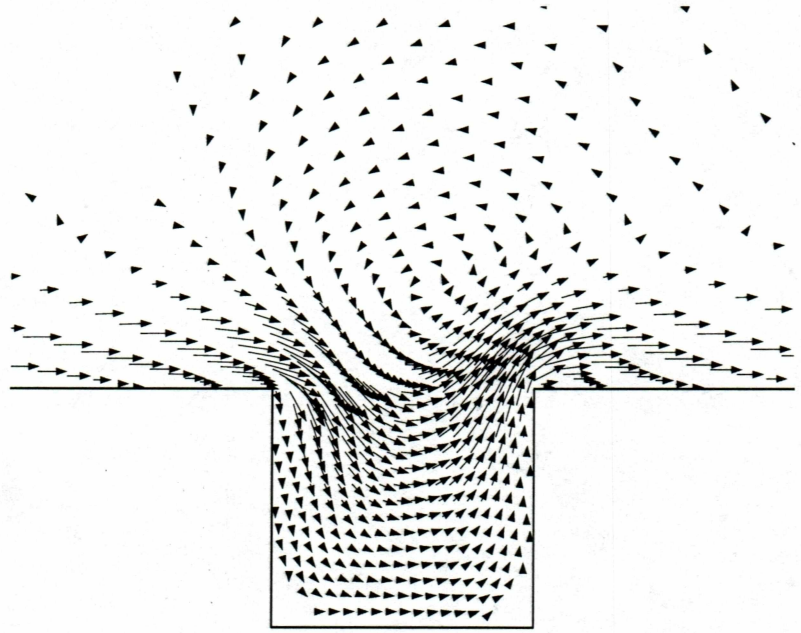

(b)

Figure 4. 7:Stream function (a) and Velocity vector plots (b) at t* = 0. A counter-clockwise vortex being shed when the cavity comes to rest.

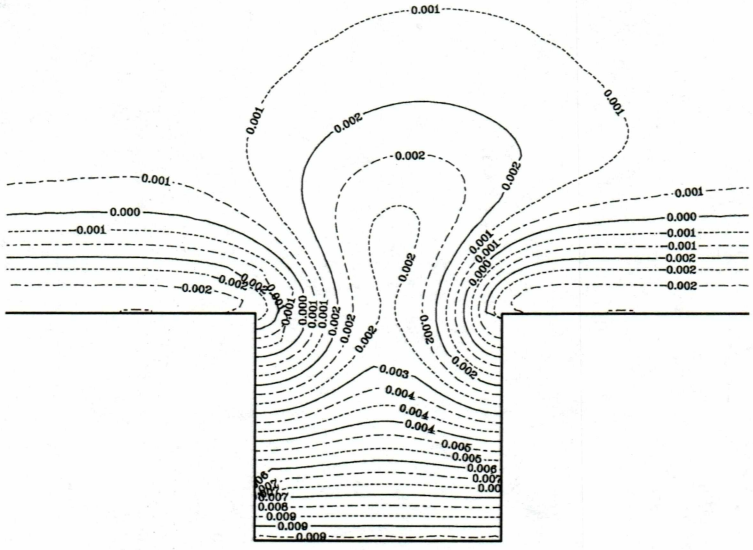

(a)

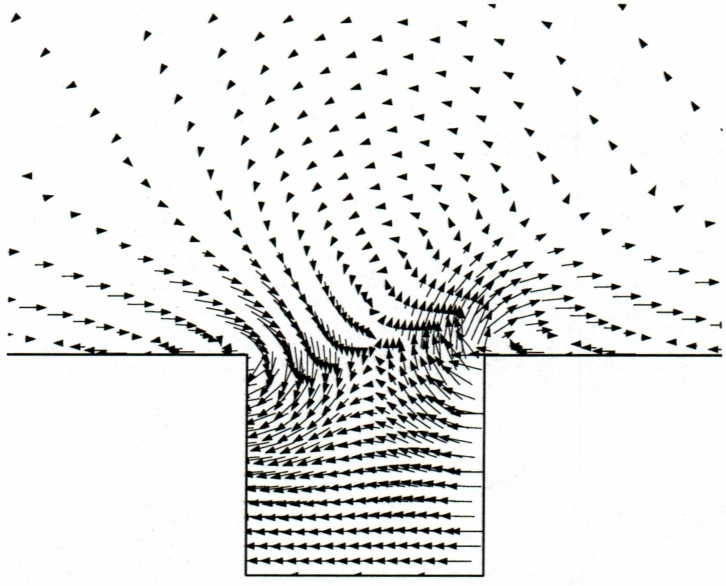

(b)

Figure 4. 8 : Stream function (a) and Velocity vector plots (b) at t* = T/20:
As the cavity starts translating to the right, fluid sloshes out and is sucked in from the other end.

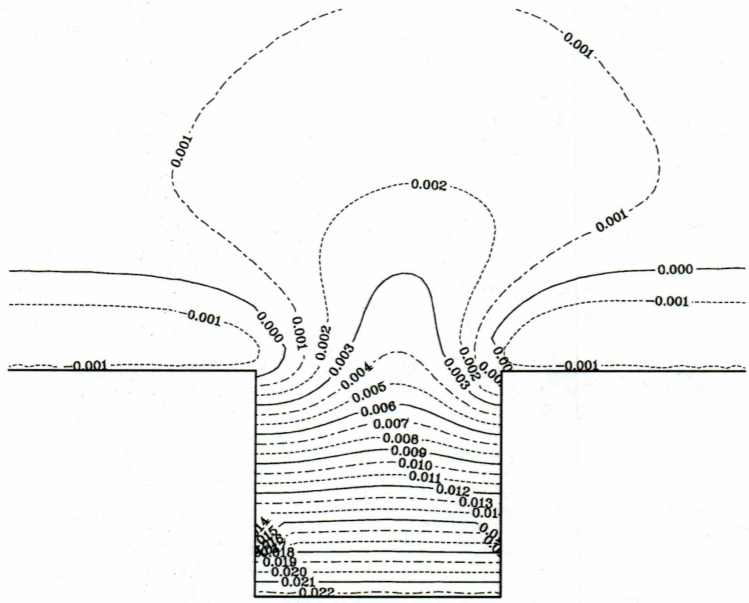

(a)

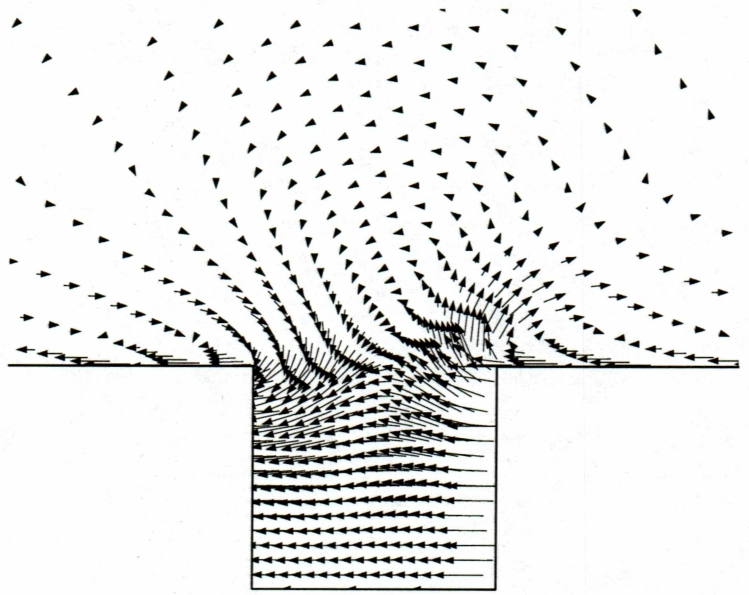

(b)

Figure 4. 9 : Stream function (a) and Velocity vector plots (b) at t* = T/10

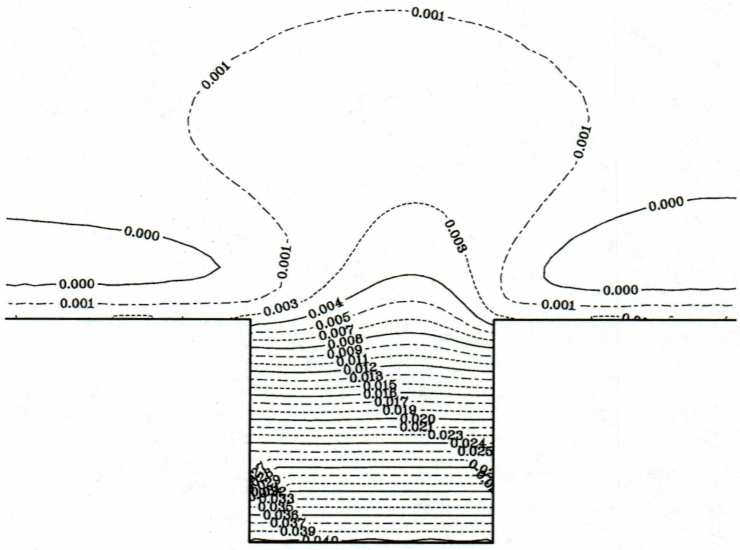

(a)

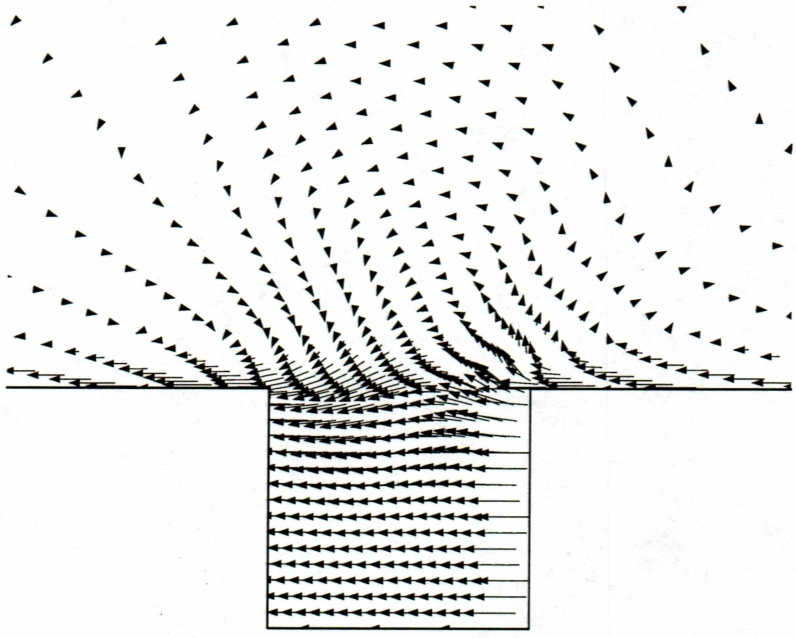

(b)

Figure 4. 10: Stream function (a) and Velocity vector plots (b) at t* = T/5.

Plug flow fills up almost the entire cavity. The vortex sheet has moved a little to the right.

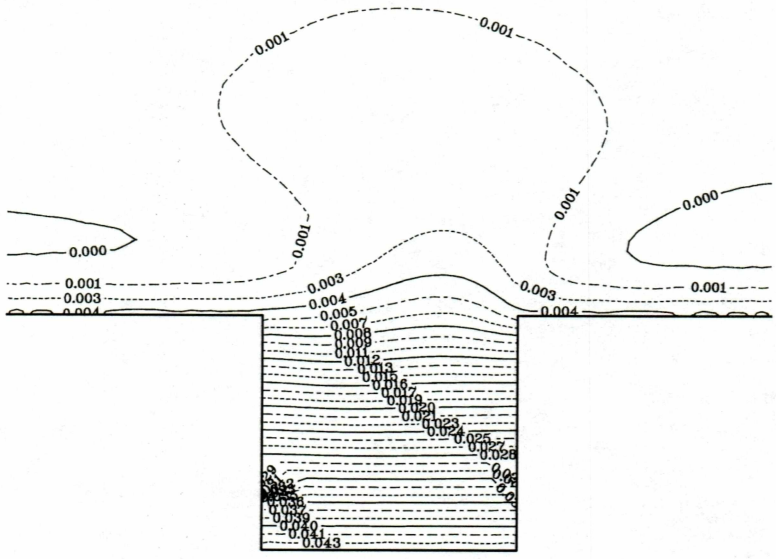

(a)

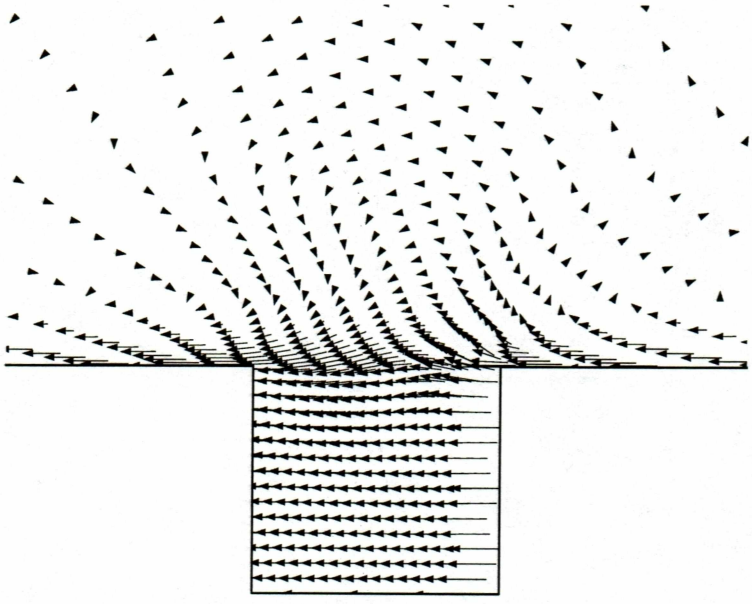

(b)

Figure 4. 11: Stream function (a) and Velocity vector plots (b) at t* = T/4

The cavity has its maximum velocity here. Plug flow fills up the entire cavity.

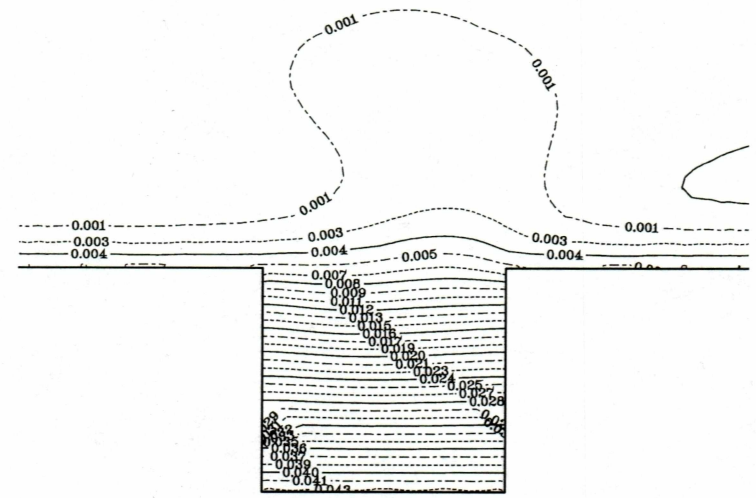

(a)

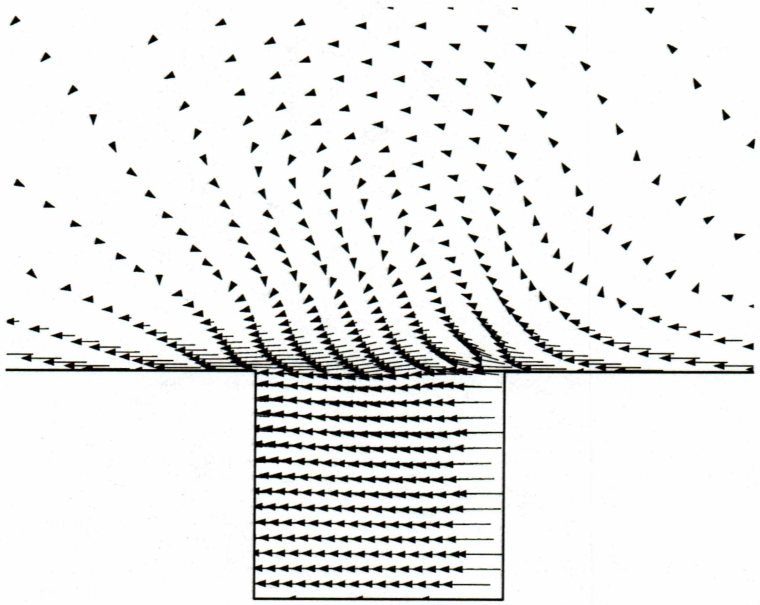

(b)

Figure 4. 12: Stream function (a) and Velocity vector plots (b) at t* = 3T/10

The cavity is in its deceleration phase. A secondary vortex is in its formative phase.

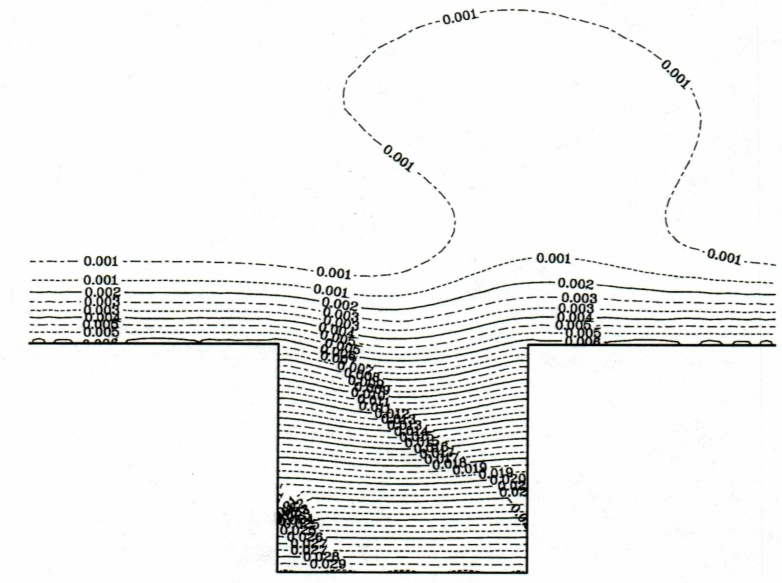

(a)

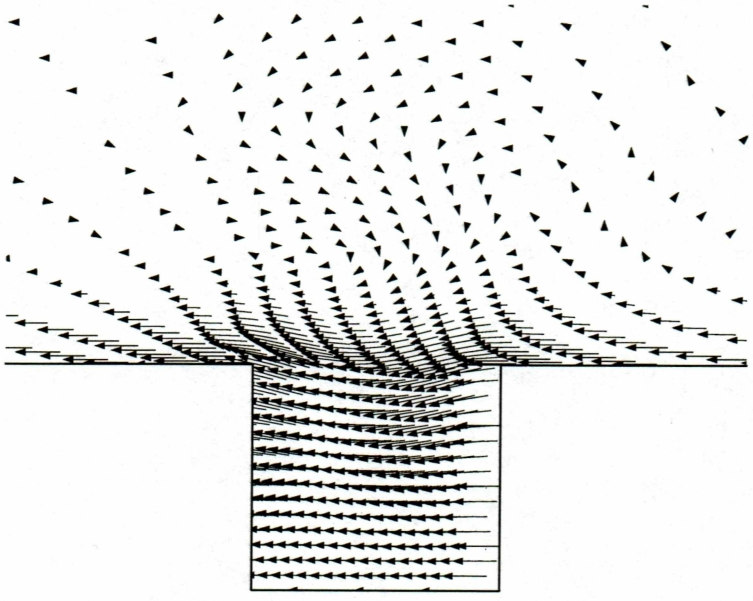

(b)

Figure 4. 13: Stream function (a) and Velocity vector plots (b) at t* = 2T/5

The cavity approaches rest at this instant. The vortex away from the cavity is stronger now.

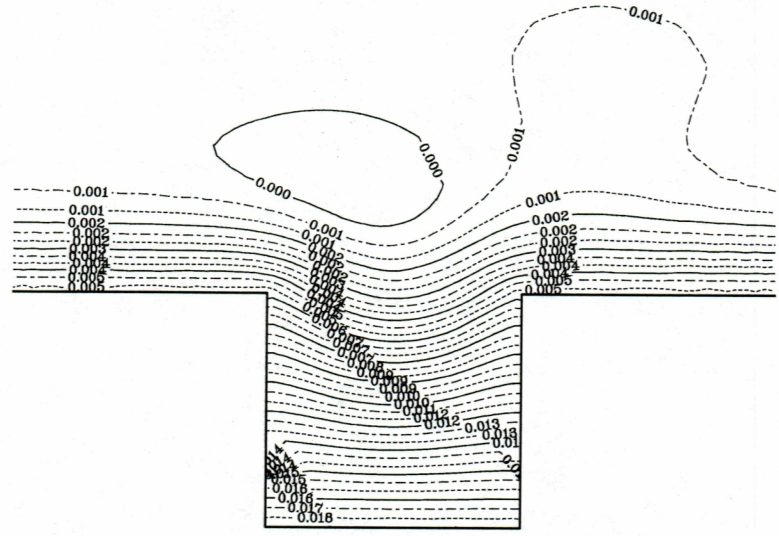

(a)

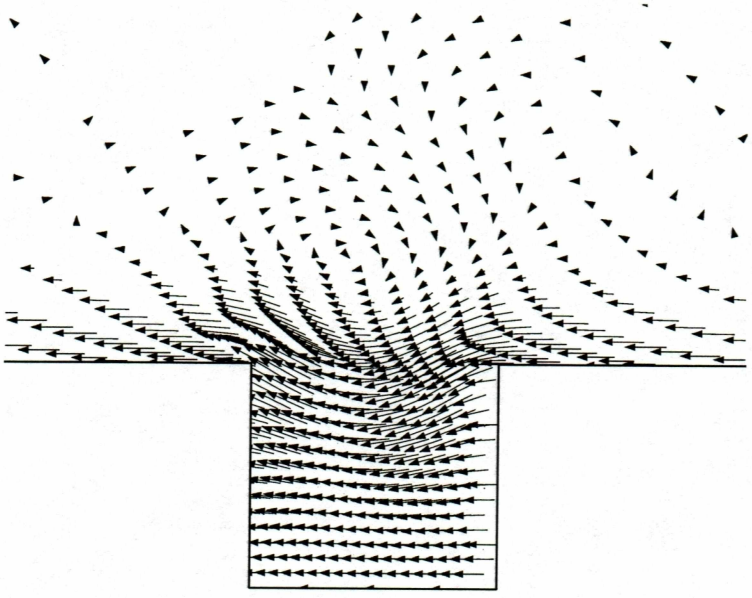

(b)

Figure 4. 14: Stream function (a) and Velocity vector plots (b) at t* = 9T/20

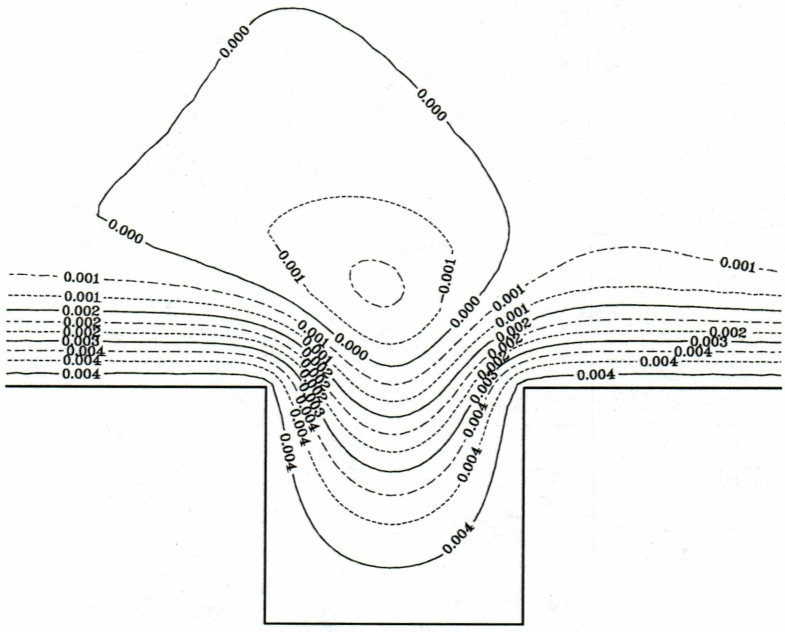

(a)

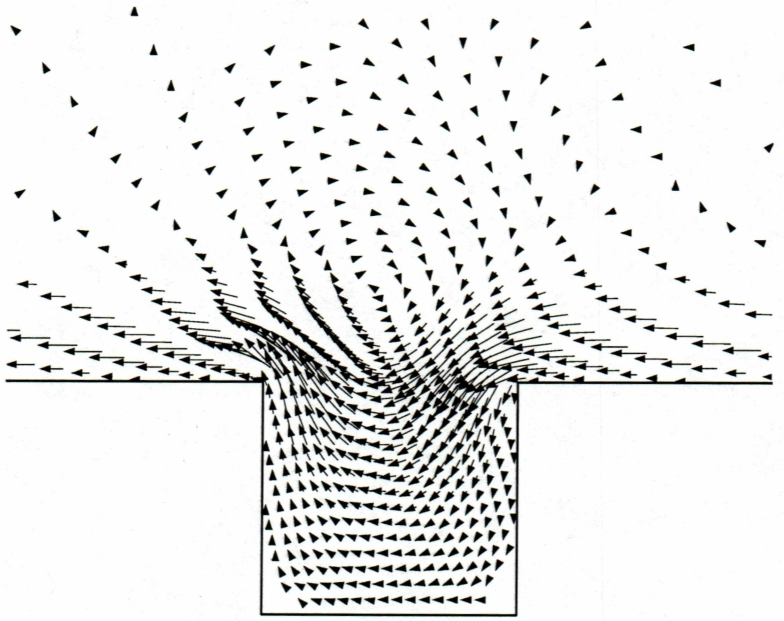

(b)

Figure 4. 15: Stream function (a) and Velocity vector plots (b) at t* = T/2

At half-time, the cavity has come to rest . A clockwise vortex is being shed.

CASE 2: $Re_d = 42$, $\delta/d = 0.5$, $\omega = 25.1472$ rad/s

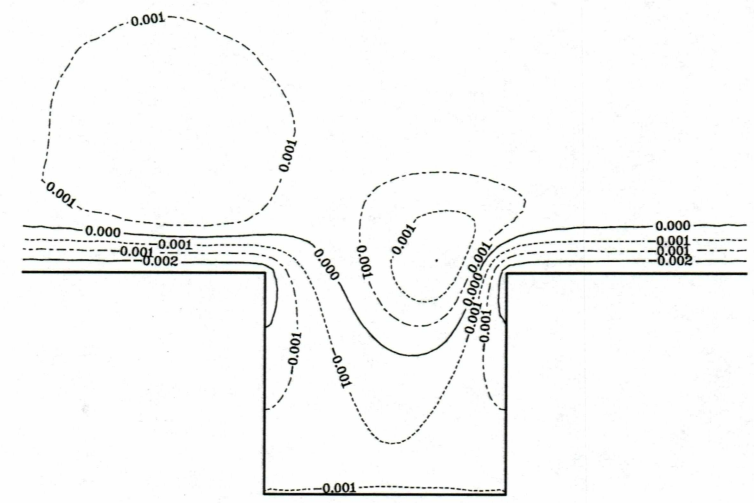

(a)

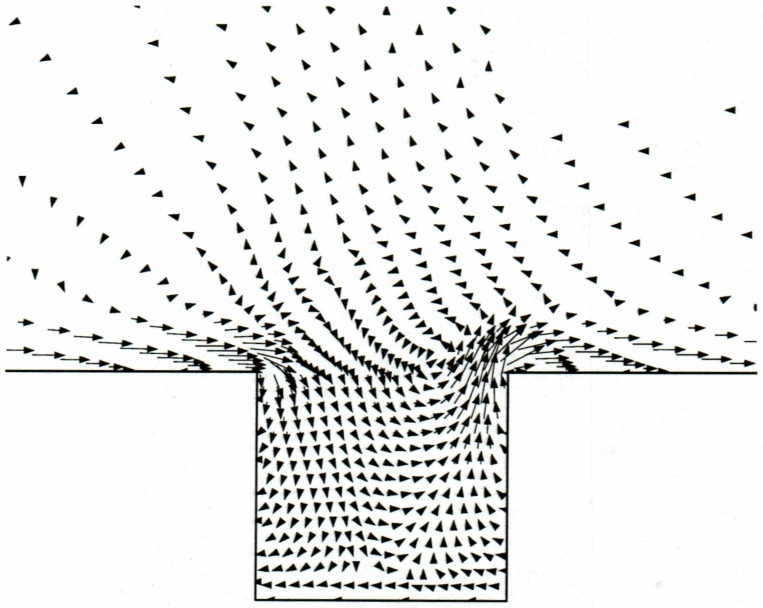

(b)

Figure 4. 16:Stream function (a) and Velocity vector plots (b) at t*= 0

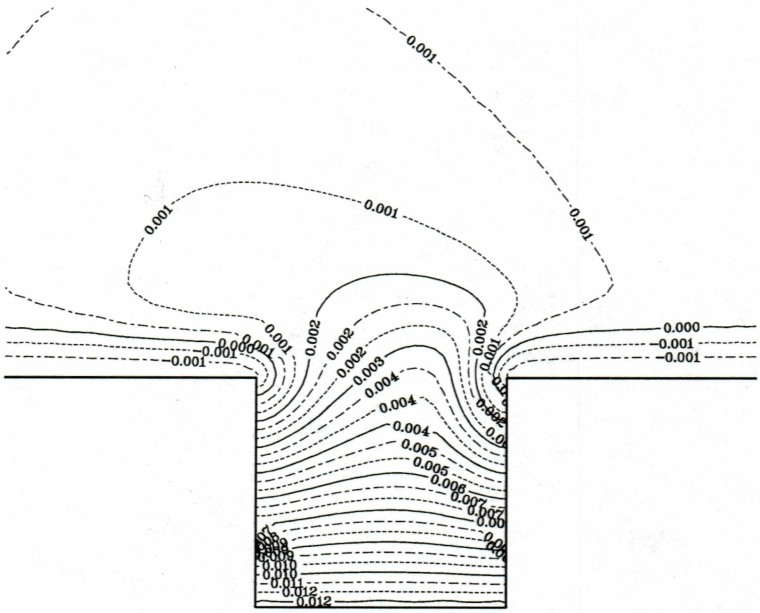

(a)

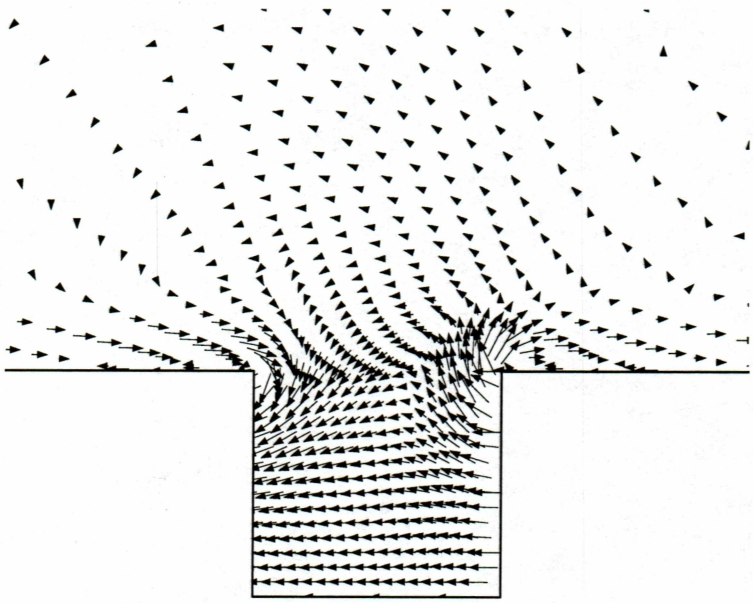

(b)

Figure 4. 17: Stream function (a) and Velocity vector plots (b) at t* = T/20

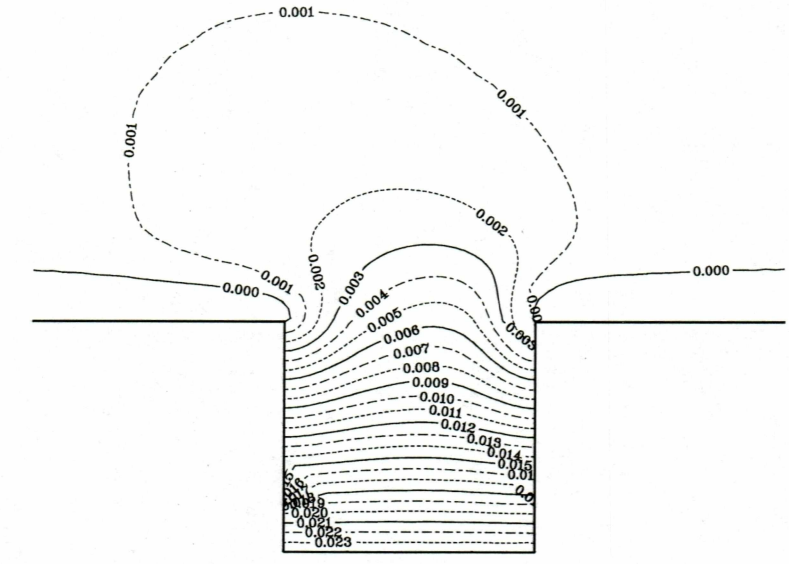

(a)

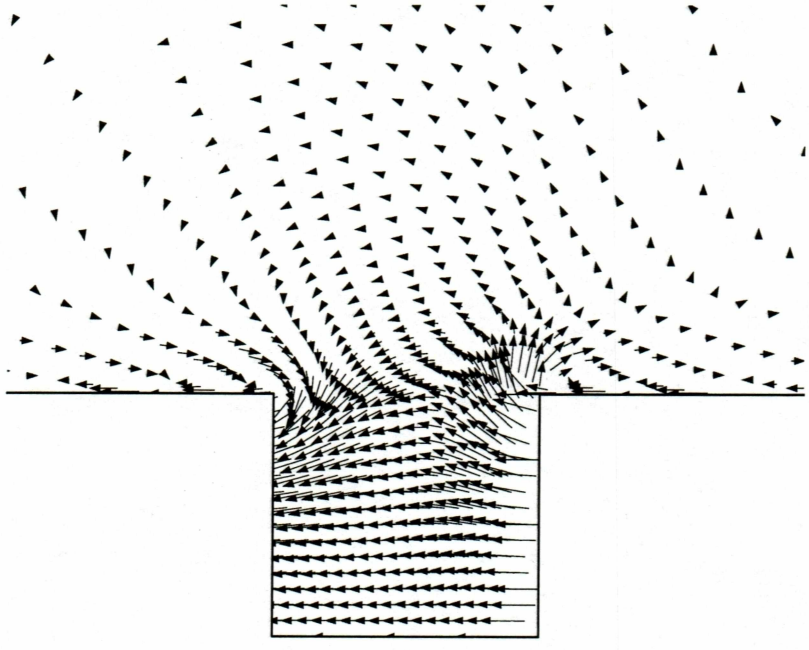

(b)

Figure 4. 18: Stream function (a) and Velocity vector plots (b) at t*= T/10

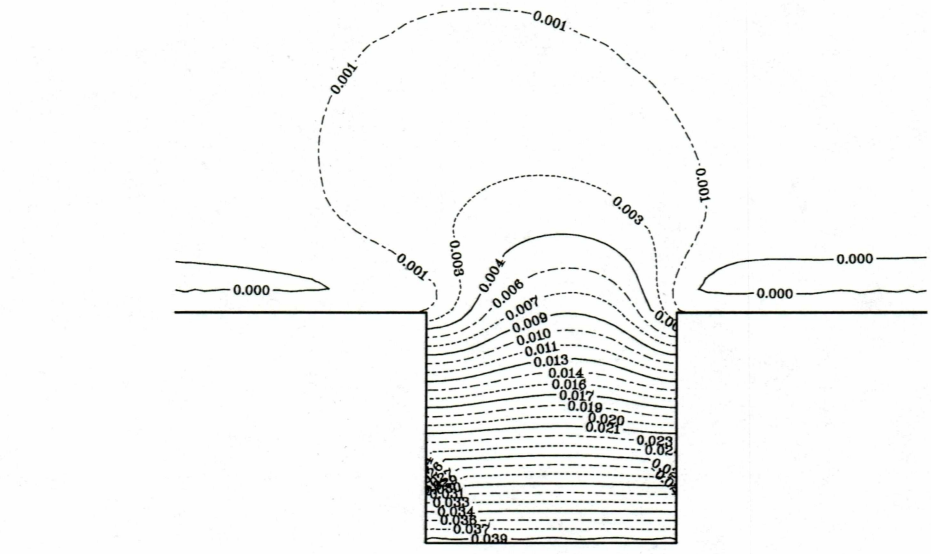

(a)

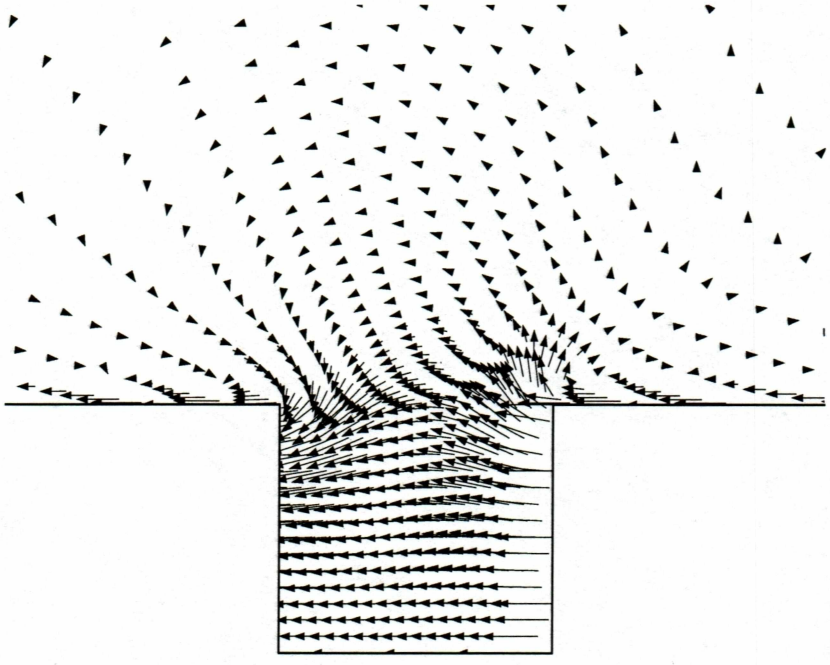

(b)

Figure 4. 19: Stream function (a) and Velocity vector plots (b) at t*= T/5

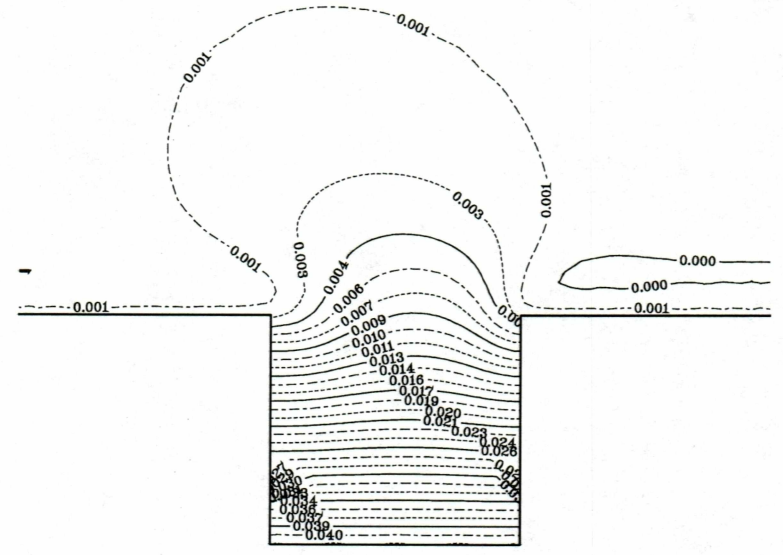

(a)

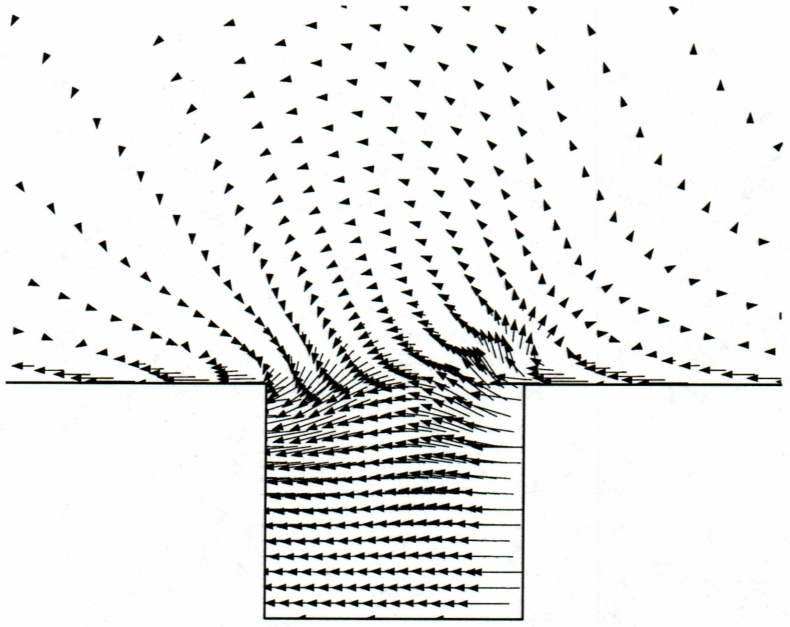

(b)

Figure 4. 20: Stream function (a) and Velocity vector plots (b) at t* = T/4

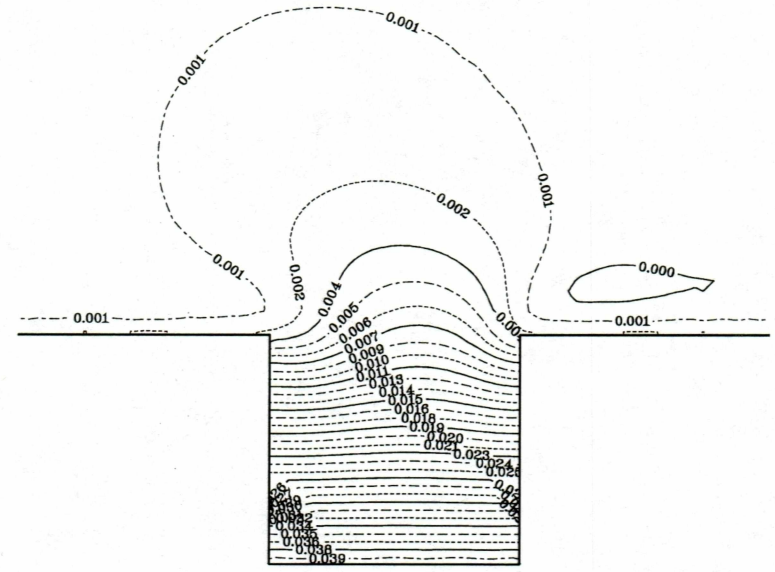

(a)

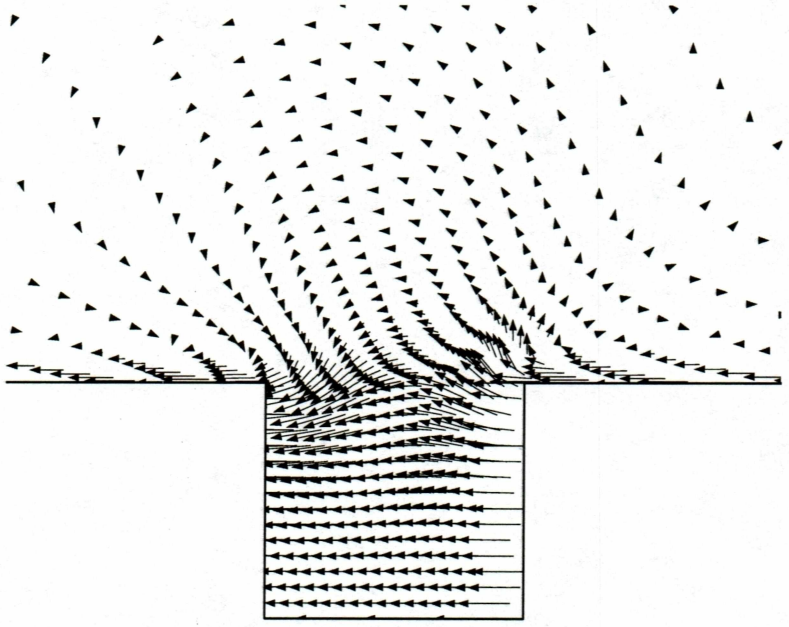

(b)

Figure 4. 21: Stream function (a) and Velocity vector plots (b) at t* = 3T/10

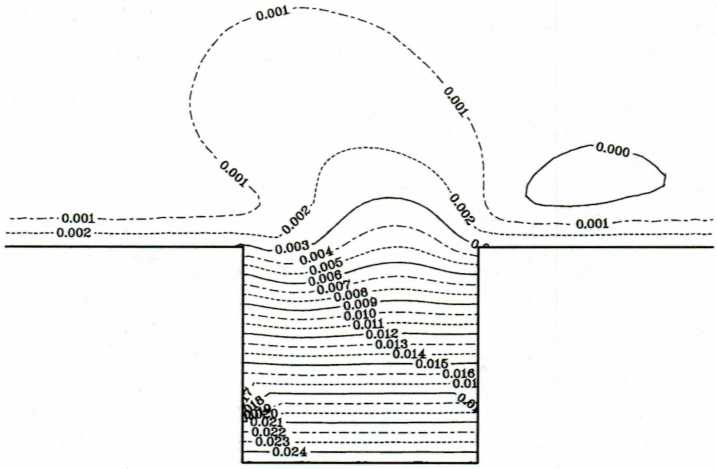

(a)

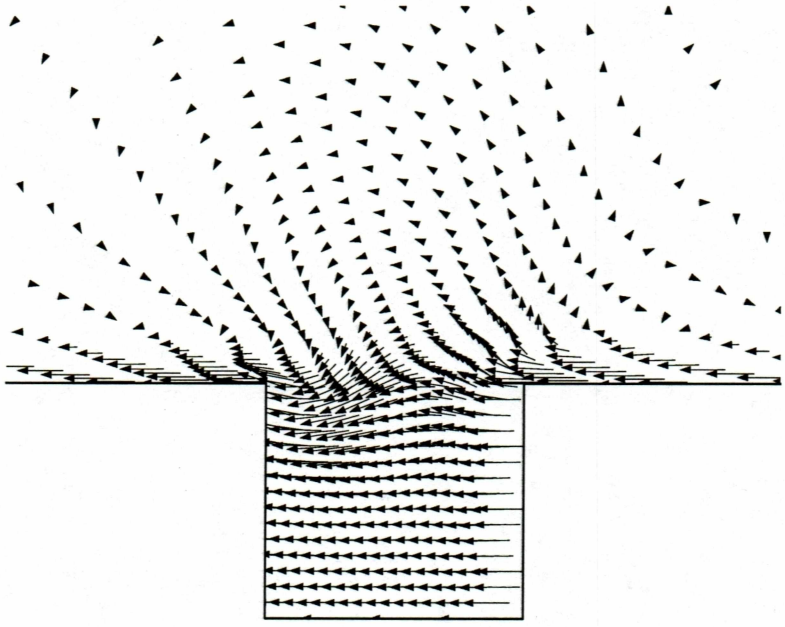

(b)

Figure 4. 22: Stream function (a) and Velocity vector plots (b) at t* = 2T/5

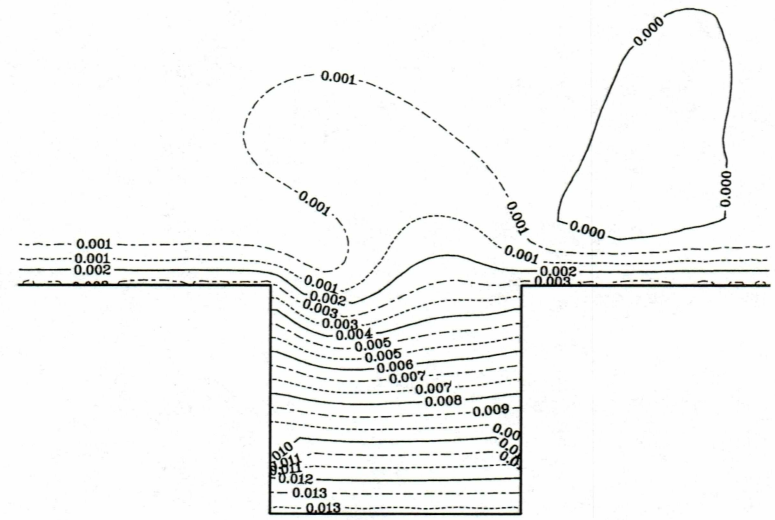

(a)

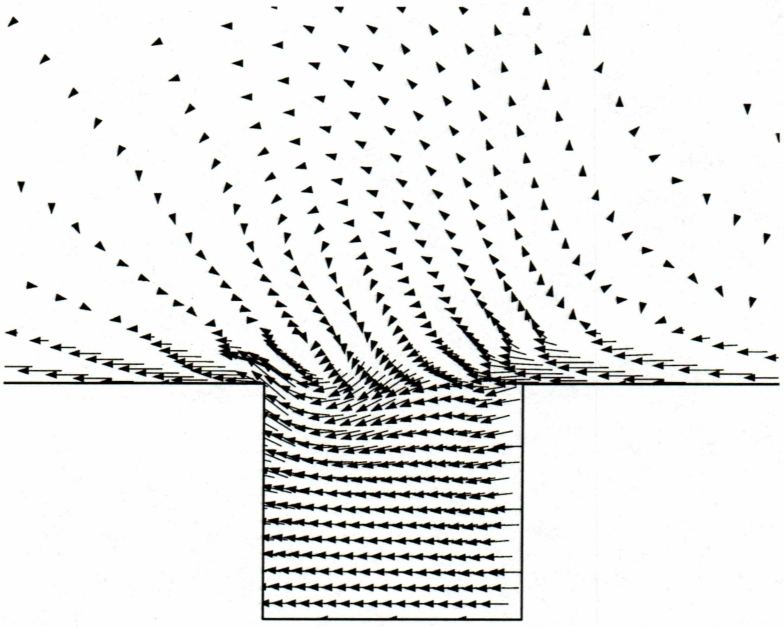

(b)

Figure 4. 23: Stream function (a) and Velocity vector plots (b) at t* = 9T/20

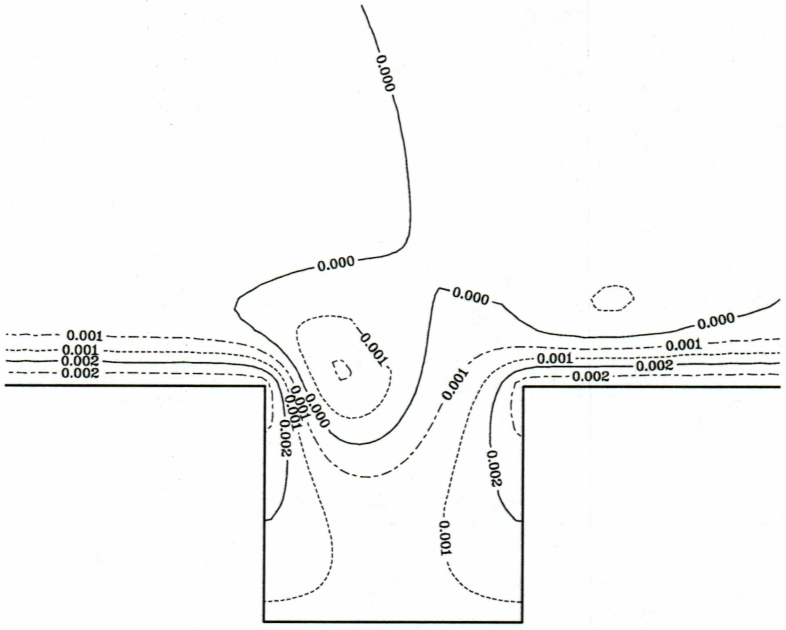

(a)

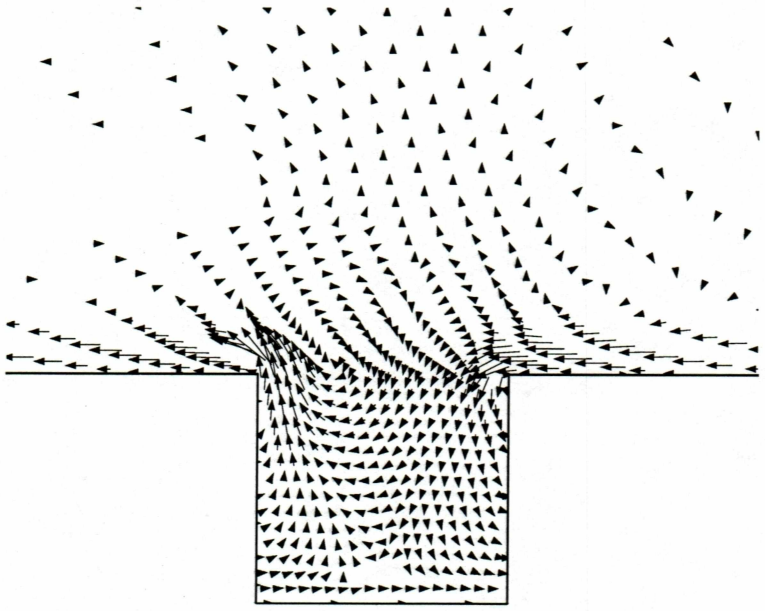

(b)

Figure 4. 24: Stream function (a) and Velocity vector plots (b) at t* = T/2

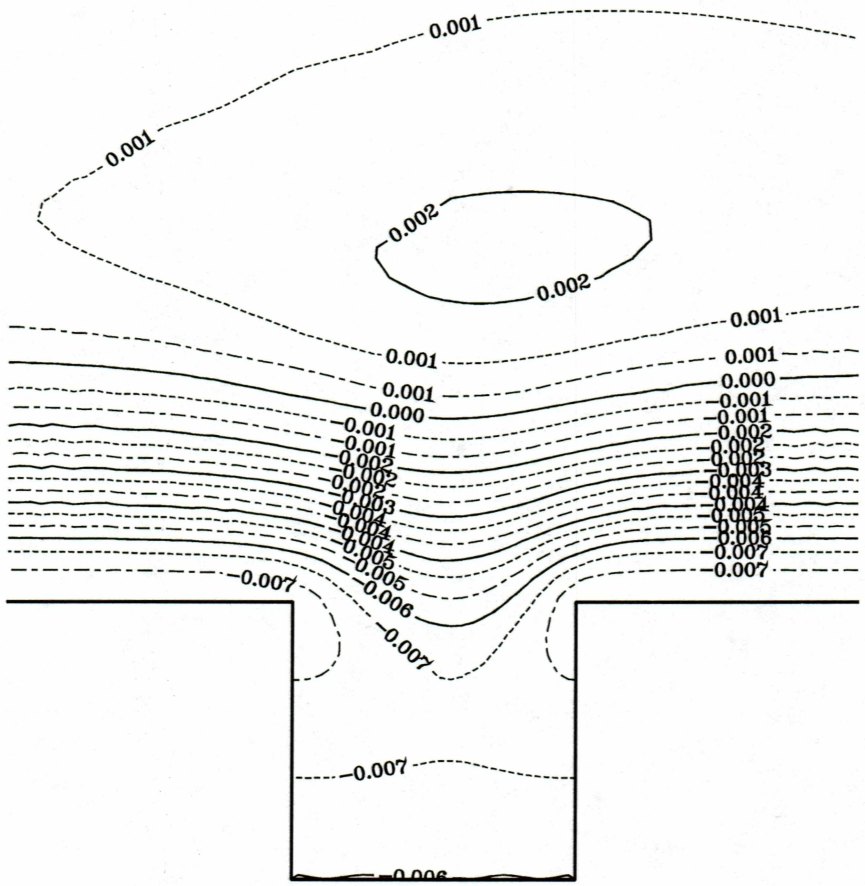

Figure 4. 25 CASE 3 Stream function Plots at t* = 0

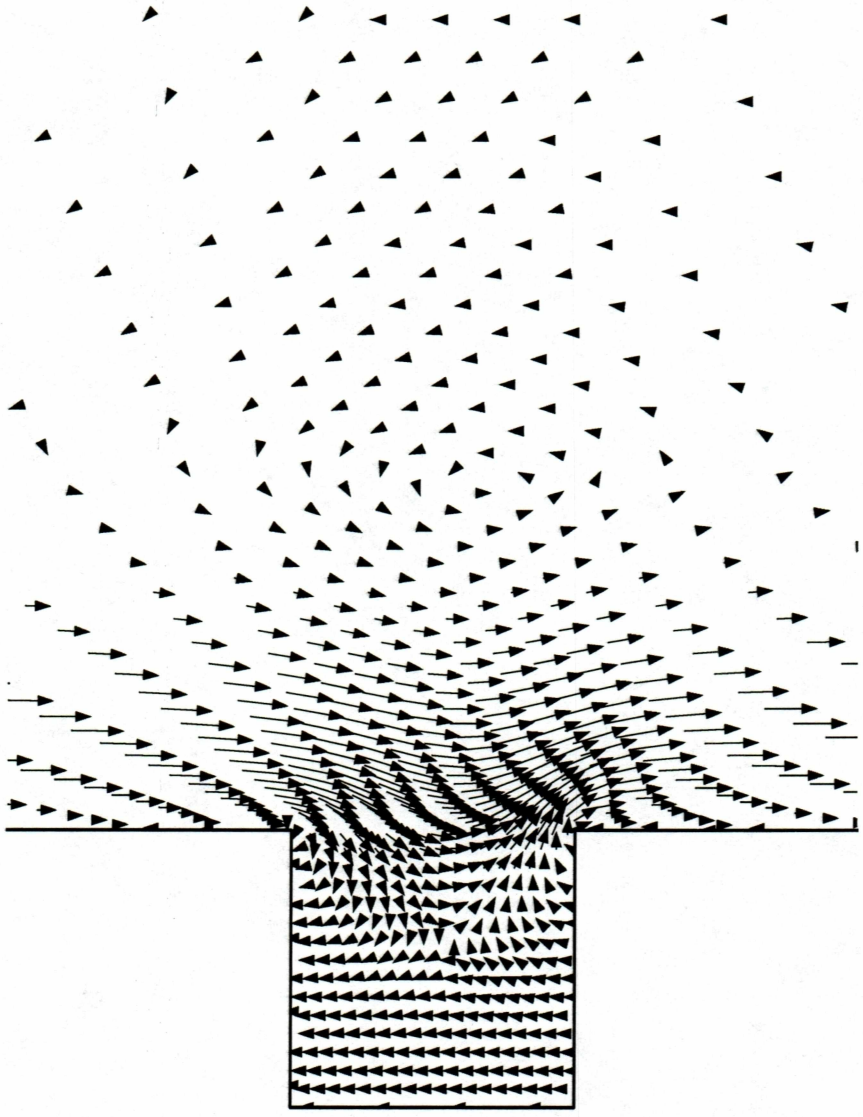

Figure 4. 26 : Velocity Vector plot at t* = 0

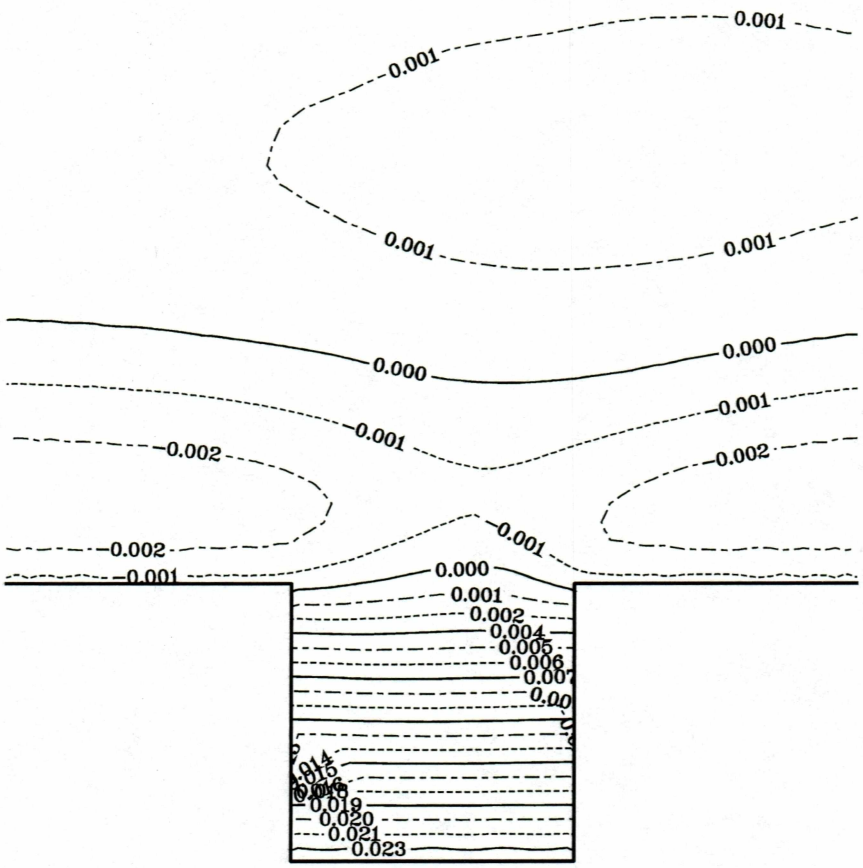

Figure 4. 27: Stream Function Contours at t* = T/10

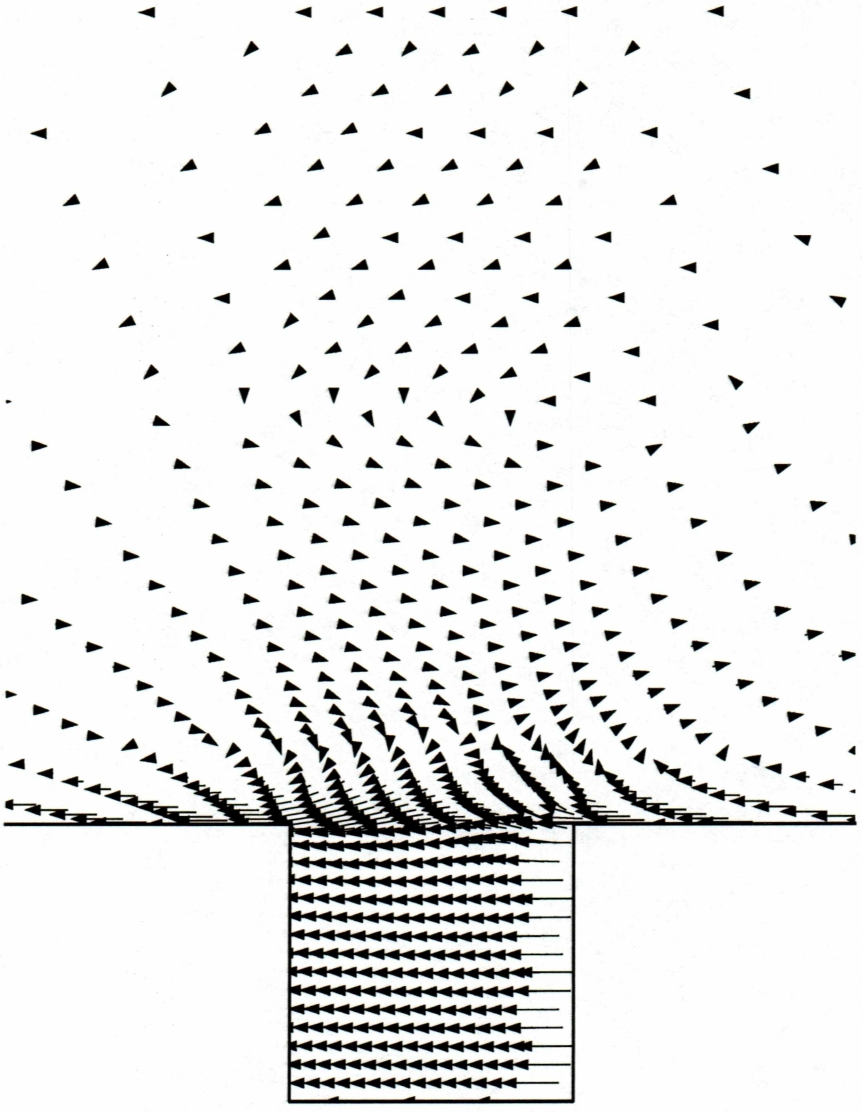

Figure 4. 28:Velocity vectors at t* = T/10

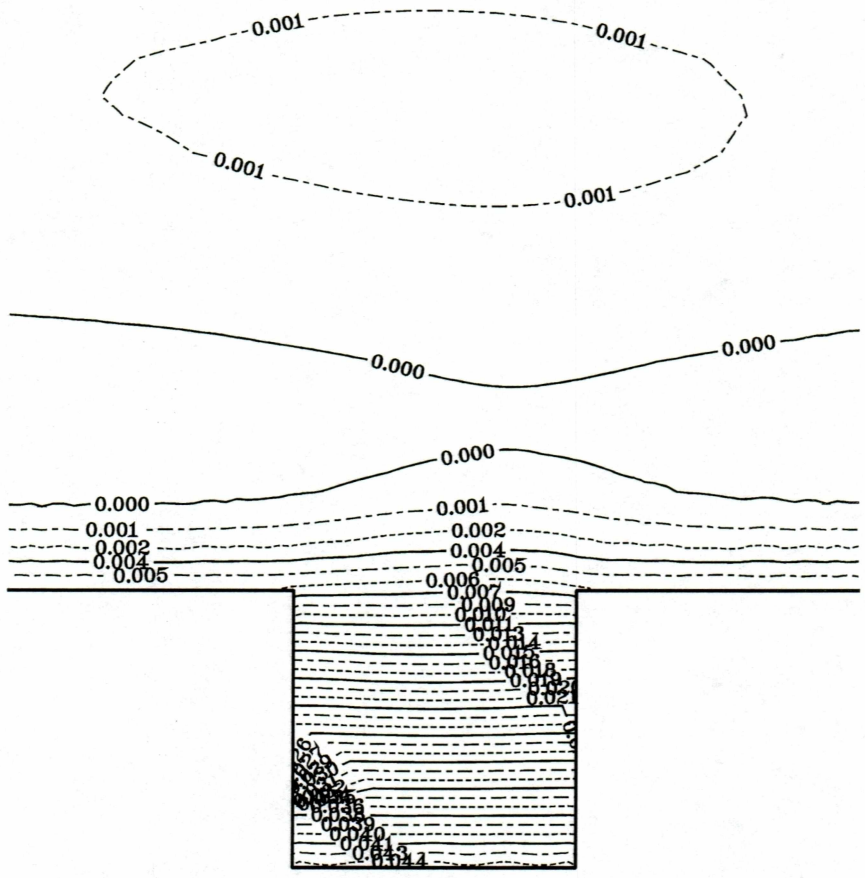

Figure 4. 29:Stream function Contours at t* = T/5

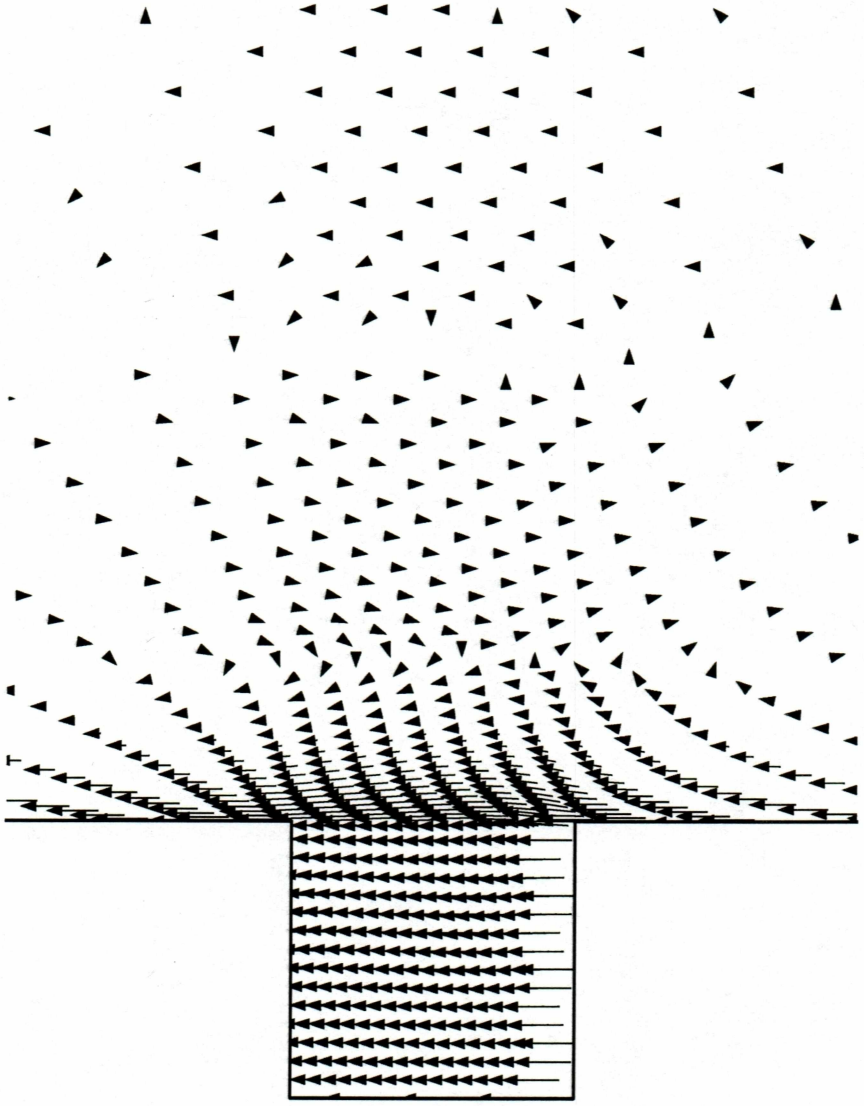

Figure 4. 30:Velocity Vector Plots at t* = T/5

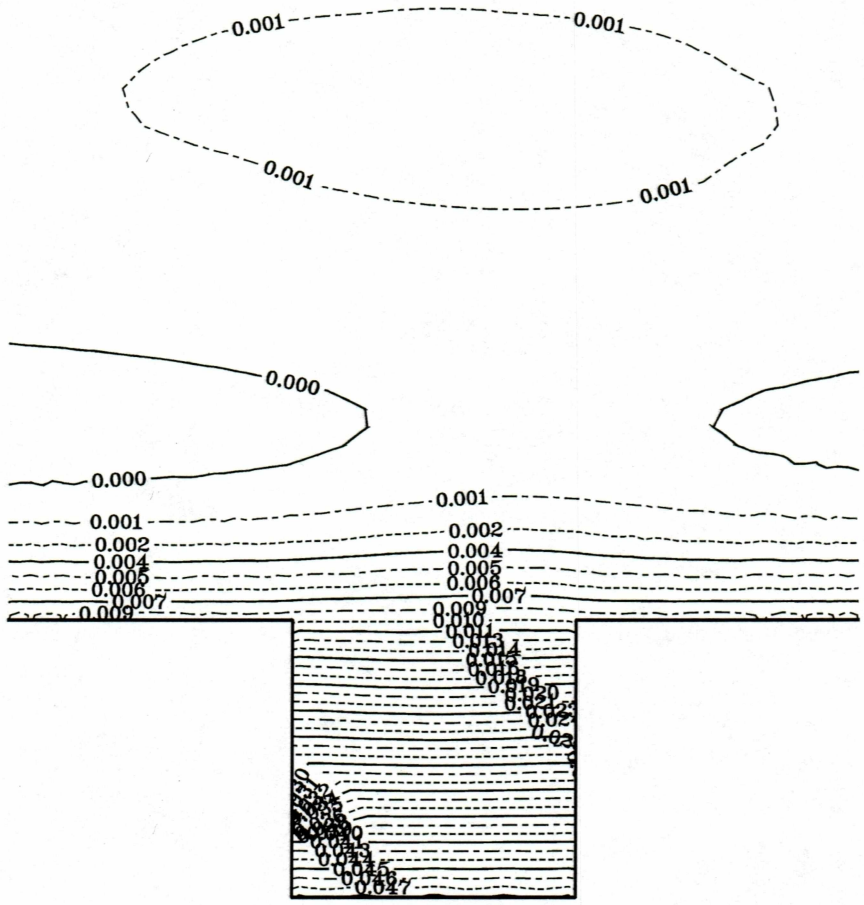

Figure 4. 31:Stream function Contours at t*= T/4

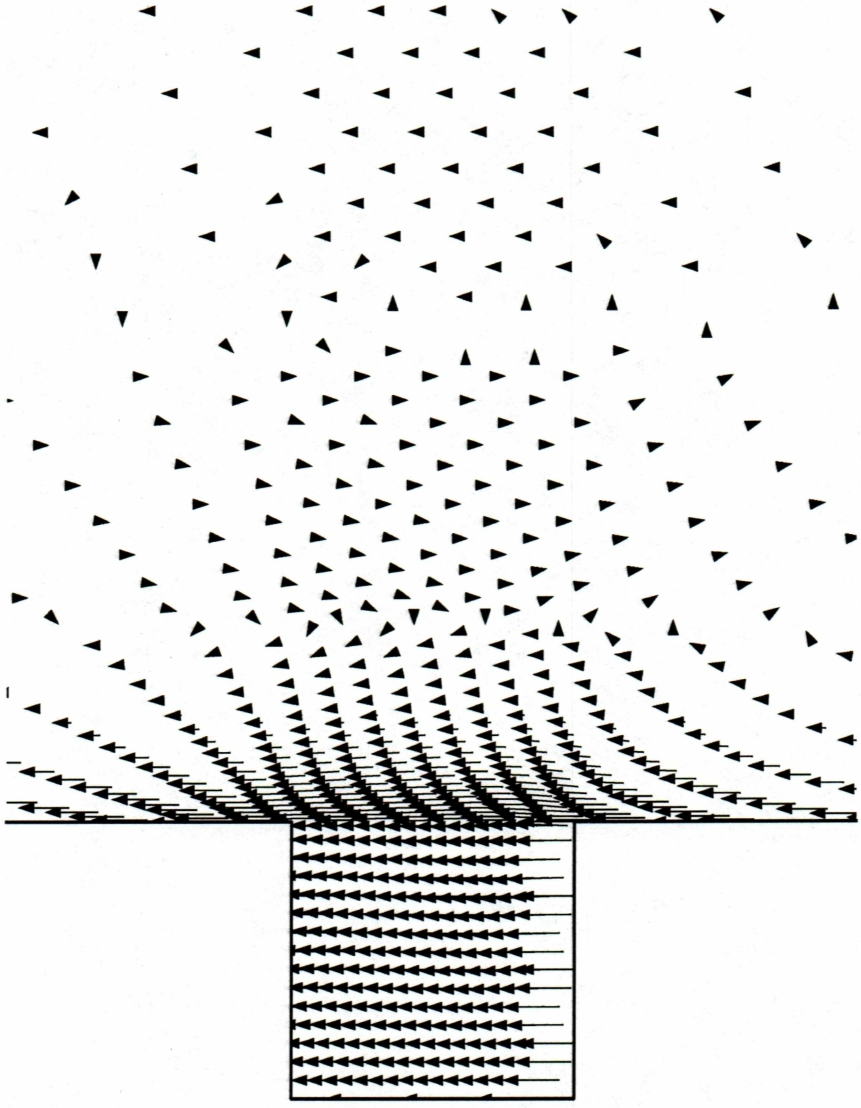

Figure 4. 32:Velocity Vector Plots at t* = T/4

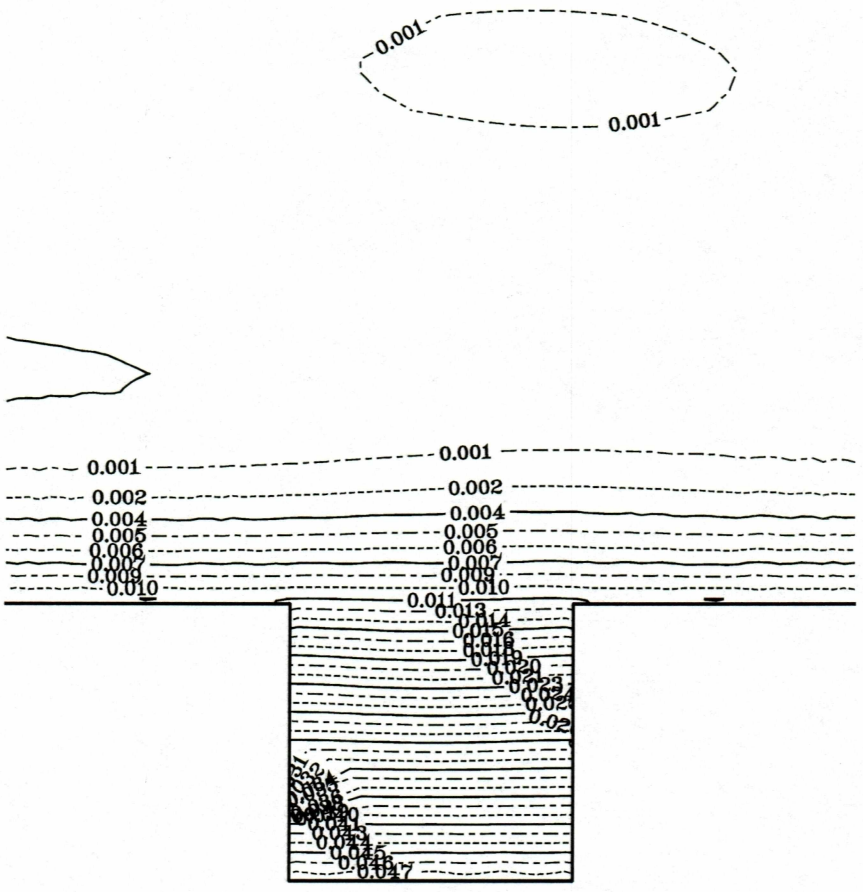

Figure 4. 33: Stream Function Plots at t* = 3T/10

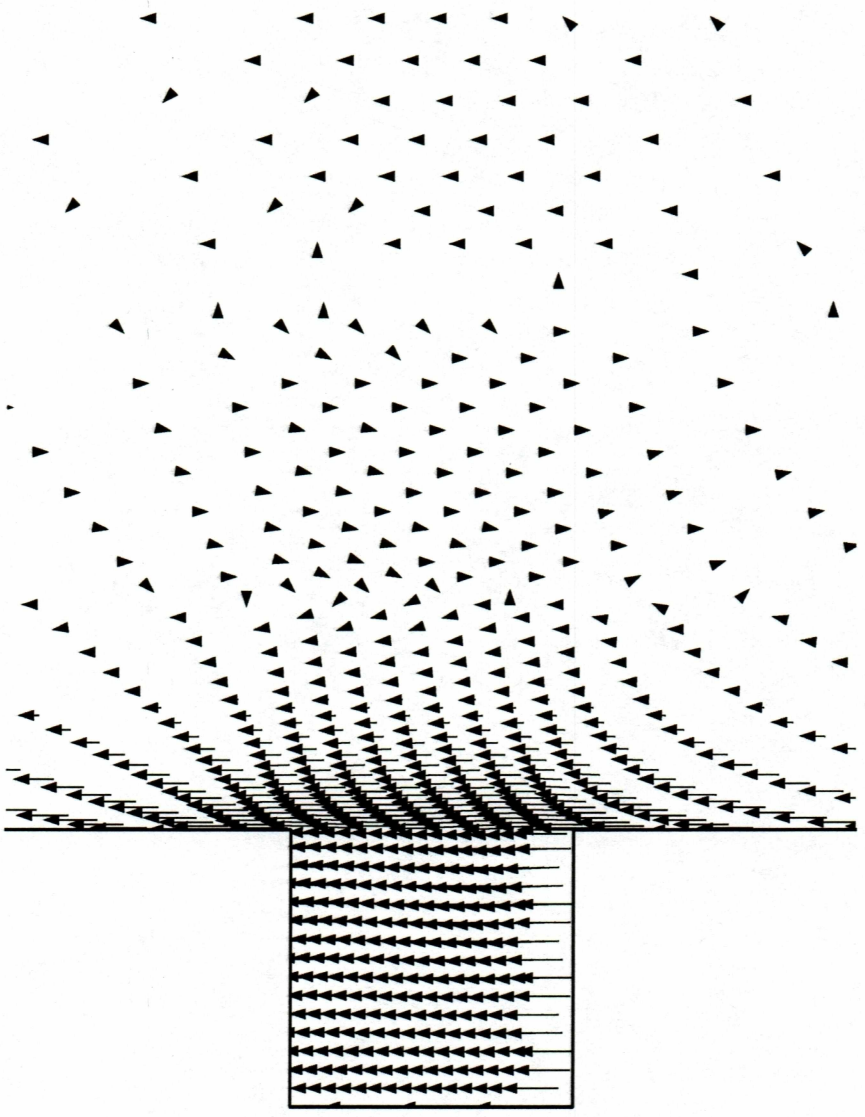

Figure 4. 34: Velocity Vector Plots at t* = 3T/10

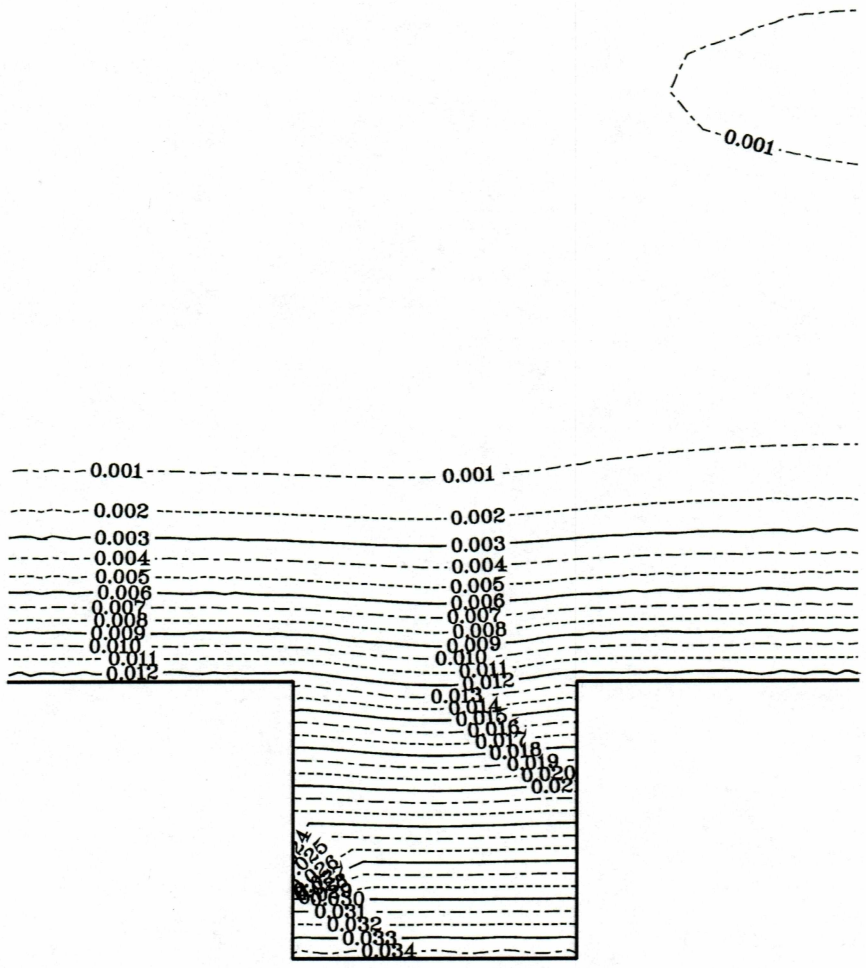

Figure 4. 35: Stream Function Plot at t* = 2T/5

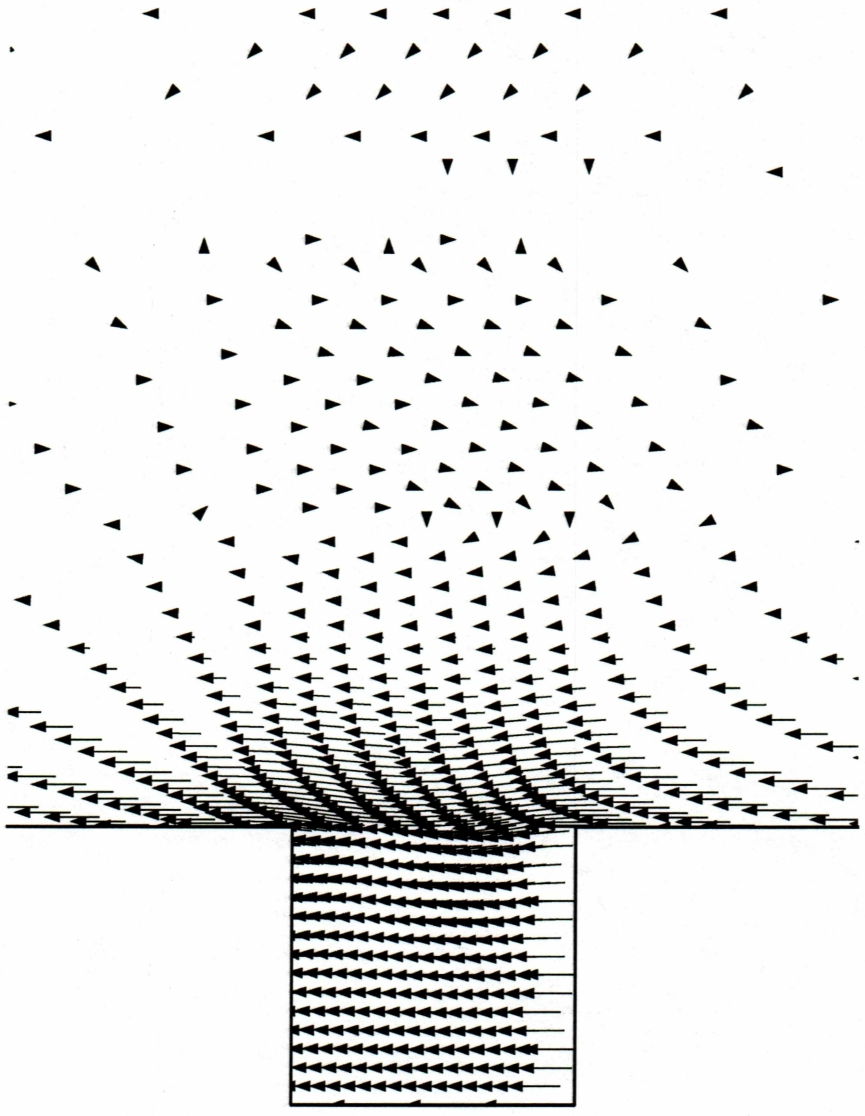

Figure 4. 36:Velocity Vectors at t* = 2T/5

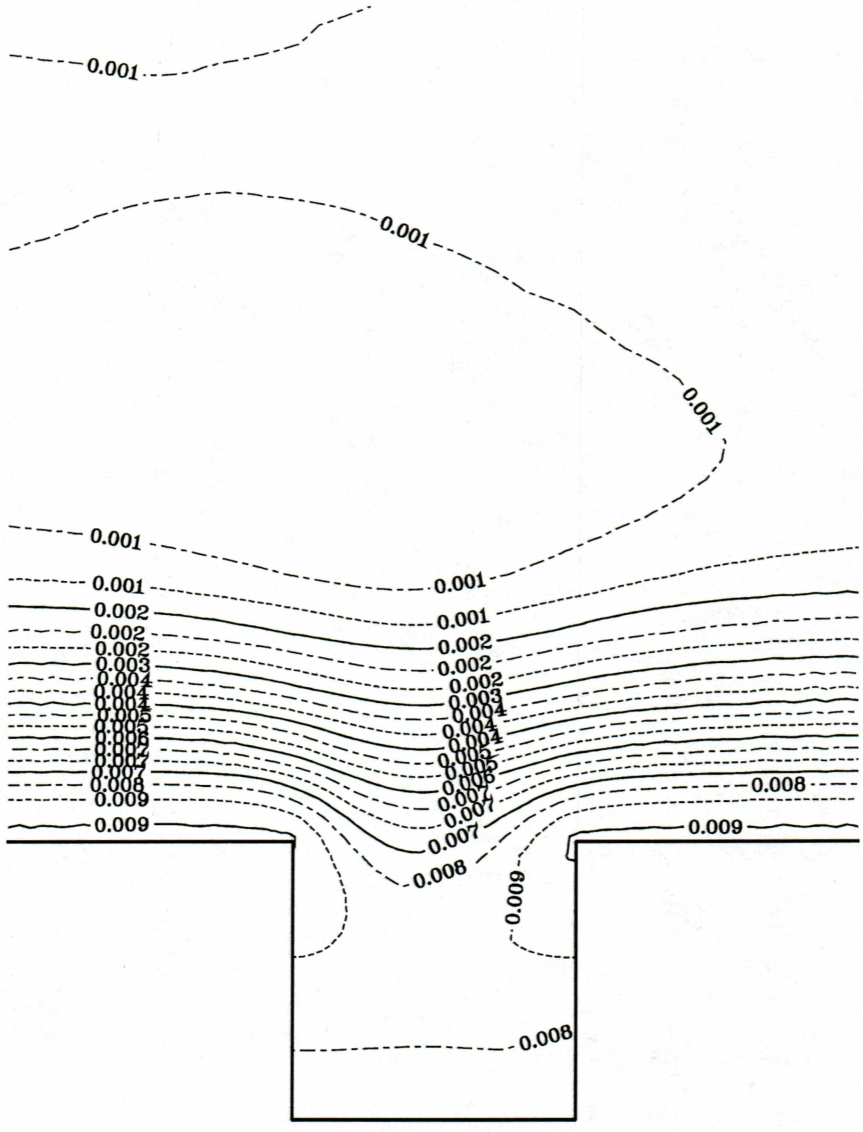

Figure 4. 37:Stream Function plot for t* = T/2

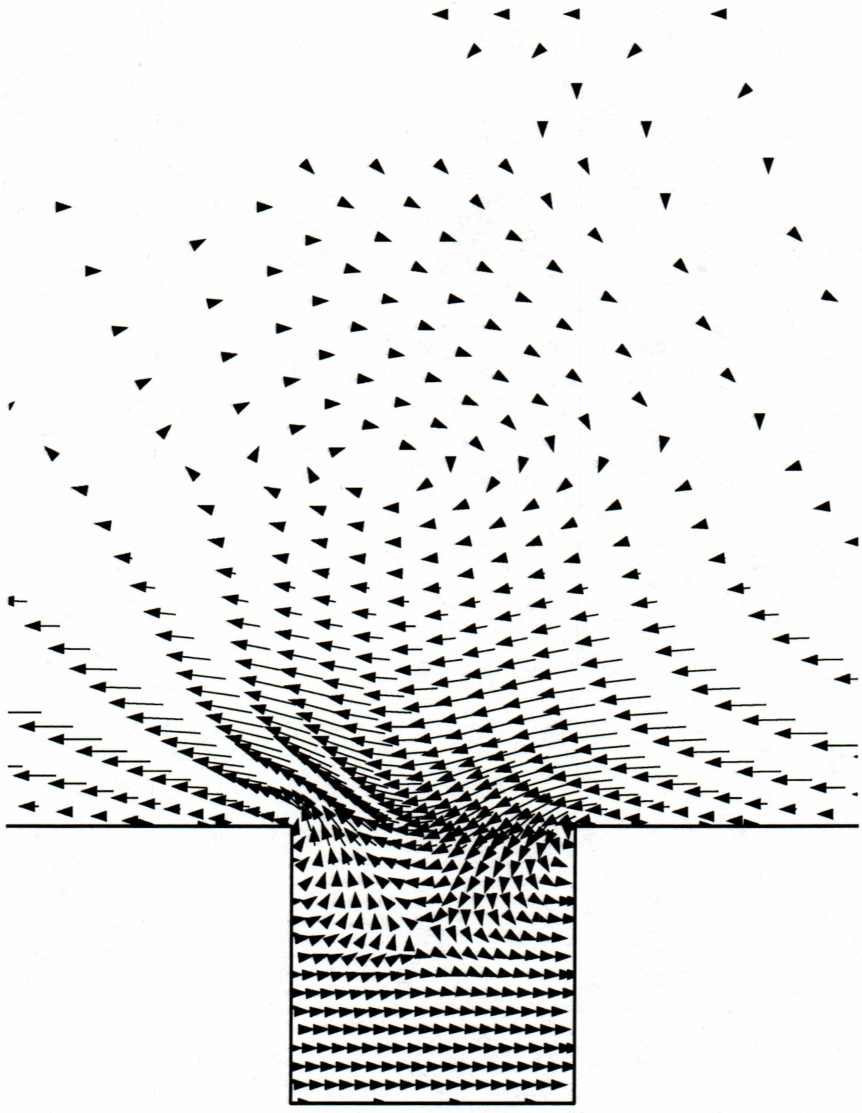

Figure 4. 38: Velocity Vector plots for t* = T/2

Chapter 5

Results and Discussion:

(5.1) Introduction:

The commercial CFD software Fluent was used for visualizing all data and the flow field in general. Stream function lines are those that are tangent to the local velocity vector at all points in the flow field. They are very useful in visualizing flow lines. Mathematically, the stream function, if integrated along the x or y directions, is defined by:

$$\psi = \int \mathbf{u} dy \qquad \textbf{(5.1)}$$

or alternatively

$$\psi = - \int \mathbf{v} dx \qquad \textbf{(5.2)}$$

where ψ is the stream function, u is the streamwise velocity, dy is a differential change in the cross streamwise coordinate (assumed to be y in this case), v is the cross streamwise velocity and dx is the differential change in the streamwise coordinate (assumed to be x here).

Fluent uses equations (5.1) and (5.2) to calculate and plot stream function values throughout the domain. Since these values were easier to analyze the flow field with, they were chosen for the discussion of results. There was one difficulty however, with the use of stream function values as generated by Fluent. In the present problem, an oscillating velocity was imposed on the fluid initially at rest. There is one positive and one negative half cycle for each complete cycle of oscillation. During the positive half cycle, stream function values calculated using equations (5.1) and (5.2) would all be positive and thus one would expect values during the negative half cycle to be negative. On the contrary, as is the convention with most CFD software, the minimum of the stream function values is taken as zero and all other values throughout the domain are calculated based on this value with the result that there are no negative values for stream function at any instant.

It is worth remembering at this point the dimensionless parameters that were used to characterize flow. The matrix that was used to run the three different cases relied mainly on changing the length ratios and keeping the cavity based Reynolds number a constant. Subtle differences were seen in all these cases but it must be mentioned that vortex development depended mainly upon the length ratios (ratio of the stokes layer thickness to the cavity size) rather than the cavity size-based Reynolds number. Response of the fluid to an increase in Reynolds number based on the geometric parameters of the cavity is an interesting digression and may lead to characterization of transition of laminar oscillatory flows to turbulence. (This is currently under investigation at MIT, albeit for a different problem). Each case (Cases 1 to 3) is explained in detail below: The problem is quite different under the Newtonian and non-Newtonian reference frames; a program to calculate velocities and stream functions in the Newtonian reference frame was written in FORTRAN. This is included in the appendix A3. In the non-Newtonian reference frame, the problem is very similar to work mentioned in the literature, most oscillatory flows deal with a sinusoidally oscillating flow rate; here, we may consider a fixed quantity of fluid that is oscillating. Incidentally, this might actually prove to be a very interesting case too (fortuitously) though this is not being described in this work.

CASE 1:

$Re_d = 42$

$\delta/d = 1$

$a/d = 1$

$\omega = 2\pi$ rad/s

$\nu = 0.0093$ cm^2/s. δ (Stokes layer thickness) =0.25 cm

This was taken as the base case for comparison. The Stokes layer thickness was set equal to the cavity size (both being equal to 0.25 cm). It is worth remembering at this point that the Stokes layer thickness is the region where almost all velocity fluctuations are confined. It is also worth comparing the cavity problem with

Stokes' second problem; one can actually see perturbations creeping into the Stokes layer because of the presence of the cavity. Vortices are shed (unlike in the Stokes problem) and the flow separated at regular intervals.

Figure 4.7 shows velocity vectors and stream function plots at time $t^*=0$ where t^* is the instantaneous cycle time as a function of the time period of oscillation T.(In fact, the exact cycle time was t = 11s). t*=0 is the instant when the cavity has just come to rest; the wall velocity and acceleration are given by:

$$\mathbf{V_w = -V_a \sin(\omega t) \mid t=11.0s = 0}$$

$$\mathbf{a_w = -V_a \omega \cos(\omega t) \mid t=11.0s = -V_a \omega}$$

The acceleration is a maximum here and the wall is about to begin translation to the left. Since the wall velocity is zero, the layers very near the wall have near-zero velocities (shown by the short tails on the velocity vectors), whereas this zero velocity has not penetrated deep enough away from the vicinity of the wall, so they still have some residual positive velocities (from the previous cycle). This can be seen in a direction change in the velocity vectors as one goes away from the wall into the Stokes layer and the stream function values increase from the wall into the Stokes layer.

Inside the cavity however, one can see zero velocity vectors filling up almost the entire cavity except at the entrance of the cavity where there are appreciable velocities; remnants of the previous cycle. Since the cavity walls have come to rest, these vectors are forced to follow a path up being restricted by the cavity walls. As the fluid at the "lip" of the cavity is being forced up, one can actually see a weak clockwise vortex being generated away from the cavity. Far away from the vicinity of the cavity, flow resembles a Stokes flow solution; the presence of a cavity does not affect flow there.

Figure 4.8 shows the velocity vectors and stream function plots at t* = T/20 where T is the time period of oscillation (the actual time t = 11.05s), when the cavity has started translating to the left with non-zero velocity and acceleration. One can actually see fluid being thrown out at the right entrance of the cavity because of the motion of the cavity walls. This can also be realized from the big "plume" out of the cavity in the stream function plot. About a third of the cavity is filled with "plug" flow due to the momentum imparted by the moving wall. The cavity "sucks" in fluid from the right entrance. The weak recirculating vortex is disturbed because of the wall motion.

The wall momentum away from the cavity diffuses into the Stokes layer through only a small distance, but remnants of the positive velocities from the previous cycle give rise to a shear layer away from the cavity.

Figure 4.9 shows velocity vectors and stream function plots at t = 11.10 s, t* = T/10; one can actually see the momentum of the wall diffusing deeper into the Stokes layer. Inside the cavity, the "plug" flow traveled to a distance that is almost half of the cavity height. There is still some ejection of the fluid at one end and entrainment at the other end going on in the cavity. It can actually be seen that the "plume" has slightly shifted towards the right.

Away from the cavity, since the momentum of the wall diffuses deeper into the cavity, the shear layer gets displaced away from the wall into the Stokes layer. A separation zone can be seen at both ends away from the cavity.

Figure 4.10 shows velocity vectors and stream function values at t=11.20s; the momentum of the wall has penetrated further, the separation zone has traveled far away from the boundary and the "plug" flow fills almost the entire cavity. The plume has shifted further toward the right (in a direction opposing the flow direction).

Figure 4.11 shows velocity vectors and stream function at t =11.25 s, when the velocity of the wall is a maximum in the leftward direction and the acceleration is

zero. The entire cavity is filled by the "plug" flow. At this point, the wall is beginning to decelerate.

Figure 4.12 shows velocity vectors and stream function at t = 11.30s. This is the period when the wall is actually decelerating; the velocity is slowly decreasing, the plume gets displaced further to the right and the momentum of the wall has diffused enough into the Stokes layer. During this deceleration phase, it can be seen that the effects inside the cavity get reversed to those found during acceleration. The flow outside the cavity tries to get inside the cavity as the wall is approaching zero velocity (at half time). This can be seen in Figures 4.13 and 4.14. Figure 4.13 (a and b) shows stream function and velocity vector plots at t = 11.40s). As the main flow (outside the cavity) tries to "bend" inside the cavity, there is a vortex sheet being shed, although this can be seen very clearly only in Figure 4.14 at (t = 11.45s) that is spinning counter-clockwise. Figure 4.15 is at cycle half-time (at t = 11.5s), with the flow "bending" nicely into the cavity and a counter-clockwise spinning vortex sheet away from the cavity. Deep inside the cavity, near the walls, there are only negligible velocities, these velocities being aligned with the wall.

The other half of the cycle comprises the same processes, in the opposite direction.

CASE 2:

$Re_d = 42$

$\delta/d = 0.5$

$a/d = 2$

It can be seen that the Stokes layer thickness for this case is 0.125 cm, half of the cavity size. Interesting results were seen when the Stokes layer thickness was halved. Entirely different vortex structure is seen when the cavity comes to a halt. Inside the cavity, since the Stokes layer thickness is only half of the cavity size, flow separation occurs. This can be seen in Figures 4.16 and 4.24. It can also be

noticed that the shedding of the vortices at these instants in time is different from those in Case 1, which can be easily explained by the difference in their Stokes layer thicknesses. There is no visible difference in the flow pattern (shear layer displacement, flow separation away from the cavity, the "plug" flow phenomenon, sloshing from the cavity and entrainment of fluid) during the acceleration phase (Figures 4.17 to 4.20) as compared to the acceleration phase in Case1; however during the deceleration phase, a secondary vortex is being generated farther away from the cavity which grows, gets displaced from the wall into the Stokes layer and moves towards the plume (Figures 4.21 to 4.24). When the oscillation reaches half-time, the wall comes to a halt (Figure 4.24), flow separation occurs inside the cavity itself. The next half of the cycle resembles the first half, with a change in direction.

CASE 3:

$Re_d = 42$

$\delta/d = 2$

$a/d = 1$

Interesting physical phenomena were seen in this case when the Stokes layer thickness was twice the cavity size. Sloshing and entrainment of fluid from and into the cavity occurs when it comes to a halt, (cycle start time and half-time, Figures 4.25 and 4.31 respectively). Much of the activity, such as flow separation and vortex generation happens outside the cavity and flow inside the cavity is almost entirely "plug" flow.

During the acceleration phase (Figures 4.26 to 4.28), the cavity is filled up by the plug flow. When the cavity starts translating to the left (Figure 4.26), the fluid sloshing out of the cavity forces the steady flow and separation occurs. The momentum of the wall keeps diffusing away from the wall into the Stokes layer and the separated zone keeps moving up too (Figures 4.27 and 4.28). The weak remnant vortex moves to the right. During the deceleration phase (Figures 4.29 to 4.31), the weak recirculating vortex moves up and father away to the right and the

wall momentum diffuses much deeper into the Stokes layer. Near half time, the wall velocities are much smaller as the wall is coming to rest. This causes the flow outside the cavity to bend down into the cavity, although not very deep. At half-time, (Figure 4.31), it can be seen that there is ejection of the fluid out of the cavity and sucking in from the other side.

(6.2) Summary:

The cavity problem showed interesting results as dimensionless numbers were varied. Of all these parameters, the Stokes layer thickness influenced fluid dynamic phenomena to the largest extent. If the Stokes layer thickness was large, the momentum of the cavity walls diffused faster and deeper into the fluid as was seen in Case3. Also the sloshing and the entrainment of the fluid occurred earlier. This might have a very significant impact on transport modulation. If the Stokes layer thickness was small, as it was in Case 2, separation could be seen even inside the cavity. A secondary vortex was also seen during the deceleration phase.

Altogether, the cavity problem paved the way for a very interesting general study and the cases discussed had a lot of significant differences in their physical nature. The study of fluid flow pattern and vortex structure, and sloshing are very important in transport problems and this work can be construed as a starting point for a detailed work on transport phenomena of engineering interest.

Chapter 6

Scope for future work:

Ever since the cavity problem was envisioned, the temptation to digress was huge since there were many potential independent areas waiting in the wings to be explored. The present work was only an initial analysis aimed at understanding and characterizing oscillatory flow phenomena. Based on this work, much more work could potentially be done .

The foremost in this line of thinking would be the extension of 2 dimensional analyses into 3-d analyses. The development of modern software has aided in 3-D flow visualizations a great deal and it is only proper to have a 3-D analysis for technically flawless, stringent design. Fluent is capable of doing 3-D analysis very efficiently.

When the fluid flow problem is accurately solved, heat transfer can be solved for easily. This is the present focus in academia and the industry alike as far as building efficient new cooling techniques for microdevices is concerned. Oscillatory heat transfer modulation will prove to be an excellent solution in places where bulk mechanical heat transfer components cannot be accommodated. A 3-D flow analysis coupled with heat transfer analysis is the next station for the cavity problem!

Transition to turbulence and stability in oscillatory flows are other areas of research that would delight a Fluid dynamics purist. Turbulence in flow brings about a great degree of unpredictability; flow phenomena become much more complex and in most cases, intractable. Prediction of the onset of turbulence is very critical in flow phenomena; one should be very comfortable with the idea of using laminar flow equations for the flow parameters one selects. Prediction of turbulence in oscillatory flows as functions of geometric and oscillation

parameters are very useful and they are being studied in many academic institutions.

Only the simplest of geometries, a square geometry was studied in this work. The choice of a square geometry was because of its inherent simplicity. The natural extension of this square geometry would be the analysis in much more complex geometries starting with a rectangular geometry. Vortex generation, spreading, residence times and their ejection would probably vary significantly with more complex geometries.

The problem could "mathematically" be advanced too with the definition of time-dependent velocity amplitude for oscillation. This, in fact, increases the non-linearity associated with the problem and could possibly have a very significant impact on transport rates, especially if we could identify amplitude decay and growth rates as functions of fluid dynamic parameters. It would help too in this regard to build local expertise in writing custom computer codes and visualization environments.

Since momentum, heat and mass transfer are analogous concepts; a careful study of mass transfer rates in oscillating cavities would be of significant importance especially in drug delivery applications. A careful follow-up on Ian Sobey's work [4] would probably reveal a lot of interesting applications oscillatory flows have on mass transfer rates. Oscillatory flows could potentially also aid in particle transport. One would probably need an *Arbitrary Eulerian Lagrangian* (ALE) formulation to solve for discrete particle transport; nevertheless fluid flow patterns described in this work would prove to be a significant basic study.

The assumption of "no-slip" flow near the oscillating walls fails when the molecular mean free path becomes comparable to the characteristic flow dimensions(Knudsen number =1). The validity of the "no-slip" assumption is being researched in microchannel flows. This offers yet another rich arena for future research in oscillating cavities (probably microcavities).

Since there is a lot of sloshing and entrainment in and out of the cavity, a study of pressure oscillations could also prove useful.

The concept of flow modulation could successfully be applied to micro-electronic device cooling if Knudsen numbers work out to be in the continuum range which is the case for most devices now.

Development of experimental expertise is another area that holds much promise for future development.

References:

(1) V.O.Brien, "Unsteady Cavity Flows: Oscillatory Flat Box flows", *Journal of Applied Mechanics, Sep 1975.*

(2) Christian Von Kerczek and Stephen H Davis, "Linear Stability of Oscillatory Stokes Layers", *Journal of Fluid Mechanics, 1974.*

(3) Ivar G Jonsson, "A new approach to oscillatory rough boundary layers", *Ocean Engineering, 1980.*

(4) Ian Sobey, "On flow through furrowed channels Part1 Calculated Flow Patterns" , *Journal of Fluid Mechanics, 1980.*

(5) Ian Sobey, "On flow through furrowed channels Part2 Observed Flow Patterns", *Journal of Fluid Mechanics, 1980.*

(6) Ian J Sobey, "The Occurrence of Separation in Oscillatory Flow", *Journal of Fluid Mechanics, 1983.*

(7) N.K. Ghaddar, K.Z.Korczak, B.B.Mikic, A.T.Patera, "Numerical Investigation of Incompressible Flow in grooved channels Parts1 and 2", *Journal of Fluid Mechanics, 1986.*

(8) D.Mateescu, M.P.Paidoussis, W.G.Sim, "A Spectral Collocation Method for confined unsteady flows with oscillating boundaries", *Journal of Fluids and Structures, 1994.*

(9) Kiril B Selverov, H.A.Stone, "Peristaltically driven channel flows with applications to micromixing", *Physics of Fluids, July2001.*

(10) Tatsuo NISHIMURA, Alexandru Mihail MOREGA and Koji KUNITSUGU, Vortex Structure and Fluid Mixing in Pulzatile through Periodically Grooved Channels at Low Reynolds Numbers, *Japan Society of Mechanical Engineers, 1997*

(11) J.M. Floryan, J.Szumbarski, X.Wu, "Stability of flow in a channel with vibrating wall", *Physics of Fluids, 2002.*

(12) Fredrik Carlsson, Mihir Sen, Lennart Lofdahl, "Analytical studies of flow effects due to Vibrating Walls", under consideration for publication in the *Journal of Fluid Mechanics (submitted Dec5, 2002).*

(13) M.J.Vogel, A.H.Hirsa, J.M.Lopez, "Spatio-Temporal Dynamics of a Periodically Driven Cavity Flow", under consideration for publication in the *Journal of Fluid Mechanics(submitted March 25, 2002).*

(14) Frank M White, *Viscous Fluid Flow*, Second edition, 1991

(15) J.L. Meriam and L.G.Kraige, *Engineering Mechanics*, Vol 2, 1992

(16) Suhas V Patankar, *Numerical Heat Transfer and Fluid Flow,* 1980

APPENDICES:

A1 C Program for an oscillating velocity boundary condition:

```
#include<udf.h>
DEFINE_PROFILE(unsteady_velocity,thread,position)
{
face_t f;
begin_f_loop(f,thread)
{
real t = RP_Get_Real("flow-time");
F_PROFILE(f,thread,position) = 0.01 *sin(6.2831853*t);
}
end_f_loop(f,thread)
}
```

A2 C Program that inputs an oscillating source terms to the x-momentum equation:

```
#include<udf.h>
#include<mem.h>
DEFINE_SOURCE(cell_x_source, cell, thread, dS, eqn)

{
real cons = 6283.1853;
real source;
real t = RP_Get_Real("flow-time");
source = cons*0.01*cos(6.2831853*t);
dS[eqn]=0;
return source;
}
```

A3 Fortran program that calculates Newtonian velocities and stream functions from Fluent results.

```
      PROGRAM cavityplot
      PARAMETER (nnmax=30000,nconx=80,ncony=60)
      REAL x(nnmax),y(nnmax),psinn(nnmax),psin(nnmax),unn(nnmax)
          REAL v(nnmax),un(nnmax),vmag(nnmax),t,w,vwamp,vw,wo(nnmax)
          real zmat(nconx,ncony),imat(nconx,ncony),wmat(nconx,ncony)
          integer ixp(11),iyp(11)

          character*80 fname,cjunk

          open(unit=8,file='c3410.dat',status='old')
c     print*,'case1,case2,case3,case4 ? (5,6,7,8)'
c     read*, ipickcase

c
c         Set number of nodes in data file
c
      print*,'velocity vector, stream function,vorticity? (3,4,5)'
          read*, ipickplot

          nnodes = 26266
          ymax = 0.045
          psimax = -100.0
          psimin = 100.0
          vmax = 0.0
          veclmax = 0.05
      print*,'enter current time'
      read*, t
      print*,'enter angular velocity'
      read*,w
      print*,'wall velocity amplitude'
      read*,vwamp
      vw = - vwamp * sin(w*t)
          print*,vw

c
c         Read in data from plotting file
c         first read title then x,y,unn,v,psinn data; subscript nn means non-newtonian,
c
```

```
      read(8,*) cjunk

      do i=1,nnodes
            read(8,*) nn,x(i),y(i),unn(i),v(i),psinn(i),wo(i)
       psin(i) = (1000*vw*y(i))+psinn(i)
c       psin(i) = psin(i)/(1000*vwamp*0.0025)
c        psin(i) = psin(i)
           un(i) = vw + unn(i)
c          un(i) = unn(i)
        vmag(i)= (un(i)**2+v(i)**2)**0.5
            if(y(i).eq.ymax) psin0 = psin(i)
            if(vmag(i).gt.vmax) vmax = vmag(i)
c                 psinzero = psin(i)
c           end if
      end do
      print*, psin0
      do i=1,nnodes
            x(i)=x(i)*100.0
            y(i)=y(i)*100.0
            psin(i)=psin(i)-psin0
c     psin(i) = psin(i)/(1000*vwamp*0.0025)
            if(psimax.lt.psin(i)) psimax = psin(i)
            if(psimin.gt.psin(i)) psimin = psin(i)
      end do

      print*,'wmf, xwin, ps or cgm output? (0,1,2,3)'
      read*, ipick
      if(ipick.eq.0) call metafl('wmf')
      if(ipick.eq.1) call metafl('xwin')
      if(ipick.eq.2) call metafl('post')
      if(ipick.eq.3) call metafl('cgm')

c     CALL SETPAG('DA4l')
      CALL PAGE(2800,3000)
c     CALL SETPAG('DA3P')

      CALL DISINI

      call triplx
c     call pagera
      call axslen(1900,2500)
      call center
```

```
c
c       Set up user coordinate system but don't plot axes
c
        call nograf
c       CALL GRAF(3.0,4.25,0.,1.0,1.0,2.0,0.,5.0)
c       CALL GRAF(0.0,6.75,0.,1.,0.,5.,0.,5.0)
        call graf(3.25,4.00,3.25,1.0,1.25,2.25,1.25,0.5)

c
c       Display time
c

c       call rlmess('Time=',0.,22.)
c       call number(time,-1,999,999)

c
c       Plot wall and cavity boarders
c

        call linwid(4)

c       call rlstrt(0.5,1.5)
    call rlstrt(3.25,1.5)
        call rlconn(3.5,1.5)
        call rlconn(3.5,1.25)
        call rlconn(3.75,1.25)
        call rlconn(3.75,1.5)
        call rlconn(4.0,1.5)
c       call rlconn(6.75,1.5)

        call linwid(1)

c**********************************************************************
c
c       The following is for mesh plotting
c

c       do i=1,nelem
c               call rline(x(no(i,1)),y(no(i,1)),x(no(i,2)),y(no(i,2)))
c               call rline(x(no(i,2)),y(no(i,2)),x(no(i,3)),y(no(i,3)))
c               call rline(x(no(i,1)),y(no(i,1)),x(no(i,3)),y(no(i,3)))
c       end do
c**********************************************************************
```

```
c**********************************************************************
c       Contouring starts here.
c
c       Set up shielding for contour plotting
c
c
        ixp(1)=nxposn(0.5)
        ixp(2)=nxposn(3.5)
        ixp(3)=nxposn(3.5)
        ixp(4)=nxposn(3.75)
        ixp(5)=nxposn(3.75)
        ixp(6)=nxposn(6.75)
        ixp(7)=nxposn(6.75)
        ixp(8)=nxposn(0.5)
c       ixp(9)=nxposn(10.)
c       ixp(10)=nxposn(0.)
c       ixp(11)=nxposn(0.)

        iyp(1)=nyposn(1.5)
        iyp(2)=nyposn(1.5)
        iyp(3)=nyposn(1.25)
        iyp(4)=nyposn(1.25)
        iyp(5)=nyposn(1.5)
        iyp(6)=nyposn(1.5)
        iyp(7)=nyposn(1.0)
        iyp(8)=nyposn(1.0)
c       iyp(9)=nyposn(23.)
c       iyp(10)=nyposn(23.)
c       iyp(11)=nyposn(0.)

        call frame(0)
        call shlpol(ixp,iyp,8)


c       Produce contours and then plot


        call getmat(x,y,psin,nnodes,zmat,nconx,ncony,0.0,imat,wmat)

        call labels('float','contur')
        call labdig(3,'contur')
```

```
c       call congap(1.0)
c       call conmod(1.0,1.5)
c       call labdis(2000,'contur')
        call height(30)
        call thkcrv(1)
        call penwid(4)
     if(ipickplot.eq.3) goto 400
     if(ipickplot.eq.5) goto 450
c    if(ipickplot.eq.4) goto sfplot.

        do i=-100,100
         IF(MOD(I+100,3).EQ.1) THEN
          CALL SOLID
          CALL THKCRV(2)
         ELSE IF(MOD(I+100,3).EQ.2) THEN
          CALL chndsh
          CALL THKCRV(1)
         ELSE
          CALL dash
          CALL THKCRV(1)
         END IF
               call conmat(zmat,nconx,ncony,float(i)/800)
        end do

        goto 500

c    velocity vector plots

 400  scale = veclmax/vmax

        do i=1,nnodes,20
         if(vmag(i).gt.0.00005) then
               xto=x(i)+un(i)*scale
               yto=y(i)+v(i)*scale
c              xto=x(i)+un(i)*veclmax/vmag(i)
c              yto=y(i)+v(i)*veclmax/vmag(i)
               call rlvec(x(i),y(i),xto,yto,1201)
         end if
        end do
     goto 500


c     vorticity plot
 450  call getmat(x,y,wo,nnodes,zmat,nconx,ncony,0.0,imat,wmat)
```

```
c       call labels('float','contur')
        call labdig(3,'contur')
        call congap(1.0)
        call conmod(1.0,1.5)
        call labdis(2000,'contur')
        call height(100)
        call thkcrv(1)
        call penwid(4)

        do i=-100,100
        IF(MOD(I+100,3).EQ.1) THEN
         CALL SOLID
         CALL THKCRV(2)
        ELSE IF(MOD(I+100,3).EQ.2) THEN
         CALL chndsh
         CALL THKCRV(1)
        ELSE
         CALL dash
         CALL THKCRV(1)
        END IF
             call conmat(zmat,nconx,ncony,float(i)/2500)
       end do

       goto 500

500    continue

   CALL DISFIN
   END
```